

AD-A182 775

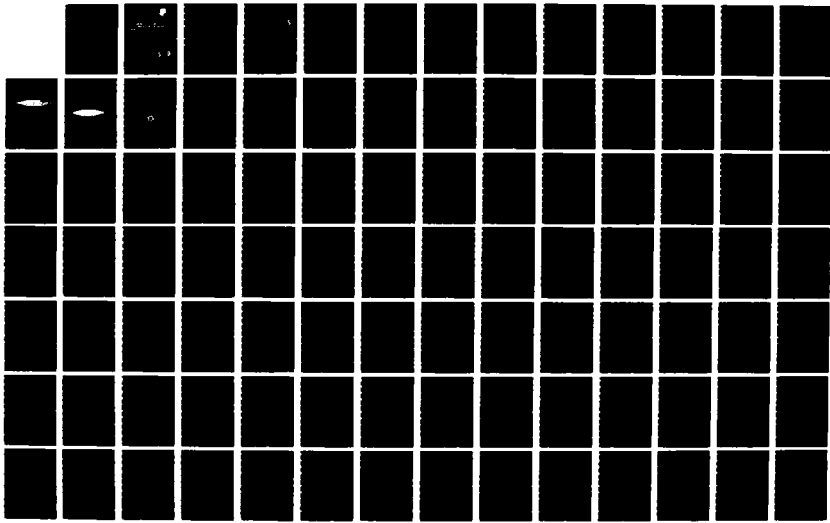
ELECTROMAGNETIC DISPERSION OF A COAXIAL WAVEGUIDE WITH 1/2
AN ARBITRARY RADIUS (U) UTAH UNIV SALT LAKE CITY DEPT
OF ELECTRICAL ENGINEERING A M PUZELLA APR 87

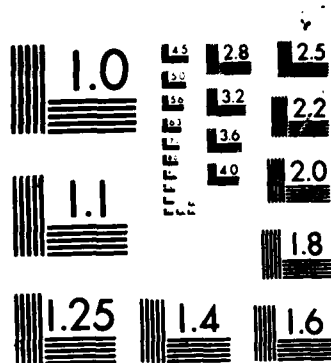
UNCLASSIFIED

UTECH-MD-86-843 RADC-TR-87-36

F/G 9/1

NL





MICROCOPY RESOLUTION TEST CHART
NATIONAL BUREAU OF STANDARDS 1963-A

DTIC FILE COPY

12

AD-A182 775

RADC-TR-87-36
Final Technical Report
April 1987



ELECTROMAGNETIC DISPERSION OF A COAXIAL WAVEGUIDE WITH AN ARBITRARY RADIAL DIELECTRIC PROFILE

University of Utah

Angelo M. Puzella

APPROVED FOR PUBLIC RELEASE; DISTRIBUTION UNLIMITED

DTIC
ELECTED
S JUL 27 1987 D
C E

**ROME AIR DEVELOPMENT CENTER
Air Force Systems Command
Griffiss Air Force Base, NY 13441-5700**

87 7 24 008

This report has been reviewed by the RADC Public Affairs Office (PA) and is releasable to the National Technical Information Service (NTIS). At NTIS it will be releasable to the general public, including foreign nations.

RADC-TR-87-36 has been reviewed and is approved for publication.

APPROVED:



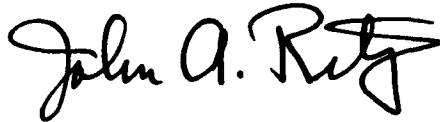
ANDREW E. CHROSTOWSKI, CAPT, USAF
Project Engineer

APPROVED:



FRED J. DEMMA
Acting Director
Directorate of Surveillance

FOR THE COMMANDER:



JOHN A. RITZ
Directorate of Plans & Programs

If your address has changed or if you wish to be removed from the RADC mailing list, or if the addressee is no longer employed by your organization, please notify RADC (OCTP) Griffiss AFB NY 13441-5700. This will assist us in maintaining a current mailing list.

Do not return copies of this report unless contractual obligations or notice on a specific document requires that it be returned.

UNCLASSIFIED
SECURITY CLASSIFICATION OF THIS PAGE

REPORT DOCUMENTATION PAGE

12
A182 775

Form Approved
OMB No. 0704-0188

1a. REPORT SECURITY CLASSIFICATION UNCLASSIFIED		1b. RESTRICTIVE MARKINGS N/A	
2a. SECURITY CLASSIFICATION AUTHORITY N/A		3. DISTRIBUTION/AVAILABILITY OF REPORT Approved for public release; distribution unlimited.	
2b. DECLASSIFICATION/DOWNGRADING SCHEDULE N/A		5. MONITORING ORGANIZATION REPORT NUMBER(S) RADC-TR-87-36	
4. PERFORMING ORGANIZATION REPORT NUMBER(S) UTEC MD-86-043		6a. NAME OF PERFORMING ORGANIZATION University of Utah	
6b. OFFICE SYMBOL (If applicable)		7a. NAME OF MONITORING ORGANIZATION Rome Air Development Center (OCTP)	
6c. ADDRESS (City, State, and ZIP Code) Department of Electrical Engineering Salt Lake City UT 84112		7b. ADDRESS (City, State, and ZIP Code) Griffiss AFB NY 13441-5700	
8a. NAME OF FUNDING/SPONSORING ORGANIZATION AFOSR		8b. OFFICE SYMBOL (If applicable) NE	
8c. ADDRESS (City, State, and ZIP Code) Bolling AFB Wash DC 20332		9. PROCUREMENT INSTRUMENT IDENTIFICATION NUMBER F30602-82-C-0161	
10. SOURCE OF FUNDING NUMBERS PROGRAM ELEMENT NO. 61102F		PROJECT NO. 2305	TASK NO. J9
		WORK UNIT ACCESSION NO. 16	
11. TITLE (Include Security Classification) ELECTROMAGNETIC DISPERSION OF A COAXIAL WAVEGUIDE WITH AN ARBITRARY RADIAL DIELECTRIC PROFILE			
12. PERSONAL AUTHOR(S) Angelo M. Puzella			
13a. TYPE OF REPORT Final	13b. TIME COVERED FROM Sep 82 TO Sep 85	14. DATE OF REPORT (Year, Month, Day) April 1987	15. PAGE COUNT 158
16. SUPPLEMENTARY NOTATION Research accomplished in conjunction with Air Force Thermionics Engineering Research Program (AFTER) AFTER-15			
17. COSATI CODES FIELD 09 GROUP 03 SUB-GROUP		18. SUBJECT TERMS (Continue on reverse if necessary and identify by block number) Microwave Tubes Direct Integration Method Coaxial Wave Guide Electromagnetic Dispersion Computer Analysis	
19. ABSTRACT (Continue on reverse if necessary and identify by block number) <p>The electromagnetic dispersion of a coaxial waveguide with an arbitrary radial dielectric profile is obtained by direct integration of Maxwell's equations. The equations are written in cylindrical coordinates and the standard Fourier transformations are performed in the time ($t + \omega$), axial ($z + k_z$), and azimuthal ($\phi + m$) coordinates. The resulting equations are combined to form either one second order differential equation ($m = 0$) or two coupled second order equations ($m \neq 0$) in the radial coordinate. These equations are integrated for fixed ω and m by a "shooting" method with k_z as the shooting parameter that is, k_z is varied until the boundary conditions are satisfied. This yields k_z as a function of ω, and hence the dispersion. The field components are directly obtained from the integration. The formulation handles both smoothly varying and discontinuous jumps in the radial dielectric profile.</p>			
20. DISTRIBUTION/AVAILABILITY OF ABSTRACT <input checked="" type="checkbox"/> UNCLASSIFIED/UNLIMITED <input type="checkbox"/> SAME AS RPT. <input type="checkbox"/> DTIC USERS		21. ABSTRACT SECURITY CLASSIFICATION UNCLASSIFIED	
22a. NAME OF RESPONSIBLE INDIVIDUAL Andrew E. Chrostowski, Capt, USAF		22b. TELEPHONE (Include Area Code) (315) 330-4381	22c. OFFICE SYMBOL RADC (OCTP)

UNCLASSIFIED

This approach is quite different from the standard normal mode expansion in terms of Bessel functions. The problem with the standard technique is that it cannot handle a smoothly varying dielectric; it does not include the TEM mode, and it is numerically unstable in the regime where the mode is propagating in one region and cutoff in another. The direct integration method overcomes all these drawbacks.

UNCLASSIFIED

ACKNOWLEDGMENTS

I thank Dr. Alan Palevsky for his time, inexhaustible patience, and optimism throughout the project. Dr. Norman J. Dionne was also of invaluable help, and I thank him. Finally, I thank Raytheon's Microwave and Power Tube Division, the United States Air Force and the University of Utah for their sponsorship and participation in the AFTER program.

Accession No.	
NTIS GRA&I	<input checked="" type="checkbox"/>
DTIC TAB	<input type="checkbox"/>
Unannounced	<input type="checkbox"/>
Justification	
By	
Distribution/	
Availability	
Dist	Avail Spec
A-1	

TABLE OF CONTENTS

	<u>Page</u>
LIST OF ILLUSTRATIONS	v
I. INTRODUCTION	1
II. MODAL EXPANSION APPROACH	6
2.1 Derivation of the Dispersion Determinant	6
2.2 Drawbacks	16
III. DIRECT INTEGRATION OF MAXWELL'S EQUATIONS	17
3.1 Derivation of the Differential Equation Systems	17
3.2 Initial and Boundary Conditions	24
3.3 Discontinuous Dielectric Profile Formulation	26
3.4 Field Equations	28
3.5 Normalization and Orthogonality Relations	29
3.6 Form for Numerical Integration	30
IV. PROGRAM OUTLINE AND USE	41
4.1 Program Flow	41
4.2 Process for a General Dielectric Profile	51
4.3 Finding a Mode	52
V. PRESENTATION OF RESULTS	56
5.1 $TM_{0,1}$ Mode	58
5.2 $TE_{0,1}$ Mode	67
5.3 TEM Mode	76
5.4 $TM_{1,1}$ ($EH_{1,1}$) Mode	85

	<u>Page</u>
5.5 Evaluation of Orthogonality	112
5.6 Dispersion Plots	114
5.7 Effect of the Dielectric Profile on k_z	118
VI. CONCLUSION	120
6.1 Advantages and Drawbacks	120
6.2 Future Goals and Applications	121
REFERENCES	122
APPENDIX A. NUMERICAL SUBROUTINES	123
APPENDIX B. NAMELISTS	128
APPENDIX C. INTERPOLATION OF A DISCONTINUOUS FUNCTION	132
APPENDIX D. VARIABLE DEFINITIONS	134
APPENDIX E. VALUES OF THE RADIAL POINTS	144

LIST OF ILLUSTRATIONS AND TABLES

<u>Figure</u>	<u>Page</u>
1 Tapered coaxial waveguide	3
2 Step approximation of the tapered coaxial waveguide . . .	4
3 (A) Stepped dielectric section, front view. (B) Linearly graded dielectric section, front view	5
4 "Build up" process to evaluate the two dielectric profile	54
5 $TM_{0,1}$ mode at 32 GHz, $ER1 = 1$; E_r component	59
6 $TM_{0,1}$ mode at 32 GHz $ER1 = 1$; E_z component	60
7 $TM_{0,1}$ mode at 32 GHz, $ER1 = 1$; H_ϕ component	61
8 $TM_{0,1}$ mode at 32 GHz, $ER1 = 1$; Poynting's vector $E_r H_\phi$. .	62
9 $TM_{0,1}$ mode at 32 GHz, $ER1 = 2$; E_r component	63
10 $TM_{0,1}$ mode at 32 GHz, $ER1 = 2$; E_z component	64
11 $TM_{0,1}$ mode at 32 GHz, $ER1 = 2$; H_ϕ component	65
12 $TM_{0,1}$ mode at 32 GHz, $ER1 = 2$; Poynting's vector $E_r H_\phi$. .	66
13 $TE_{0,1}$ mode at 32 GHz, $ER1 = 1$; E_ϕ component	68
14 $TE_{0,1}$ mode at 32 GHz, $ER1 = 1$; H_r component	69
15 $TE_{0,1}$ mode at 32 GHz, $ER1 = 1$; H_z component	70
16 $TE_{0,1}$ mode at 32 GHz, $ER1 = 1$; Poynting's vector $E_\phi H_r$. .	71
17 $TE_{0,1}$ mode at 32 GHz, $ER1 = 2$; E_ϕ component	72
18 $TE_{0,1}$ mode at 32 GHz, $ER1 = 2$; H_r component	73
19 $TE_{0,1}$ mode at 32 GHz, $ER1 = 2$; H_z component	74
20 $TE_{0,1}$ mode at 32 GHz, $ER1 = 2$; Poynting's vector $E_\phi H_r$. .	75
21 TEM mode at 32 GHz, $ER1 = 1$; E_r component	77
22 TEM mode at 32 GHz, $ER1 = 1$; E_z component	78

<u>Figure</u>		<u>Page</u>
23	TEM mode at 32 GHz, ERL = 1; H_ϕ component	79
24	TEM mode at 32 GHz, ERL = 1; Poynting's vector $E_r H_\phi$. . .	80
25	TEM mode at 32 GHz, ERL = 2; E_r component	81
26	TEM mode at 32 GHz, ERL = 2; E_z component	82
27	TEM mode at 32 GHz, ERL = 2; H_ϕ component	83
28	TEM mode at 32 GHz, ERL = 2; Poynting's vector $E_r H_\phi$. . .	84
29	TM _{1,1} mode at 32 GHz, ERL = 1; E_r component	86
30	TM _{1,1} mode at 32 GHz, ERL = 1; E_ϕ component	87
31	TM _{1,1} mode at 32 GHz, ERL = 1; E_z component	88
32	TM _{1,1} mode at 32 GHz, ERL = 1; H_r component	89
33	TM _{1,1} mode at 32 GHz, ERL = 1; H_ϕ component	90
34	TM _{1,1} mode at 32 GHz, ERL = 1; H_z component	91
35	TM _{1,1} mode at 32 GHz, ERL = 1; Poynting's vector $E_r H_\phi$. .	93
36	TM _{1,1} mode at 32 GHz, ERL = 1; Poynting's vector $E_\phi H_r$. .	94
37	EH _{1,1} mode 1 at 32 GHz, ERL = 2; E_r component	95
38	EH _{1,1} mode 1 at 32 GHz, ERL = 2; E_ϕ component	96
39	EH _{1,1} mode 1 at 32 GHz, ERL = 2; E_z component	97
40	EH _{1,1} mode 1 at 32 GHz, ERL = 2; H_r component	98
41	EH _{1,1} mode 1 at 32 GHz, ERL = 2; H_ϕ component	99
42	EH _{1,1} mode 1 at 32 GHz, ERL = 2; H_z component	100
43	EH _{1,1} mode 1 at 32 GHz, ERL = 2; Poynting's vector $E_r H_\phi$.	101
44	EH _{1,1} mode 1 at 32 GHz, ERL = 2; Poynting's vector $E_\phi H_r$.	103
45	EH _{1,1} mode 2 at 32 GHz, ERL = 2; E_r component	104
46	EH _{1,1} mode 2 at 32 GHz, ERL = 2; E_ϕ component	105
47	EH _{1,1} mode 2 at 32 GHz, ERL = 2; E_z component	106

I. INTRODUCTION

In the interest of building an axial gain cross field amplifier, analysis was desired for the tapered waveguide (Fig. 1.). A stepped dielectric profile was chosen to model the linearly tapered profile (Fig. 2). The formulation presented in this paper is based on the geometry of Fig. 3, where a given slab is removed from the step. Particular interest in the behavior of certain modes in the presence of a discontinuous dielectric included the $TE_{0,1}$, $TM_{0,1}$, TEM, and several $TE_{m,n}$ and $TM_{m,n}$ modes.

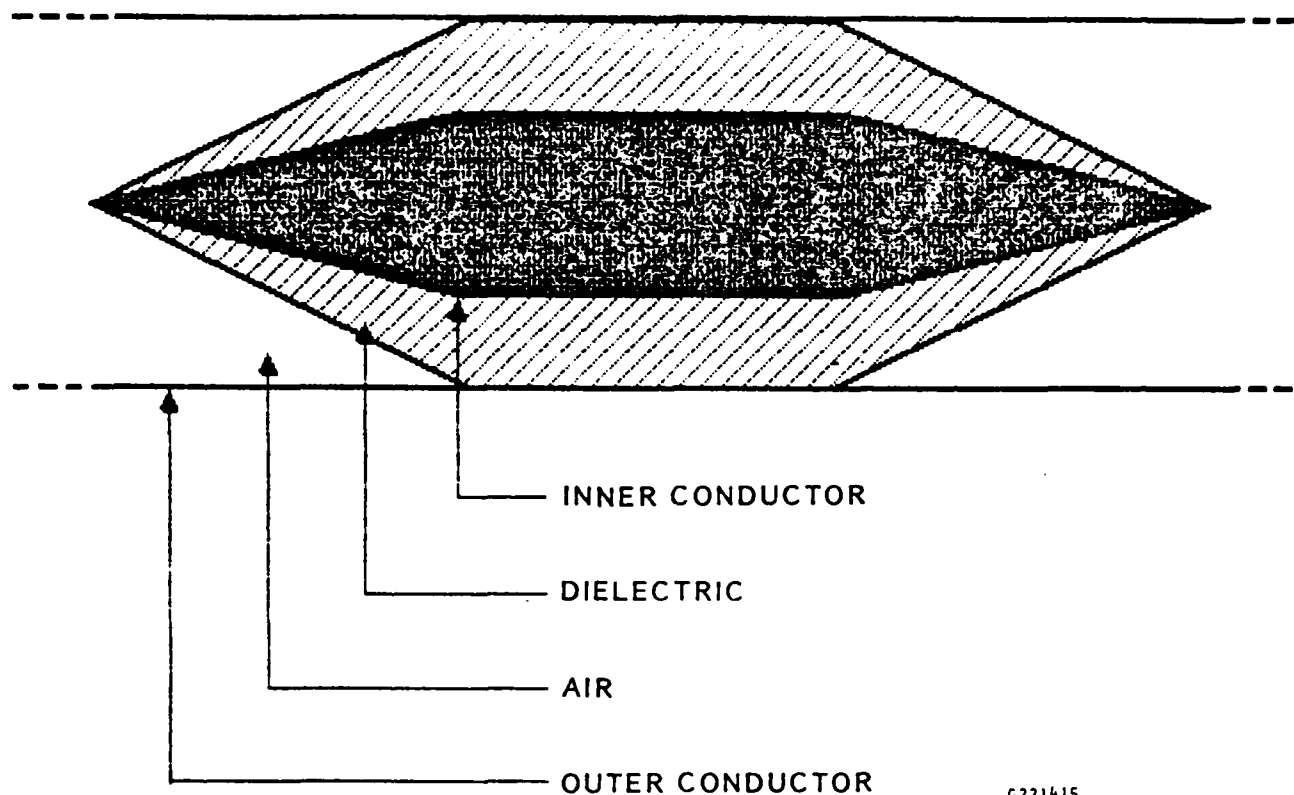
The original approach taken for the problem was the modal expansion technique. This traditional approach generates a dispersion determinant by enforcing continuity of certain fields across an interface between two mediums. Roots (k_z as a function of ω) are obtained by finding the zeros of the determinant formed from these boundary conditions. The formulation is straightforward, but numerical difficulties arise when it is translated to code and run. This motivated the need for a fresh approach to the problem.

The direct integration approach simply involves integrating two second order linear differential equations for $TE_{m,n}$ and $TM_{m,n}$ modes ($m \neq 0$) or one second order linear differential equation for $TE_{0,n}$, $TM_{0,n}$, and TEM modes. The formulation can handle discontinuous and linearly tapered (as a function of r) dielectric profiles. Theoretically, it can also handle combinations of both to produce a general dielectric profile. Irrelevant of the number of dielectric layers comprising the profile, the number and format of the second order

differential equations does not change for a given mode. There are no Bessel functions, and consequently no need to evaluate Bessel function expansions in a computer program. A major advantage regards the ability to analyze the TEM mode for a discontinuous dielectric profile, as shown in Fig. 3A. This seems logical based on the fact that all modes must obey Maxwell's equations for a given dielectric profile. In stark contrast, the modal expansion technique sheds no light regarding analysis of the TEM mode for a discontinuous dielectric profile. Finally, upon completing the integration, all field components of a given mode are easily computed using the values of the integration parameters, the mode propagation constant, and Maxwell's equations.

The code analyzes the geometry of Fig. 3A and its effects on the following mode types: $TM_{m,n}$ ($EH_{m,n}$), $TE_{0,n}$, $TM_{0,n}$, and TEM modes. The user inputs a desired dielectric profile, mode type, and initial conditions from which the propagation constant k_z and all relevant field patterns (as a function of r) are produced. For $TE_{m,n}$ and $TM_{m,n}$ modes, an additional parameter, α , is produced which interprets the degree of hybridization due to the dielectric profile. The program also checks the orthogonality between any two modes of a given mode type and similar azimuthal mode number.

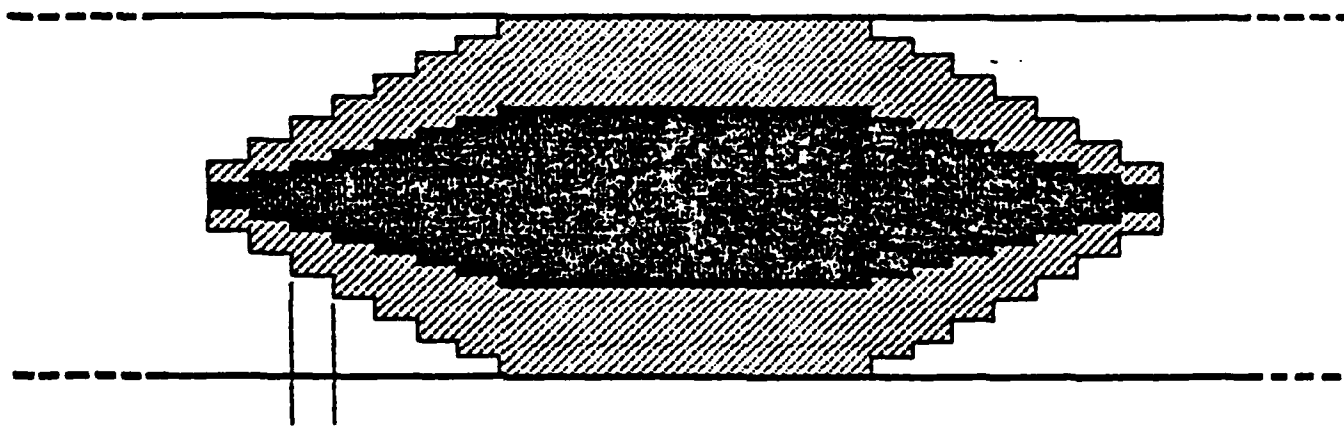
TAPERED COAXIAL WAVEGUIDE



6221415

Fig. 1. Tapered coaxial waveguide.

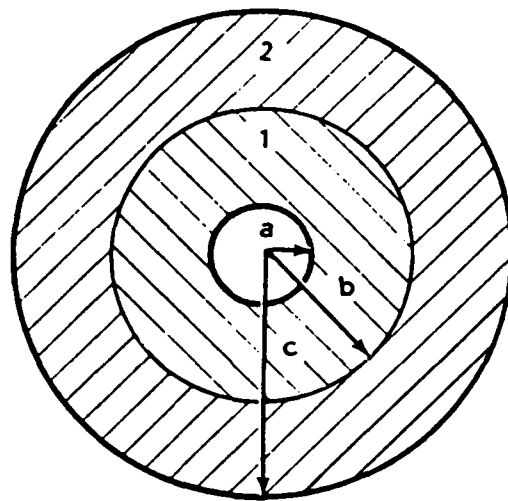
STEP APPROXIMATION
OF THE
TAPERED COAXIAL WAVEGUIDE



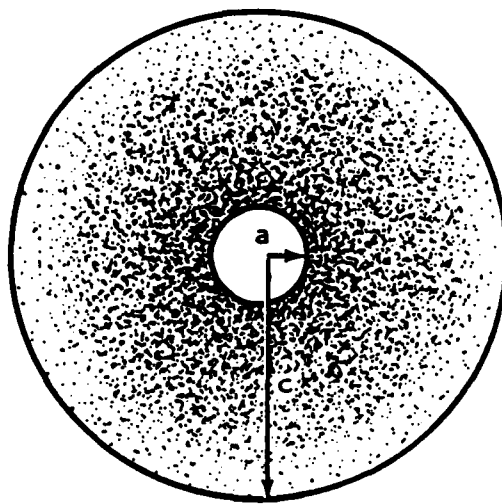
TYPICAL SECTION USED IN FORMULATION

6221416

Fig. 2. Step approximation of the tapered coaxial waveguide.



A. STEPPED DIELECTRIC SECTION
FRONT VIEW



B. LINEARLY GRADED DIELECTRIC SECTION
FRONT VIEW

6221413

Fig. 3. (A) Stepped dielectric section, front view.
(B) Linearly graded dielectric section, front view.

1.. MODAL EXPANSION APPROACH

The modal expansion technique is presented in this chapter. Section 2.1 derives the dispersion determinant for the geometry of Fig. 3A. We start with the scalar Helmholtz equation and proceed to separate the variables. The scalar wave functions (eigen functions) are constructed, which then allows the appropriate boundary conditions to be applied at the dielectric interface ($r = b$). Finally, the dispersion determinant is found which describes the modes propagating in our system. Section 2.2 discusses the drawbacks using this approach. We note that primes in the equations represent the derivative with respect to the radial coordinate r .

2.1 Derivation of the Dispersion Determinant

The derivation that follows is based on that of Harrington¹ and Rothwell.² The scalar wave functions for the geometry of Fig. 3 must obey the scalar Helmholtz equation written here in cylindrical coordinates:

$$\frac{1}{r} \frac{\partial}{\partial r} \left[r \frac{\partial \psi}{\partial r} \right] + \frac{1}{r^2} \frac{\partial^2 \psi}{\partial \phi^2} + \frac{\partial^2 \psi}{\partial z^2} + k^2 \psi = 0 \quad (1)$$

where

ψ = scalar wave function

k = constant

The common approach taken to solve Eq. 1 is to separate the variables.

The usual form for the solution is

$$\psi = R(r)\Phi(\phi)Z(z) \quad (2)$$

Following the standard procedure, the separated equations are

$$r \frac{d}{dr} \left[r \frac{dR}{dr} \right] + \left[k_r r - m^2 \right] R = 0 \quad (3)$$

$$\frac{d^2\Phi}{d\phi^2} + m^2\Phi = 0 \quad (4)$$

$$\frac{d^2Z}{dz^2} + k_z^2 Z = 0 \quad (5)$$

where

$$k_z^2 + k_r^2 = k^2$$

Solutions to Eqs. 4 and 5 are harmonic functions. Equation 3 is known as Bessel's equation of order m and argument $k_r \cdot r$ with solutions having the general form

$$R(r) = Z_m(k_r r, r, A, B) \equiv AJ_m(k_r r) + BY_m(k_r r) \quad (6)$$

where

$J_m(k_r r)$ = Bessel's function of the first kind

$Y_m(k_r r)$ = Bessel's function of the second kind

A, B = constants

and k_r may be real or imaginary. Solutions to Eqs. 4 and 5 are of the form

$$\Phi(\phi) = \cos(m\phi) \quad (7)$$

$$\Phi(\phi) = \sin(m\phi) \quad (8)$$

$$Z(z) = e^{-jk_z z} \quad (9)$$

where k_z is the propagation constant. The scalar wave functions for each region of Fig. 3A are:

Region 1

$$\psi_m^{(m1)} = Z_m^{(m1)}(k_{r1}, r, A_1, A_2) \cos(m\phi) e^{-jk_z z} \quad (10a)$$

$$\phi_m^{(e1)} = Z_m^{(e1)}(k_{r1}, r, B_1, B_2) \sin(m\phi) e^{-jk_z z} \quad (10b)$$

Region 2

$$\psi_m^{(m2)} = Z_m^{(m2)}(k_{r2}, r, C_1, C_2) \cos(m\phi) e^{-jk_z z} \quad (11a)$$

$$\phi_m^{(e2)} = Z_m^{(e2)}(k_{r2}, r, D_1, D_2) \sin(m\phi) e^{-jk_z z} \quad (11b)$$

where A_i , B_i , and D_i are constants ($i = 1, 2$). The superscripts $m1$ and $m2$ denote the contributions from TM modes for regions 1 and 2; the superscripts $e1$ and $e2$ denote contributions from TE modes for regions 1 and 2. The separation equations which the wave functions must satisfy are:

$$k_z^2 + k_{r1}^2 = k_1^2 = \omega^2 \epsilon_1 \mu_1 \quad (12a)$$

$$k_z^2 + k_{r2}^2 = k_2^2 = \omega^2 \epsilon_2 \mu_2 \quad (12b)$$

for regions 1 and 2, respectively. The resultant electric and magnetic fields in each region have contributions from both the TE and TM modes. Consequently, hybrid modes will propagate in our system.

Boundary conditions were applied to the following field components written in general for region i ($i = 1, 2$):

$$E_\phi = \left[\frac{mk}{\omega \epsilon_1 r} Z_m^{(mi)}(k_{r1}, r, K_1, K_2) + k_{r1} Z_m^{(ei)}(k_{r1}, r, K_3, K_4) \right] \sin(m\phi) e^{-jk_z z} \quad (13a)$$

$$E_z = \frac{k_{r1}^2}{j\omega \epsilon_1} Z_m^{(mi)}(k_{r1}, r, K_5, K_6) \cos(m\phi) e^{-jk_z z} \quad (13b)$$

$$H_\phi = - \left[k_{r1} Z_m^{(mi)}(k_{r1}, r, K_7, K_8) + \frac{mk}{\omega \mu_1 r} Z_m^{(ei)}(k_{r1}, r, K_9, K_{10}) \right] \cos(m\phi) e^{-jk_z z} \quad (13c)$$

$$H_z = \frac{k_{r1}^2}{j\omega \mu_1} Z_m^{(ei)}(k_{r1}, r, K_{11}, K_{12}) \sin(m\phi) e^{-jk_z z} \quad (13d)$$

where I_1 ($i = 1, \dots, 12$) is a constant.

For compactness, we define the following constants:

$$\begin{array}{ll}
 s_1 = J_n(k_{r1}a) & s'_1 = J'_n(k_{r1}a) \\
 s_2 = Y_n(k_{r1}a) & s'_2 = Y'_n(k_{r1}a) \\
 s_3 = J_n(k_{r1}b) & s'_3 = J'_n(k_{r1}b) \\
 s_4 = Y_n(k_{r1}b) & s'_4 = Y'_n(k_{r1}b) \\
 s_5 = J_n(k_{r2}b) & s'_5 = J'_n(k_{r2}b) \\
 s_6 = Y_n(k_{r2}b) & s'_6 = Y'_n(k_{r2}b) \\
 s_7 = J_n(k_{r2}c) & s'_7 = J'_n(k_{r2}c) \\
 s_8 = Y_n(k_{r2}c) & s'_8 = Y'_n(k_{r2}c) \quad (14)
 \end{array}$$

We are now in a position to evaluate the following boundary conditions:

$$E_\phi = 0 \quad (15a)$$

$$E_z = 0 \quad (15b)$$

at $r = a$ and $r = c$. Applying the above boundary conditions to Eq. 6 and using Eq. 14, we have

$$A_2 = -A_1 \frac{s_1}{s'_2} \quad (16a)$$

$$B_2 = -A_1 \frac{s'_1}{s'_2} \quad (16b)$$

at $r = a$ and

$$C_2 = -C_1 \frac{s_7}{s_8} \quad (17a)$$

$$E_2 = -D_1 \frac{s'_7}{s'_8} \quad (17b)$$

at $r = c$. Using Eq. 6, we eliminate A_2 , B_2 , C_2 , and D_2 with the aid of Eqs. 16 and 17,

$$\psi_m^{(m1)} = A_1 Z_m(k_{rl}, r, 1, -s_1 s_2^{-1}) \quad (18a)$$

$$\psi_m^{(e1)} = B_1 Z_m(k_{rl}, r, 1, -s'_1 (s'_2)^{-1}) \quad (18b)$$

for region 1. and

$$\psi_m^{(m2)} = C_1 Z_m(k_{r2}, r, 1, -s_7 s_8^{-1}) \quad (19a)$$

$$\psi_m^{(e2)} = D_1 Z_m(k_{r2}, r, 1, -s'_7 (s'_8)^{-1}) \quad (19b)$$

for region 2. At the dielectric interface ($r = b$) E_ϕ , E_z , H_ϕ , and H_z must be continuous. Using equation sets of Eqs. 13 and 14 for each region produces:

E_ϕ Continuous

$$\left[S_3 - S_4 \frac{S_1}{S_2} \right] \frac{A_1 \frac{mk}{\omega \epsilon_1 b} z}{\omega \epsilon_1 b} + \left[S'_3 - S'_4 \frac{S'_1}{S'_2} \right] B_1 k_{rl} - \left[S_5 - S_6 \frac{S_7}{S_8} \right] \frac{C_1 \frac{mk}{\omega \epsilon_2 b} z}{\omega \epsilon_2 b} - \left[S'_5 - S'_6 \frac{S'_7}{S'_8} \right] D_1 k_{r2} = 0 \quad (20)$$

E_z Continuous

$$\left[S_3 - S_4 \frac{S_1}{S_2} \right] \frac{A_1 k_{rl}^2}{\epsilon_1} - \left[S_5 - S_6 \frac{S_7}{S_8} \right] \frac{C_1 k_{r2}^2}{\epsilon_2} = 0 \quad (21)$$

H_ϕ Continuous

$$\begin{aligned} & - \left[S'_3 - S'_4 \frac{S_1}{S_2} \right] A_1 k_{rl} - \left[S_3 - S_4 \frac{S_1}{S_2} \right] \frac{B_1 \frac{mk}{\omega \mu_1 b} z}{\omega \mu_1 b} \\ & + \left[S'_5 - S'_6 \frac{S_7}{S_8} \right] C_1 k_{r2} + \left[S_5 - S_6 \frac{S_7}{S_8} \right] \frac{D_1 \frac{mk}{\omega \mu_2 b} z}{\omega \mu_2 b} = 0 \end{aligned} \quad (22)$$

H_z Continuous

$$\left[S_3 - S_4 \frac{S'_1}{S'_2} \right] \frac{B_1 k_{rl}^2}{\mu_1} - \left[S_5 - S_6 \frac{S'_7}{S'_8} \right] \frac{D_1 k_{r2}^2}{\mu_2} = 0 \quad (23)$$

To further simplify Eqs. 20 through 23, we define the following constants:

$$\begin{array}{ll}
G_1 = S_2 S_3 - S_1 S_4 & G_5 = S_5 S_8 - S_6 S_7 \\
G_2 = S'_2 S'_3 - S'_1 S'_4 & G_6 = S'_5 S'_8 - S'_6 S'_7 \\
G_3 = S_2 S'_3 - S_1 S'_4 & G_7 = S_5 S'_8 - S_6 S'_7 \\
G_4 = S'_2 S'_3 - S'_1 S'_4 & G_8 = S'_5 S'_8 - S'_6 S'_7
\end{array} \quad (24)$$

With the definition of Eq. 24, Eqs. 20 through 23 become

$$A_1 \frac{mG_1 k_z}{\omega \epsilon_1 b S_2} + B_1 \frac{G_4 k_{r1}}{S'_2} - C_1 \frac{mG_5 k_z}{\omega \epsilon_2 b S_8} - D_1 \frac{G_8 k_{r2}}{S'_8} = 0 \quad (25)$$

$$A_1 \frac{G_1 k_{r1}^2}{\epsilon_1 S_2} - C_1 \frac{G_5 k_{r2}^2}{\epsilon_2 S_8} = 0 \quad (26)$$

$$A_1 \frac{G_3 k_{r1}}{S_2} - B_1 \frac{mG_2 k_z}{\omega \mu_1 b S'_2} + C_1 \frac{G_6 k_{r2}}{S_8} + D_1 \frac{mG_7 k_z}{\omega \mu_2 b S'_8} = 0 \quad (27)$$

$$B_1 \frac{G_2 k_{r1}^2}{\mu_1 S'_2} - D_1 \frac{G_7 k_{r2}^2}{\mu_2 S'_8} = 0 \quad (28)$$

for E_ϕ , E_z , H_ϕ , and H_z , respectively. Based on Eqs. 25 through 28, the characteristic equation in determinantal form is

$$\begin{vmatrix}
 \underline{A_1} & \underline{B_1} & \underline{C_1} & \underline{D_1} \\
 0 & \frac{G_2 k_{rl}^2}{\mu_1' S_2'} & 0 & -\frac{G_7 k_{r2}^2}{\mu_2' S_8'} \\
 \frac{G_1 k_{rl}^2}{\epsilon_1' S_2'} & 0 & -\frac{G_5 k_{r2}^2}{\epsilon_2' S_8'} & 0 \\
 -\frac{G_3 k_{rl}}{S_2} & -\frac{m G_2 k_z}{\omega \mu_1' b S_2'} & \frac{G_6 k_{r2}}{S_8} & \frac{m G_7 k_z}{\omega \mu_2' b S_8'} \\
 \frac{m G_1 k_z}{\omega \epsilon_1' b S_2} & \frac{G_4 k_{rl}}{S_2'} & -\frac{m G_5 k_z}{\omega \epsilon_2' b S_8} & -\frac{G_8 k_{r2}}{S_8'} \\
 \end{vmatrix} = 0 \quad (29)$$

TM TE TM TE

This determinant represents solutions for hybrid modes and columns marked TM or TE denote the relative contributions to the hybridization. In general, the zeros of this determinant lie in the complex plane.

If we set $m = 0$, the determinant simplifies to

$$\begin{vmatrix}
 0 & \frac{G_2 k_{rl}^2}{\mu_1' S_2'} & 0 & \frac{G_7 k_{r2}^2}{\mu_2' S_8'} \\
 \frac{G_1 k_{rl}^2}{\epsilon_1' S_2'} & 0 & -\frac{G_5 k_{r2}^2}{\epsilon_2' S_8'} & 0 \\
 -\frac{G_3 k_{rl}}{S_2} & 0 & \frac{G_6 k_{r2}}{S_8} & 0 \\
 0 & \frac{G_4 k_{rl}}{S_2'} & 0 & -\frac{G_8 k_{r2}}{S_8'} \\
 \end{vmatrix} = 0 \quad (30)$$

Determinant Eq. 30 is the uncoupled version of Eq. 29 and it represents solutions to pure TE and TM modes. This is illustrated by interchanging the first and third rows of Eq. 30, producing

$$\begin{vmatrix} \Gamma_1 & 0 \\ 0 & \Gamma_2 \end{vmatrix} = 0$$

where

$$\Gamma_1 = \begin{vmatrix} -\frac{G_3 k_{r1}}{S_2} & \frac{G_6 k_{r2}}{S_8} \\ \frac{G_1 k_{r1}^2}{\epsilon_1 S_2} & -\frac{G_5 k_{r2}^2}{\epsilon_2 S_8} \end{vmatrix}$$

for TM modes, and

$$\Gamma_2 = \begin{vmatrix} \frac{G_2 k_{r1}^2}{\mu_1 S_2} & -\frac{G_7 k_{r2}^2}{\mu_2 S_8} \\ \frac{G_4 k_{r1}}{S_2} & -\frac{G_8 k_{r2}}{S_8} \end{vmatrix}$$

for TE modes.

2.2 Drawbacks

As dielectric layers are added to the profile, the increasing number of continuity conditions applied at each interface results in a dispersion determinant that grows as the square of the number of transitions. This drawback has two consequences. The first is that the dispersion determinant must be rederived for each new layer of dielectric added. The second is, obviously, the increasingly complex determinant for which a zero must be found.

The modal expansion approach is a technique where continuity of certain field components is applied at the boundary where the characteristics of the medium change abruptly. Cases where the dielectric is tapered continuously as a function of r cannot be handled by this formulation. Another drawback results from numerically approximating Bessel's function in a computer program. Problems arise when the arguments of the expansions used approach zero due to k_r approaching zero. Instabilities and/or numerical overflow result, placing restrictions on investigating modes which are in transition between the fast and slow wave regions of the structure. Due to the above mentioned problems, we could not analyze the dielectric loaded coaxial waveguide successfully. This led us to develop the technique described in the next chapter.

III. DIRECT INTEGRATION OF MAXWELL'S EQUATIONS

This chapter will lay the foundations used to calculate the electromagnetic dispersion of a coaxial waveguide with an arbitrary radial dielectric profile. Starting with Maxwell's equations,³ Section 3.1 will develop a coupled second order differential equation system in the radial coordinate. The propagation constant sought, k_z , is found by integrating this system of differential equations at a given frequency (ω) and azimuthal eigenvalue (m). Integration is performed using a "shooting" method, where the shooting parameter, k_z , is varied until certain boundary conditions are satisfied. Section 3.2 discusses the initial and boundary conditions used in the integration. For discontinuous dielectric profiles, Section 3.3 formulates the jump conditions for the equations. The equations for the field components, which are directly obtained from the solutions to the integration, are given in Section 3.4. The normalization of the field components and computation of orthogonality are discussed in Section 3.5. Finally, in Section 3.6, the equations are transformed into a format suitable for numerical integration. We note that boldface type will represent vector quantities.

3.1 Derivation of the Differential Equation Systems

The general Maxwell's equations for a region free of charges and currents ($\rho = 0$, $\mathbf{J} = 0$) are

$$\nabla \cdot \mathbf{E} = 0 \quad (31a)$$

$$\nabla \cdot \mathbf{B} = 0 \quad (32a)$$

$$\nabla \times \mathbf{H} = \frac{\partial \mathbf{D}}{\partial t} \quad (33a)$$

$$\nabla \times \mathbf{E} = -\frac{\partial \mathbf{B}}{\partial t} \quad (34a)$$

For linear dielectric media, the following relation holds:

$$\mathbf{D} = \epsilon \mathbf{E} \quad (35)$$

The formulation will be limited to the case where $\mu = \mu_0$ (μ_0 is the permeability of vacuum):

$$\mathbf{B} = \mu_0 \mathbf{H} \quad (36)$$

Assuming harmonic variation and uniform propagation in the $+z$ direction, $e^{j(\omega t - k_z z)}$, Eqs. 31a through 34a become

$$\nabla \cdot \mathbf{D} = 0 \quad (31b)$$

$$\nabla \cdot \mathbf{H} = 0 \quad (32b)$$

$$\nabla \times \mathbf{H} = j\omega \mathbf{D} \quad (33b)$$

$$\nabla \times \mathbf{E} = -j\omega \mu_0 \mathbf{H} \quad (34b)$$

where Eq. 36 was used in Eq. 34b for \mathbf{B} . Rewriting Eqs. 31b through 34b in cylindrical coordinates yields

$$\frac{\partial D_r}{\partial r} + \frac{1}{r} \frac{\partial D_\phi}{\partial \phi} + \frac{\partial D_z}{\partial z} + \frac{D_r}{r} = 0 \quad (31c)$$

$$\frac{\partial H_r}{\partial r} + \frac{1}{r} \frac{\partial H_\phi}{\partial \phi} + \frac{\partial H_z}{\partial z} + \frac{H_r}{r} = 0 \quad (32c)$$

$$\frac{1}{r} \frac{\partial H_z}{\partial \phi} - \frac{\partial H_\phi}{\partial z} - j\omega D_r = 0 \quad (33c-r)$$

$$- \frac{\partial H_z}{\partial r} + \frac{\partial H_r}{\partial z} - j\omega D_\phi = 0 \quad (33c-\phi)$$

$$\frac{\partial H_\phi}{\partial r} - \frac{1}{r} \frac{\partial H_r}{\partial \phi} + \frac{H_\phi}{r} - j\omega D_z = 0 \quad (33c-z)$$

$$\frac{1}{r} \frac{\partial E_z}{\partial \phi} - \frac{\partial E_\phi}{\partial z} + j\omega \mu_0 H_r = 0 \quad (34c-r)$$

$$- \frac{\partial E_z}{\partial r} + \frac{\partial E_r}{\partial z} + j\omega \mu_0 H_\phi = 0 \quad (34c-\phi)$$

$$\frac{\partial E_\phi}{\partial r} - \frac{1}{r} \frac{\partial E_r}{\partial \phi} + \frac{\partial_\phi}{r} + j\omega \mu_0 H_z = 0 \quad (34c-z)$$

The following polarization is chosen for the ϕ dependence:

$$D_r(r, \phi) \rightarrow D_r(r) \cos(m\phi) \quad (37a)$$

$$E_r(r, \phi) \rightarrow E_r(r) \cos(m\phi) \quad (37b)$$

$$D_\phi(r, \phi) \rightarrow D_\phi(r) \sin(m\phi) \quad (37c)$$

$$E_\phi(r, \phi) \rightarrow E_\phi(r) \sin(m\phi) \quad (37d)$$

$$D_z(r, \phi) \rightarrow D_z(r) \cos(m\phi) \quad (37e)$$

$$E_z(r, \phi) \rightarrow E_z(r) \cos(m\phi) \quad (37f)$$

$$H_r(r, \phi) \rightarrow H_r(r) \sin(m\phi) \quad (37g)$$

$$H_\phi(r, \phi) + H_\phi(r) \cos(m\phi) \quad (37h)$$

$$H_z(r, \phi) + H_z(r) \sin(m\phi) \quad (37i)$$

Using this polarization in Eqs. 31c through 34c-z and canceling common cosine and sine terms gives

$$\frac{\partial D_r}{\partial r} + \frac{mD_\phi}{r} - jk_z D_z + \frac{D_r}{r} = 0 \quad (31d)$$

$$\frac{\partial H_r}{\partial r} + \frac{mH_\phi}{r} - jk_z H_z + \frac{H_r}{r} = 0 \quad (32d)$$

$$\frac{mH_z}{r} + jk_z H_\phi - j\omega D_r = 0 \quad (33d-r)$$

$$- \frac{\partial H_z}{\partial r} - jk_z H_r - j\omega D_\phi = 0 \quad (33d-\phi)$$

$$\frac{\partial H_\phi}{\partial r} - \frac{mH_r}{r} + \frac{H_\phi}{r} - j\omega D_z = 0 \quad (33d-z)$$

$$- \frac{mE_z}{r} + jk_z E_\phi + j\omega \mu_0 H_r = 0 \quad (34d-r)$$

$$- \frac{\partial E_z}{\partial r} - jk_z E_r + j\omega \mu_0 H_\phi = 0 \quad (34d-\phi)$$

$$\frac{\partial E_\phi}{\partial r} + \frac{mE_r}{r} + \frac{E_\phi}{r} + j\omega \mu_0 H_z = 0 \quad (34d-z)$$

Equations 31d through 34d-z will provide the basis for determining a system of second order linear differential equations. Before proceeding, we further assume that ϵ is a function of the r coordinate only.

We begin by solving Eq. 34c- ϕ for $\frac{\partial E_z}{\partial r}$ and then using the constitutive relation (Eq. 35) to generate $\frac{\partial D_z}{\partial r}$, which yields

$$\frac{\partial D_z}{\partial r} - E_z \frac{\partial \epsilon}{\partial r} - j\omega\mu_0 \epsilon H_\phi + jk_z D_z = 0 \quad (38)$$

If we solve Eq. 31d for jD_z and then take the radial derivative, we have

$$\frac{\partial(jD_z)}{\partial r} = \left[\frac{\partial^2 D_r}{\partial r^2} + \frac{1}{r} \frac{\partial D_r}{\partial r} - \frac{D_r}{r^2} + \frac{m\epsilon}{r} \frac{\partial E_\phi}{\partial r} + \frac{mE_\phi}{r} \frac{\partial \epsilon}{\partial r} - \frac{m\epsilon E_\phi}{r^2} \right] \frac{1}{k_z} \quad (39)$$

where the constitutive relationship for D_ϕ was used. By taking Eq. 39 and substituting for $\frac{\partial D_z}{\partial r}$ in Eq. 38, we can solve for $\frac{\partial^2 D_r}{\partial r^2}$,

$$\frac{\partial^2 D_r}{\partial r^2} = -\frac{1}{r} \frac{\partial D_r}{\partial r} + \frac{D_r}{r^2} - \frac{m\epsilon}{r} \frac{\partial E_\phi}{\partial r} - \frac{mE_\phi}{r} \frac{\partial \epsilon}{\partial r} + \frac{m\epsilon E_\phi}{r^2} + jk_z E_z \frac{\partial \epsilon}{\partial r} - \omega\mu_0 \epsilon k_z H_\phi + k_z^2 D_r \quad (40)$$

In order to put Eq. 40 into a form involving only electric field components and their derivatives, we substitute for H_ϕ and H_z from Eqs. 33d-r and 34d-z, respectively,

$$\frac{\partial^2 D_r}{\partial r^2} = D_r \left[k_z^2 - k^2 + \frac{m^2 + 1}{r^2} + \frac{1}{r} \frac{\partial(\ln \epsilon)}{\partial r} \right] + \frac{\partial D_r}{\partial r} \left[\frac{\partial(\ln \epsilon)}{\partial r} - \frac{1}{r} \right] + \frac{2m\epsilon E_\phi}{r^2} \quad (41)$$

where the following relations were used:

$$\frac{\partial(\ln\epsilon)}{\partial r} = \frac{1}{r} \frac{\partial\epsilon}{\partial r} \quad (42)$$

$$k^2 = \omega^2 \mu_0 \epsilon \quad (43)$$

Equation 41 represents the first half of our differential equation system.

To generate the other half of our differential equation system, we take the radial derivative of Eq. 34d-z and solve for $\frac{\partial^2 E_\phi}{\partial r^2}$:

$$\begin{aligned} \frac{\partial^2 E_\phi}{\partial r^2} = & -\frac{m}{r\epsilon} \frac{\partial D_r}{\partial r} + \frac{mD_r}{r^2\epsilon} - \frac{1}{\epsilon} \frac{\partial\epsilon}{\partial r} \frac{\partial E_\phi}{\partial r} - \frac{1}{r} \frac{\partial E_\phi}{\partial r} - \frac{E_\phi}{r\epsilon} \frac{\partial\epsilon}{\partial r} + \frac{E_\phi}{r^2} \\ & - j\omega\mu_0 \frac{\partial H_z}{\partial r} - \frac{j\omega\mu_0 H_z}{\epsilon} \frac{\partial\epsilon}{\partial r} \end{aligned} \quad (44)$$

where the constitutive relation for E_r was used. Using Eqs. 33d- ϕ and 34d-z, a solution for $\frac{\partial H_z}{\partial r}$ as a function of E_ϕ and E_z is obtained. Substituting $\frac{\partial H_z}{\partial r}$ into Eq. 44 yields

$$\begin{aligned} \frac{\partial^2 E_\phi}{\partial r^2} = & E_\phi \left[k_z^2 - k^2 + \frac{1}{r^2} - \frac{1}{r} \frac{\partial(\ln\epsilon)}{\partial r} \right] - \frac{\partial E_\phi}{\partial r} \left[\frac{\partial(\ln\epsilon)}{\partial r} + \frac{1}{r} \right] \\ & - \frac{m}{r\epsilon} \frac{\partial D_r}{\partial r} + \frac{mD_r}{r^2\epsilon} + \frac{jmk_z D_z}{r\epsilon} - j\omega\mu_0 H_z \frac{\partial(\ln\epsilon)}{\partial r} \end{aligned} \quad (45)$$

where Eqs. 42 and 43 were again used. Equation 45 is finally put into a form involving only electric field components by substituting for D_z and H_z from Eqs. 31d and 34d-z, respectively:

$$\frac{\partial^2 E_\phi}{\partial r^2} = E_\phi \left[k_z^2 - k^2 + \frac{m^2 + 1}{r^2} \right] - \frac{1}{r} \frac{\partial E_\phi}{\partial r} + \frac{mD_r}{r^2\epsilon} \left[\frac{2}{r} + \frac{\partial(\ln\epsilon)}{\partial r} \right] \quad (46)$$

Equation 46 completes the formulation of the differential equation system.

Upon normalizing Eq. 41 by dividing by ϵ_0 (permittivity of vacuum) in order to have consistent units with Eq. 46, the second order differential equation system is

$$\frac{\partial^2 D_r}{\partial r^2} \frac{1}{\epsilon_0} = \frac{D_r}{\epsilon_0} \left[k_z^2 - k^2 + \frac{m^2 + 1}{r^2} + \frac{1}{r} \frac{\partial(\ln\epsilon)}{\partial r} \right] + \frac{1}{\epsilon_0} \frac{\partial D_r}{\partial r} \left[\frac{\partial(\ln\epsilon)}{\partial r} - \frac{1}{r} \right] + \frac{2meE_\phi}{r^2} \quad (47a)$$

$$\frac{\partial^2 E_\phi}{\partial r^2} = E_\phi \left[k_z^2 - k^2 + \frac{m^2 + 1}{r^2} \right] = \frac{1}{r} \frac{\partial E_\phi}{\partial r} + \frac{mD_r}{r\epsilon} \left[\frac{2}{r} + \frac{\partial(\ln\epsilon)}{\partial r} \right] \quad (47b)$$

where $\epsilon = \epsilon_0 \epsilon_r$ (ϵ_r is the relative dielectric permittivity). Equation 47 is used to find the propagation constant, k_z , for the $TE_{m,n}$ and $TM_{m,n}$ modes as well as the "TE_{m,n} like" ($HE_{m,n}$) and "TM_{m,n} like" ($EH_{m,n}$) modes. For the special case of $m = 0$, Eq. 47 becomes

$$\frac{\partial^2 D_r}{\partial r^2} \frac{1}{\epsilon_0} = \frac{D_r}{\epsilon_0} \left[k_z^2 - k^2 + \frac{1}{r^2} + \frac{1}{r} \frac{\partial(\ln\epsilon)}{\partial r} \right] + \frac{1}{\epsilon_0} \frac{\partial D_r}{\partial r} \left[\frac{\partial(\ln\epsilon)}{\partial r} - \frac{1}{r} \right] \quad (48a)$$

$$\frac{\partial^2 E_\phi}{\partial r^2} = E_\phi \left[k_z^2 - k^2 + \frac{1}{r^2} \right] - \frac{1}{r} \frac{\partial E_\phi}{\partial r} \quad (48b)$$

Equation 48 is the uncoupled form of Eq. 47, with Eq. 48a applying to $TM_{0,n}$ and TEM modes, and Eq. 48b applying to $TE_{0,n}$ modes. It is interesting to note the analogous relationship between Eqs. 47 and 48 and the dispersion determinants of Eq. 29 and 30.

3.2 Initial and Boundary Conditions

For $TE_{0,n}$, $TM_{0,n}$, and TEM modes, a one-dimensional "shooting" method is used, with k_z being the shooting parameter. However, " $TE_{m,n}$ like" and " $TM_{m,n}$ like" modes require a two-dimensional "shooting" method. The shooting parameters here are k_z and the dimensionless parameter α , which we define as

$$\alpha \equiv \frac{jH_z}{c_0 D_r} \quad (49)$$

at $r = a$ and c_0 = speed of light in vacuum. The degree to which a mode has characteristic TE behavior (H_z component dominant) or characteristic TM behavior (E_z component dominant) is represented by α . The initial magnitude of α points the integration in the direction of an $HE_{m,n}$ or $EH_{m,n}$ mode when a nonuniform dielectric is present. When the boundary conditions are satisfied, the final magnitude of α describes the degree of actual hybridization. There are two limiting cases for α which occur when a nonuniform dielectric profile approaches a uniform profile:

$$|\alpha| \rightarrow 0$$

as pure TM modes are approached, and

$$|\alpha| \sim 10$$

as pure TE modes are approached.

Integration of Eqs. 47 and 48 requires the value of a given field component and its derivative with respect to the radial coordinate at the inner conductor of Fig. 3A ($r = a$). The tangential electric field components must satisfy the boundary condition

$$E_\phi = 0 \quad (50a)$$

$$E_z = 0 \quad (50b)$$

at $r = a$ and $r = c$, respectively. Using this result in Eq. 31d and 34d- z yields

$$\frac{\partial D_r}{\partial r} + \frac{D_r}{r} = 0 \quad (51)$$

$$\frac{\partial E_\phi}{\partial r} = - \left[\frac{mE_r}{r} + j\omega\mu_0 H_z \right] \quad (52)$$

Using Eqs. 49 and the constitutive relation for E_r , Eq. 52 becomes

$$\frac{\partial E_\phi}{\partial r} = - \left[\frac{\omega\epsilon_r a}{c_0} + \frac{m}{r} \right] \frac{D_r}{\epsilon} \quad (53)$$

Summarizing the initial conditions for uniform and nonuniform dielectric profiles:

1. Equations 50b and 51 are used for the $TM_{0,n}$ and TEM modes.
2. Equation 50a is used for $TE_{0,n}$ modes.
3. Equations 50, 51, and 53 are used for $TE_{m,n}$ ($HE_{m,n}$) and $TM_{m,n}$ ($EH_{m,n}$) modes.

As mentioned, the "shooting" method varies the shooting parameters until the boundary condition at $r = c$ is satisfied. For $TM_{0,n}$ and TEM modes, Eq. 50b must be satisfied, while $TE_{0,n}$ modes require Eq. 50a to be satisfied. Finally, Eqs. 50a and 50b are combined to form the boundary condition for $TE_{m,n}$ ($HE_{m,n}$) and $TM_{m,n}$ ($EH_{m,n}$) modes:

$$\sqrt{E_z^2 + E_\phi^2} = 0 \quad (54)$$

We note that for the two-dimensional shooting, k_z enters only in the differential equations and does not appear in the initial or boundary conditions. Conversely, α enters only in the initial conditions and does not appear in the differential equations.

3.3 Discontinuous Dielectric Profile Formulation

When discontinuities in the dielectric profile are present, as in Fig. 3A, integration of Eqs. 47 or 48 cannot proceed past a discontinuous point unless expressions for $\frac{\partial D_r}{\partial r}$ and $\frac{\partial E_\phi}{\partial r}$ can be developed.

At the dielectric interface of Fig. 3A, the following field components are continuous:

$$D_r^{[1]} = D_r^{[2]} \quad (55a)$$

$$E_\phi^{[1]} = E_\phi^{[2]} \quad (55b)$$

$$E_z^{[1]} = E_z^{[2]} \quad (55c)$$

$$H_{\phi}^{[1]} = H_{\phi}^{[2]} \quad (55d)$$

$$H_z^{[1]} = H_z^{[2]} \quad (55e)$$

where superscripts 1 and 2 denote the dielectric regions. Substituting for $E_z^{[1]}$ and $E_z^{[2]}$, using Eq. 31d, we generate Eq. 56 from Eq. 55c,

$$\left[\frac{\partial D_r^{[1]}}{\partial r} + \frac{D_r^{[1]}}{r} + \frac{m\epsilon_1 E_{\phi}^{[1]}}{r} \right] \frac{1}{\epsilon_1} = \left[\frac{\partial D_r^{[2]}}{\partial r} + \frac{D_r^{[2]}}{r} + \frac{m\epsilon_2 E_{\phi}^{[2]}}{r} \right] \frac{1}{\epsilon_2} \quad (56)$$

where ϵ_1 and ϵ_2 represent the dielectric permittivities of regions 1 and 2, respectively. Solving Eq. 56 for $\partial D_r^{[2]}/\partial r$,

$$\frac{\partial D_r^{[2]}}{\partial r} = \frac{\epsilon_2}{\epsilon_1} \frac{\partial D_r^{[1]}}{\partial r} + \left[\frac{\epsilon_2}{\epsilon_1} - 1 \right] \frac{D_r^{[1]}}{r} \quad (57)$$

Similarly, we substitute for $H_z^{[1]}$ and $H_z^{[2]}$, using Eq. 34d-z into Eq. 55e,

$$\left[\frac{\partial E_{\phi}^{[1]}}{\partial r} + \frac{E_{\phi}^{[1]}}{r} \right] \frac{1}{\omega\mu_0} + \frac{mD_r^{[1]}}{r\epsilon_1} = \left[\frac{\partial E_{\phi}^{[2]}}{\partial r} + \frac{E_{\phi}^{[2]}}{r} \right] \frac{1}{\omega\mu_0} + \frac{mD_r^{[2]}}{r\epsilon_2} \quad (58)$$

Solving Eq. 58 for $\frac{\partial E_{\phi}^{[2]}}{\partial r}$,

$$\frac{\partial E_{\phi}^{[2]}}{\partial r} = \frac{\partial E_{\phi}^{[1]}}{\partial r} + \left[\frac{\epsilon_2}{\epsilon_1} - 1 \right] \frac{mD_r^{[1]}}{r\epsilon_2} \quad (59)$$

For the special case of $m = 0$, Eq. 59 becomes

$$\frac{\partial E_{\phi}^{[2]}}{\partial r} = \frac{\partial E_{\phi}^{[1]}}{\partial r} \quad (60)$$

Summarizing Eqs. 57, 59, and 60 for reference (Eq. 57 is divided by ϵ_0),

$$\frac{\partial D_r^{[2]}}{\partial r} \frac{1}{\epsilon_0} = \frac{\epsilon_2}{\epsilon_0 \epsilon_1} * \frac{\partial D_r^{[1]}}{\partial r} + \left[\frac{\epsilon_2}{\epsilon_1} - 1 \right] \frac{D_r^{[1]}}{\epsilon_0 r} \quad (61a)$$

$$\frac{\partial E_{\phi}^{[2]}}{\partial r} = \frac{\partial E_{\phi}^{[1]}}{\partial r} + \left[\frac{\epsilon_2}{\epsilon_1} - 1 \right] \frac{m D_r^{[1]}}{r \epsilon_2} \quad (61b)$$

Equation 61 is used for $TE_{m,n}$ ($HE_{m,n}$) and $TM_{m,n}$ ($EH_{m,n}$) modes.

$$\frac{\partial D_r^{[2]}}{\partial r} \frac{1}{\epsilon_0} = \frac{\epsilon_2}{\epsilon_0 \epsilon_1} \frac{\partial D_r^{[1]}}{\partial r} + \left[\frac{\epsilon_2}{\epsilon_1} - 1 \right] \frac{D_r^{[1]}}{\epsilon_0 r} \quad (62)$$

Equation 62 is used for $TM_{0,n}$ and TEM modes.

$$\frac{\partial E_{\phi}^{[2]}}{\partial r} = \frac{\partial E_{\phi}^{[1]}}{\partial R} \quad (63)$$

Equation 63 is used for $TE_{0,n}$ modes.

3.4 Field Equations

The following field components may be computed once the parameters $\frac{D_r}{\epsilon_0}$, E_{ϕ} , $\frac{1}{\epsilon_0} \frac{\partial D_r}{\partial r}$, and $\frac{\partial E_{\phi}}{\partial r}$ have been determined. Equations 31d, 34d-z, 34d-r, and 33d-r are used to derive Eqs. 64 through 67, respectively,

$$jD_z = \left[\frac{\partial D_r}{\partial r} + \frac{D_r}{r} + \frac{m \epsilon E_{\phi}}{r} \right] \frac{1}{k_z} \quad (64)$$

$$jH_z = - \left[\frac{\partial E_\phi}{\partial r} + \frac{E_\phi}{r} + \frac{mD_r}{r\epsilon} \right] \frac{1}{\omega\mu_0} \quad (65)$$

$$H_r = \left[\frac{jmE_z}{r} + k_z E_\phi \right] \frac{1}{\omega\mu_0} \quad (66)$$

$$H_\phi = \frac{jmH_z}{r} + \omega D_r \frac{1}{k_z} \quad (67)$$

3.5 Normalization and Orthogonality Relations

Once computed, all field components are normalized with respect to Poynting's vector taken over the cross-sectional area of the waveguide:

$$\begin{aligned} \delta_{l,k} &\equiv \int_0^{2\pi} \int_a^c \mathbf{E}_l \times \mathbf{H}_k^* \cdot d\mathbf{A} \\ &= \int_0^{2\pi} \int_a^c \mathbf{E}_l \times \mathbf{H}_k^* \cdot \hat{\mathbf{n}} d\mathbf{A} \\ &= \int_0^{2\pi} \int_a^c [E_{r,l}^* H_{r,k}^* - E_{\phi,l}^* H_{\phi,k}^*] r dr d\phi \end{aligned} \quad (68)$$

where

$\delta_{l,k}$ = Kronecker delta function

$d\mathbf{A} = r dr d\phi$

$\hat{\mathbf{n}}$ = unit vector normal to $d\mathbf{A}$ in $+z$ direction

Normalization for a given mode requires computing Eq. 68 with $l = k$ using the unnormalized fields, taking the square root of the absolute value and dividing each component by the result.

Orthogonality between two given modes l and k ($l \neq k$) is an important condition that must be satisfied in order to have any confidence in the solutions for $k_{z,l}$ and $k_{z,k}$. Equation 68 is used to evaluate the orthogonality between the normalized modes l and k . Due to the normalization, Eq. 68 gives the value of 1 when self orthogonality is computer ($l = k$).

3.6 Form for Numerical Integration

Integration of Eqs. 47 and 48 is facilitated if they are transformed into a dimensionless form. We define the following normalization:

$$r_0 = \frac{r}{a} \quad (69a)$$

where

$$a < r < c$$

As a consequence of Eq. 69a, we have

$$\frac{\partial}{\partial r_{0d}} = \frac{\partial}{\partial \left[\frac{r}{a} \right]} = a \frac{\partial}{\partial r} \quad (69b)$$

Using Eq. 69, Eq. 47 becomes

$$\frac{\partial^2 D_r}{\partial(r_0)^2} \frac{1}{\epsilon_0} = \frac{D_r}{\epsilon_0} \left[(k_z^2 - k^2) a^2 + \frac{m^2 + 1}{r_0^2} + \frac{1}{r_0} \frac{\partial(\ln\epsilon)}{\partial r_0} \right] + \frac{1}{\epsilon_0} \frac{\partial D_r}{\partial r_0} \left[\frac{\partial(\ln\epsilon)}{r_0} - \frac{1}{r_0} \right] + \frac{2m\epsilon E_\phi}{r_0^2} \quad (70a)$$

$$\frac{\partial^2 E_\phi}{\partial(r_0)^2} = E_\phi \left[(k_z^2 - k^2) a^2 + \frac{m^2 + 1}{r_0^2} \right] - \frac{1}{r_0} \frac{\partial E_\phi}{\partial r_0} + \frac{m D_r}{r_0 \epsilon} \left[\frac{2}{r_0} + \frac{\partial(\ln\epsilon)}{\partial r_0} \right] \quad (70b)$$

Similarly for Eq. 48, we have

$$\frac{\partial^2 D_r}{\partial(r_0)^2} \frac{1}{\epsilon_0} = \frac{D_r}{\epsilon_0} \left[(k_z^2 - k^2) a^2 + \frac{1}{r_0^2} + \frac{1}{r_0} \frac{\partial(\ln\epsilon)}{\partial r_0} \right] + \frac{1}{\epsilon_0} \frac{\partial D_r}{\partial r_0} \left[\frac{\partial(\ln\epsilon)}{r_0} - \frac{1}{r_0} \right] \quad (71a)$$

$$\frac{\partial^2 E_\phi}{\partial(r_0)^2} = E_\phi \left[(k_z^2 - k^2) a^2 + \frac{1}{r_0^2} \right] - \frac{1}{r_0} \frac{\partial E_\phi}{\partial r_0} \quad (71b)$$

Equations 70 and 71 are dimensionless.

The jump discontinuity equations, Eq. 61, 62, and 63, are also put into dimensionless form, since they are used in the integration process:

$$\frac{\partial D_r^{[2]}}{\partial r_0} \frac{1}{\epsilon_0} = \frac{\epsilon_2}{\epsilon_0 \epsilon_1} \frac{\partial D_r^{[1]}}{\partial r_0} + \left[\frac{\epsilon_2}{\epsilon_1} - 1 \right] \frac{D_r^{[1]}}{\epsilon_0 r_0} \quad (72a)$$

$$\frac{\partial E_{\phi}^{[2]}}{\partial r_0} = \frac{\partial E_{\phi}^{[1]}}{\partial r_0} + \left[\frac{\epsilon_2}{\epsilon_1} - 1 \right] \frac{mD_r^{[1]}}{r_0 \epsilon_2} \quad (72b)$$

$$\frac{\partial D_r^{[2]}}{\partial r_0} \frac{1}{\epsilon_0} = \frac{\epsilon_2}{\epsilon_0 \epsilon_1} \frac{\partial D_r^{[1]}}{\partial r_0} + \left[\frac{\epsilon_2}{\epsilon_1} - 1 \right] \frac{D_r^{[1]}}{\epsilon_0 r_0} \quad (73)$$

$$\frac{\partial E_{\phi}^{[2]}}{\partial r_0} = \frac{\partial E_{\phi}^{[1]}}{\partial r_0} \quad (74)$$

The IMSL routine DGEAR (see Appendix A.1) is used to integrate Eqs. 70 and 71. But DGEAR requires a first order linear differential equation system. To accomodate DGEAR, Eqs. 70 and 71 must be transformed into a first order linear differential equation system.

For $TE_{m,n}$ ($HE_{m,n}$) and $TM_{m,n}$ ($EH_{m,n}$) modes, we define the following variables:

$$Y_1 = \frac{\partial D_r}{\partial r_0} \frac{1}{\epsilon_0} \quad (75a)$$

$$Y_2 = \frac{\partial E_{\phi}}{\partial r_0} \quad (75b)$$

$$Y_3 = \frac{D_r}{\epsilon_0} \quad (75c)$$

$$Y_4 = E_{\phi} \quad (75d)$$

and

$$Y'_1 = \frac{\partial Y_1}{\partial r_0} \quad (76a)$$

$$Y'_2 = \frac{\partial Y_2}{\partial r_0} \quad (76b)$$

$$Y'_3 = Y_1 \quad (76c)$$

$$Y'_4 = Y_2 \quad (76d)$$

where the prime denotes the derivative with respect to the normalized radial coordinate. With the aid of Eqs. 75 and 76, Eq. 70 becomes

$$Y'_1 = Y_3 \left[(k_z^2 - k^2) a^2 + \frac{m^2 + 1}{r_0^2} + \frac{1}{r_0} \frac{\partial(\ln\epsilon)}{\partial r_0} \right] + Y_1 \left[\frac{\partial(\ln\epsilon)}{\partial r_0} - \frac{1}{r_0} \right] + \frac{2m\epsilon Y_4}{r_0^2} \quad (77a)$$

$$Y'_2 = Y_4 \left[(k_z^2 - k^2) a^2 + \frac{m^2 + 1}{r_0^2} \right] - \frac{Y_2}{r_0} + \frac{mY_3}{r_0\epsilon} \left[\frac{2}{r_0} + \frac{\partial(\ln\epsilon)}{\partial r_0} \right] \quad (77b)$$

$$Y'_3 = Y_1 \quad (77c)$$

$$Y'_4 = Y_2 \quad (77d)$$

Equation 77 constitutes the first order differential equation system which is integrated by DGEAR.

Similarly, for $TM_{0,n}$ and TEM modes, we define

$$Y_1 = \frac{\partial D_r}{\partial r_0} \frac{1}{\epsilon_0} \quad (78a)$$

$$Y_2 = \frac{D_r}{\epsilon_0} \quad (78b)$$

$$Y'_1 = \frac{\partial Y_1}{\partial r_0} \quad (79a)$$

$$Y'_2 = Y_1 \quad (79b)$$

With the definition of Eqs. 78 and 79, Eq. 71a is transformed:

$$Y'_1 = Y_2 \left[(k_z^2 - k^2) a^2 + \frac{1}{r_0^2} + \frac{1}{r_0} \frac{\partial(\ln\epsilon)}{\partial r_0} \right] \\ + Y_1 \left[\frac{\partial(\ln\epsilon)}{\partial r_0} - \frac{1}{r_0} \right] \quad (80a)$$

$$Y'_2 = Y_1 \quad (80b)$$

Finally, for $TE_{0,n}$ modes, we define

$$Y_1 = \frac{\partial E_\phi}{\partial r_0} \quad (81a)$$

$$Y_2 = E_\phi \quad (81b)$$

$$Y'_1 = \frac{\partial Y_1}{\partial r_0} \quad (82a)$$

$$Y'_2 = Y_1 \quad (82b)$$

Transforming Eq. 71b using Eqs. 81 and 82,

$$Y'_1 = Y_2 \left[(k_z^2 - k^2) a^2 + \frac{1}{r_0^2} \right] - \frac{Y_1}{r_0} \quad (83a)$$

$$Y'_2 = Y_1 \quad (83b)$$

Equations 80 and 83 represent first order linear differential equation systems integrated by DGEAR.

Another requirement for DGEAR is a system of partial derivatives $PD_{i,j}$ defined as the partial derivative of Y'_i with respect to Y_j . In light of this definition, Eq. 77 generates

$$PD_{1,1} = \frac{\partial(\ln \epsilon)}{\partial r_0} - \frac{1}{r_0} \quad (84a)$$

$$PD_{1,2} = 0 \quad (84b)$$

$$PD_{1,3} = [k_z^2 - k^2] a^2 + \frac{m^2 + 1}{r_0^2} + \frac{1}{r_0} \frac{\partial(\ln \epsilon)}{\partial r_0} \quad (84c)$$

$$PD_{1,4} = \frac{2m\epsilon}{r_0^2} \quad (84d)$$

$$PD_{2,1} = 0 \quad (84e)$$

$$PD_{2,2} = -\frac{1}{r_0} \quad (84f)$$

$$PD_{2,3} = \left[\frac{2}{r_0} + \frac{\partial(\ln \epsilon)}{\partial r_0} \right] \frac{m}{r_0 \epsilon} \quad (84g)$$

$$PD_{2,4} = [k_z^2 - k^2] a^2 + \frac{m^2 + 1}{r_0^2} \quad (84h)$$

$$PD_{3,1} = 1 \quad (84i)$$

$$PD_{3,2} = 0 \quad (84j)$$

$$PD_{3,3} = 0 \quad (84k)$$

$$PD_{3,4} = 0 \quad (84l)$$

$$PD_{4,1} = 0 \quad (84m)$$

$$PD_{4,2} = 1 \quad (84n)$$

$$PD_{4,3} = 0 \quad (84o)$$

$$PD_{4,4} = 0 \quad (84p)$$

Equation 84 represents the partial derivative system for $TE_{m,n}$ ($HE_{m,n}$) and $TM_{m,n}$ ($HE_{m,n}$) modes. Repeating the process for $TM_{0,n}$ and TEM modes, Eq. 80 produces the partial derivative system,

$$PD_{1,1} = \frac{\partial(\ln\epsilon)}{\partial r_0} - \frac{1}{r_0} \quad (85a)$$

$$PD_{1,2} = [k_z^2 - k^2] a^2 + \frac{1}{r_0^2} + \frac{1}{r_0} \frac{\partial(\ln\epsilon)}{\partial r_0} \quad (85b)$$

$$PD_{2,1} = 1 \quad (85c)$$

$$PD_{2,2} = 0 \quad (85d)$$

Similarly for $TE_{0,n}$ modes, Eq. 83 produces the partial derivative system,

$$PD_{1,1} = \frac{1}{r_0} \quad (86a)$$

$$PD_{1,2} = [k_z^2 - k^2] a^2 + \frac{1}{r_0^2} \quad (86b)$$

$$PD_{2,1} = 1 \quad (86c)$$

$$PD_{2,2} = 0 \quad (86d)$$

With the first order differential equation and partial derivative equation systems constructed, we now turn our attention to initial and boundary conditions. In each case to follow, we are free to choose the value of one variable, since it affects only the magnitude of the results.

Choosing $\frac{D_r}{\epsilon_0} = 1$ coupled with the aid of Eqs. 50, 51, and 53, Eq. 75 yields the initial conditions for $TE_{m,n}$ ($HE_{m,n}$) and $TM_{m,n}$ ($EH_{m,n}$) modes,

$$Y_1 = -1 \quad (87a)$$

$$Y_2 = - \left[\frac{\omega \epsilon_r \alpha a}{c_0} + \frac{m}{r_0} \right] \frac{1}{\epsilon_r} \quad (87b)$$

$$Y_3 = 1 \quad (87c)$$

$$Y_4 = 0 \quad (87d)$$

where ϵ_r is the relative permittivity at the boundary (Fig. 3). The corresponding unnormalized field components are

$$\frac{\partial D_r}{\partial r} = \frac{Y_1 \epsilon_0}{a} \quad (88a)$$

$$\frac{\partial E_\phi}{\partial r} = \frac{Y_2}{a} \quad (88b)$$

$$D_r = Y_3 \epsilon_0 \quad (88c)$$

$$E_\phi = 0 \quad (88d)$$

For $TM_{0,n}$ and TEM modes, we again choose $\frac{D_r}{\epsilon_0} = 1$ and use Eqs. 50b and 51 from which Eq. 78 yields

$$Y_1 = -1 \quad (89a)$$

$$Y_2 = 1 \quad (89b)$$

The corresponding unnormalized field components are

$$\frac{\partial D_r}{\partial r} = \frac{Y_1 \epsilon_0}{a} \quad (90a)$$

$$D_r = Y_2 \epsilon_0 \quad (90b)$$

Finally, for $TE_{0,n}$ modes, we choose $\frac{\partial E_\phi}{\partial r} = 1$ and the use of Eq. 50a from which Eq. 81 yields

$$Y_1 = 1 \quad (91a)$$

$$Y_2 = 0 \quad (91b)$$

The corresponding unnormalized field components are

$$\frac{\partial E_\phi}{\partial r} = \frac{Y_1}{a} \quad (92a)$$

$$E_\phi = 0 \quad (92b)$$

The boundary conditions that must be satisfied at $r = c$ in the shooting method are taken from Eqs. 50 and 51. For $TM_{0,n}$ and TEM modes, we have from Eq. 51,

$$Y_1 + \frac{Y_2}{r_0} = 0 \quad (93)$$

Equation 50a is used for $TE_{0,n}$ modes,

$$Y_2 = 0 \quad (94)$$

Finally, for $TE_{m,n}$ ($HE_{m,n}$) and $TM_{m,n}$ ($EH_{m,n}$) modes, Eq. 54 yields the boundary condition

$$\sqrt{\left[Y_1 + \frac{Y_2}{r_0}\right]^2 + Y_4^2} = 0 \quad (95)$$

IV. PROGRAM OUTLINE AND USE

Chapter 4 presents the key aspects of the computer program used to implement the theory and equations of Chapter 3. Section 4.1 starts with an overview of the program, showing the general flow of logic. The techniques used to handle a general dielectric profile are discussed in Section 4.2. The process for finding a mode is presented in Section 4.3.

4.1 Program Flow

The Fortran code is laid out in blocks with a number and comment delimiting each block. If necessary, a block will include a brief explanation of its function. The blocks making up each procedure (main program and subroutines) are presented below. Any variable used in the discussion is defined in Appendix D.

Main Program (COAD7R)

1.00 INITIALIZATION SECTION

Initialize constants and logicals used throughout program.

1.10 VARIABLES USED IN ZREAL1

Initialize variables used in the calling argument of the zero finding routine ZREAL1.

1.15 VARIABLES USED IN EO4JBF

Initialize variables used in the calling argument of the minimization routine EO4JBF.

1.20 VARIABLES USED IN DCADRE

Initialize variables used in the calling argument of the integration routine DCADRE.

1.30 SET DEFAULTS

Initialize constants and logicals which are input parameters.

1.40 OPEN NAMELIST AND PRINT FILES

Input variables are read in via the NAMELIST file. The print file COAD7P is opened.

1.46 CHECK MODE LOGIC

A check is made to ensure that only one mode type is chosen.

1.47 DIELECTRIC TAPER

If desired, a linearly tapered dielectric profile is constructed.

1.50 INITIALIZE DIELECTRIC AND RADIAL ARRAYS

1.52 DEFAULT FOR NJUMP EQUAL TO ZERO

Initialize NJUMP equal to zero. Set default values for DRATIO(1), AJUMP(1) and IJUMP(1).

1.54 EXAMINE DIELECTRIC PROFILE FOR ANY DISCONTINUITIES

Assign appropriate values to pertinent arrays when a discontinuity is encountered.

1.59 PRINT OUT PHYSICAL CONDITIONS

Variables representing physical conditions are written to the output file COAD7P.

1.60 SMOOTH DRELD AND DRELN

Discontinuities, if any, in DRELD and DRELN are removed.

1.65 INITIALIZE DIFFERENCE ARRAYS

1.70 GENERATE SPLINE COEFFICIENTS FOR DRELA AND DRELN

1.90 OUTER LOOP ON MODE NUMBER

This loop evaluates K distinct modes.

2.00 OUTER FREQUENCY LOOP

This loop finds the propagation constant k_z at L distinct frequencies for the kth mode.

2.10 CASE FOR $TE_{0,n}$, $TM_{0,n}$, OR TEM MODES

The propagation constant k_z for the $TE_{0,n}$, $TM_{0,n}$, or TEM mode is sought.

2.15 CALL ZREAL1

The zero finding routine ZREAL1 is called.

2.20 CASE FOR $TE_{m,n}$ OR $TM_{m,n}$ mode is sought.

2.30 CALL EO4JBF

Minimization routine EO4JBF is called.

4.00 EVALUATE FIELD COMPONENTS

Depending on the mode type chosen, initial conditions are set for one of the following pairs of equations:

$TE_{m,n}$ and $TM_{m,n}$ modes : equations 87 and 88

$TM_{0,n}$ and TEM modes : equations 89 and 90

$TE_{0,n}$ modes : equations 91 and 92.

4.10 SET UP FOR DGEAR

Initialize variables used in the calling argument of the integration routine DGEAR.

4.15 SET UP FOR NEXT INTEGRATION

Depending on the mode type chosen and if integration is currently at a discontinuity in the dielectric profile, compute one of the following cases:

$TE_{m,n}$ and $TM_{m,n}$ modes : equations 61 and 88

$TM_{0,n}$ and TEM modes : equations 62 and 80

$TE_{0,n}$ modes : equations 63 and 82.

4.20 UNNORMALIZED FIELDS

Depending on the mode type chosen, compute the remaining field components.

4.30 Define difference field arrays for one of the following mode types:

$TE_{m,n}$ and $TM_{m,n}$ modes : ERD(1), DTD(1), DZD(1)

$TM_{0,n}$ and TEM modes : ERD(1), DZD(1)

$TE_{0,n}$ modes : DTD(1)

4.45 SMOOTH DIFFERENCE FIELDS FOR SPLINE PURPOSES

If necessary, the difference field arrays will be "smoothed" for one of the following modes:

$TE_{m,n}$ and $TM_{m,n}$ modes : ERD(1), DTD(1), DZD(1)

$TM_{0,n}$ and TEM modes : ERD(1), DZD(1)

$TE_{0,n}$ modes : DTD(1).

5.00 CALL NORMALIZING ROUTINE

Normalize field components of a chosen mode type.

7.00 END OF OUTER FREQUENCY LOOP.

7.20 PRINTOUT RESULTS

For a given mode type, write appropriate results to file COAD7P.

7.40 PLOT DATA

For a given mode type, plot appropriate graphs of field components and write to file COAD7P.

7.60 CALL GRAPHING ROUTINE

For a given mode type, appropriate field components are plotted and hard copy printouts are made.

7.90 END OF OUTER LOOP ON MODE NUMBER

7.95 ORTHOGONALITY CHECK

Orthogonality between two chosen modes is evaluated by computing Poynting's vector over the cross-sectional area.

8.00 TERMINATION

9.00 FORMAT STATEMENTS

Subroutine DERIV

The integration routine DGEAR calls subroutine DERIV, which defines and evaluates the derivatives of the second order linear differential equation system (Eqs. 47 and 48).

2.00 DEFINE DIELECTRIC AND FIRST DERIVATIVE VALUES

This section evaluates FDRV and DREL based on the present radial position used by the integration routine DGEAR.

2.20 EVALUATE DERIVATIVES

Compute one of the following first order differential equation systems for a given mode type:

$TE_{m,n}$ and $TM_{m,n}$ modes : equation 77

$TM_{0,n}$ and TEM modes : equation 80

$TE_{0,n}$ modes : equation 83.

8.00 TERMINATION

9.00 FORMAT STATEMENTS

Subroutine PARDRV

Subroutine PARDRV is also called by the integration routine DGEAR and it evaluates an $N \times N$ Jacobian matrix of partial derivatives.

2.00 DEFINE DIELECTRIC AND FIRST DERIVATIVE VALUES

This section evaluates FDRV and DREL based on the present radial position used by the integration routine DGEAR.

2.20 EVALUATE PARTIAL DERIVATIVES

Compute one of the following first order partial differential equation systems for a given mode type:

$TE_{m,n}$ and $TM_{m,n}$ modes : equation 84

$TM_{0,n}$ and TEM modes : equation 85

$TE_{0,n}$ modes : equation 86.

8.00 TERMINATION

9.00 FORMAT STATEMENTS

Function FNCT1

The zero finding routine ZREAL1 calls FNCT1, which defines the functions for which the roots of the $TE_{0,n}$, $TM_{0,n}$ ($n > 1$) and TEM modes are found.

1.00 INITIALIZATION

Initialize variables used in the calling argument of the integration routine DGEAR. Also, set initial conditions for one of the following mode types:

$TM_{0,n}$ and TEM modes : equation 89

$TE_{0,n}$ modes : equation 91.

3.00 CALL DGEAR

The integration routine DGEAR is called.

3.50 SET UP FOR NEXT DIELECTRIC SECTION

If a $TM_{0,n}$ or TEM mode type is chosen, set equation 73

4.10 DEFINE FUNCTION STATEMENT FNCT1

According to which mode type is chosen, evaluate one of the following equations:

$TM_{0,n}$ and TEM modes : equation 93

$TE_{0,n}$ modes : equation 94.

8.00 TERMINATION

9.00 FORMAT STATEMENTS

Function FNCT2

The N dimensional minimization routine E04JBF calls FNCT2, which defines the function for the roots of the $TE_{m,n}$ and $TM_{m,n}$ ($n > 1$) modes.

1.00 INITIALIZATION

Initialize variables used in the calling argument of the integration routine DGEAR and equation 87.

3.00 CALL DGEAR

The integration routine DGEAR is called.

3.50 SET UP FOR NEXT DIELECTRIC SECTION

Compute equation 72.

4.10 DEFINE FUNCTION STATEMENT FNCT2

Evaluate equation 95.

8.00 TERMINATION

9.00 FORMAT STATEMENTS

Subroutine NORMAL

Subroutine NORMAL normalizes the field components of a given mode.

2.00 COMPUTE SPLINE COEFFICIENTS

Compute the spline interpolation of the field components for one of the following mode types:

$TE_{m,n}$ and $TM_{m,n}$ modes : E_r, E_ϕ, H_r, H_ϕ

$TM_{0,n}$ and TEM modes : E_r, H_ϕ

$TE_{0,n}$ modes : E_ϕ, H_r .

3.00 TRANSVERSE COMPONENT INTEGRATION

Using the integration routine DCADRE (which calls Function CXINT), equation 68 is computed.

4.00 NORMALIZE FIELD COMPONENTS

Normalize the field components of the chosen mode by dividing by the square root of the computed integral in section 3.00.

8.00 TERMINATION

9.00 FORMAT STATEMENTS

Subroutine ORTHO

Subroutine ORTHO computes the orthogonality between two chosen modes.

2.00 OUTER FREQUENCY LOOP

Compute orthogonality at L multiple frequencies.

3.00 INNER LOOP TO EVALUATE ORTHOGONALITY BETWEEN TWO MODES

Determine which pair of modes (K_1, K_2) are to be evaluated.

4.00 COMPUTE SPLINE COEFFICIENTS

Compute the spline interpolation of the field components for one of the following mode types:

TE_{m,n} and TM_{m,n} modes : E_r, E_φ, H_r, H_φ

TM_{0,n} and TEM modes : E_r, H_φ

TE_{0,n} modes : E_φ, H_r.

5.00 TRANSVERSE COMPONENT INTEGRATION

Using the integration routine DCADRE (which calls Function CXINT) on equation 68, orthogonality is computed.

6.00 END OF INNER LOOP

7.00 END OF OUTER LOOP

8.00 TERMINATION

9.00 FORMAT STATEMENTS

Function CXINT

Function CXINT is called by the integration routine DCADRE and defines the argument of Eq. 68.

2.00 EVALUATE SPLINE COEFFICIENTS

Evaluate the spline coefficients for the field components of one of the following mode types:

TE_{m,n} and TM_{m,n} modes : E_r, E_φ, H_r, H_φ

TM_{0,n} and TEM modes : E_r, H_φ

TE_{0,n} modes : E_φ, H_r.

3.00 DEFINE ARGUMENT FOR NORMALIZATION

Based on whether k_z is real (propagating) or imaginary (nonpropagating), compute one of the following arguments for equation 68:

k_z real : E_rH_φ - E_φH_r

k_z imaginary : E_φH_r - E_rH_φ.

4.00 DEFINE ARGUMENT TO COMPUTE ORTHOGONALITY

Compute arguments of equation 68 based on one of the following cases:

4.10 MODE 1 PROPAGATING, MODE 2 PROPAGATING

k_z for both modes is real; define E_rH_φ - E_φH_r

4.20 MODE 1 PROPAGATING, MODE 2 CUTOFF

k_z for mode 1 is real and imaginary for mode 2; define

E_φH_r - E_rH_φ

4.30 MODE 1 CUTOFF, MODE 2 PROPAGATING

k_z for mode 1 is imaginary and real for mode 2: define

$$E_r H_\phi - E_\phi H_r$$

4.40 MODE 1 AND MODE 2 CUTOFF

k_z is imaginary for both modes; define $E_\phi H_r - E_r H_\phi$

8.00 TERMINATION

9.00 FORMAT STATEMENTS

Subroutine DPLOT

Subroutine DPLOT generates the field plots for a given mode which can be processed into making hard copy printouts.

4.2 Process for a General Dielectric Profile

The two major tasks in the program concern finding the propagation constant k_z (and where appropriate, α) and corresponding field components for a desired mode. To accomplish this, the second order differential equation system (Eqs. 47 or 48) must be integrated in the radial coordinate across the dielectric profile. For a dielectric profile free of any discontinuities, there is a single integration from the inner to outer conductor radius. If there are N discontinuities, then integration must be performed $N + 1$ times.

The dielectric profile is originally defined at discreet points. As the integration is being performed from the inner to outer conductor radius, a point may be chosen by the integration routine at which the dielectric is not defined. Thus, before the integration is carried out, cubic spline interpolation is performed to generate a smooth curve for

the dielectric. A discussion involving the theory of cubic splines used in the program is presented by de Boor.⁴ The interpolatory subroutines used are presented in Appendix A (Section A.5). Once the interpolation has been completed, integration may proceed as before. For a dielectric profile free of any discontinuities, the standard cubic spline interpolation is performed. If the dielectric profile is discontinuous, the standard spline approach generates a large "ringing" in the vicinity of the jump. The approach taken in solving this problem is described in Appendix C.

Once k_z has been determined for a given mode, the field components as a function of r need to be generated. The integration routine used to integrate the field components from the inner to outer conductor is the same as that used in the "shooting" method to find k_z (and a). Again, cubic spline interpolation must be used on the dielectric profile in order to carry out the integration.

4.3 Finding a Mode

In order to find the mode propagation constant k_z and resulting field patterns for a given mode, an initial guess for k_z must be provided. Whenever a dielectric different from air is introduced into a waveguide, the cutoff frequency of a given mode is lowered with respect to that of air. This is due to the fact that electromagnetic waves travel at a reduced velocity governed by the following equation:

$$c_{\epsilon} = \frac{c_0}{\sqrt{\epsilon_r}} \quad (96)$$

where

c_ϵ = speed of light in dielectric

c_0 = speed of light in air

ϵ_r = relative dielectric permittivity

With this fact in mind, the initial guess for k_z falls between the values of k_z in the limiting cases of $\epsilon_{r1} = \epsilon_{r2} = 1$ (air) and $\epsilon_{r1} = \epsilon_{r2}$ = desired relative dielectric permittivity,

$$k_{za} < k_{zg} < k_{zh} \quad (97)$$

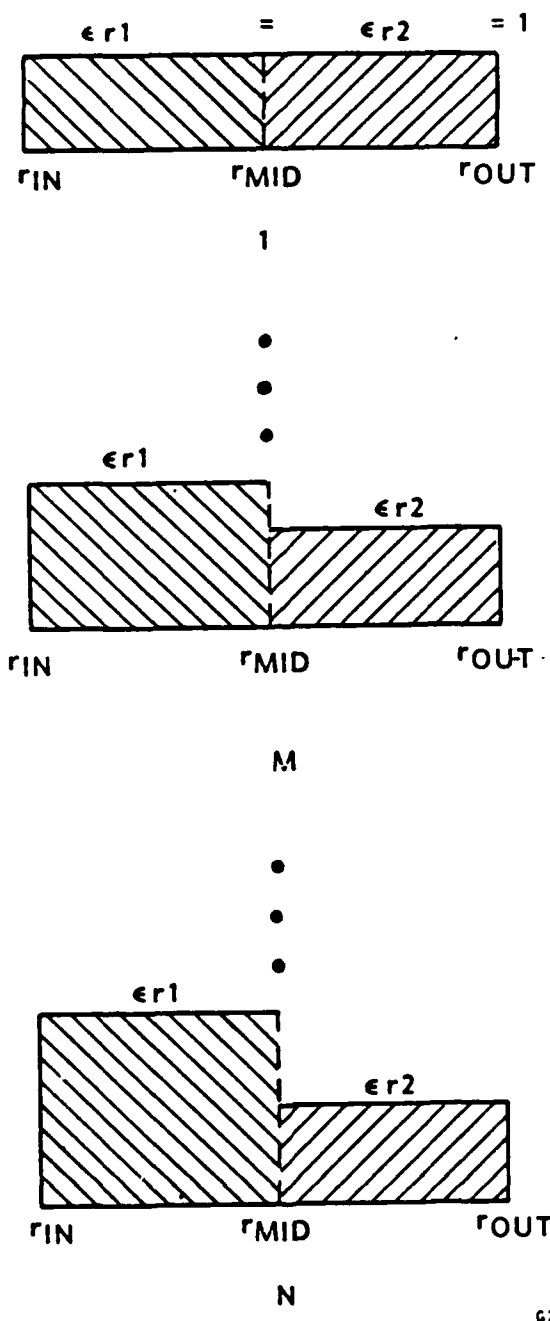
where

k_{za} = mode propagation constant for $\epsilon_{r1} = \epsilon_{r2} = 1$

k_{zh} = mode propagation constant for $\epsilon_{r1} = \epsilon_{r2}$ = desired dielectric value

As mentioned in Section 3.2, an additional guess for the dimensionless parameter α is required for $TE_{m,n}$ ($HE_{m,n}$) and $TM_{m,n}$ ($EH_{m,n}$) modes.

To evaluate the geometry of Fig. 3A for a chosen dielectric profile, one must "build up" to the final desired dielectric profile. This is achieved by starting with $\epsilon_{r1} = \epsilon_{r2} = 1$ and gradually perturbing the system by increasing the value of ϵ_{r1} and/or ϵ_{r2} . This is schematically shown in Fig. 4. The initial guess for k_z at the M th step is based on Eq. 97, where k_{zh} is the mode propagation constant for the homogeneously filled coax with the current dielectric value. For the $m \neq 0$ modes, the initial guess for α at the M th step is set equal to the final value from the previous step,



G221414

Fig. 4. "Build up" process to evaluate the two dielectric profile.

$$\alpha_M = \alpha_{M-1} \quad (98)$$

When $m = 0$, a one-dimensional zero finding routine (ZREAL1, Section A.2) is used to find the zero. When $m \neq 0$, a two-dimensional minimum finding routine (E04JBF, Section A.3) is used to find the minimum. In this second case, a relatively poor initial guess for k_z or α will nudge E04JBF towards an undesired minimum. In particular, the initial guess for α was critical. This result was found empirically by running the program and observing the affects of varying α . Conversely, for the $m = 0$ cases, the initial guess for k_z was not as critical.

To have any confidence that the final value of k_z at the M th step represents the desired mode, certain conditions are examined. The first condition requires that k_z fall between the limits of k_{za} and k_{zh} , as specified by Eq. 97. If this is not the case, then the program has unwittingly "walked" to another solution. The next check involves examining the evolution of the field plots from the air filled case to the present dielectric profile. Characteristics which should be scrutinized include:

1. The number of zero crossings
2. Conformance to the boundary condition that the tangential components of the electric field E and the normal components of the magnetic field H at $r = a$ and $r = c$ are zero
3. Relative magnitudes of similar field components
4. Poynting's vector

The last major criterion to be satisfied is orthogonality, which is computed between the current mode of interest and another conveniently chosen mode.

V. PRESENTATION OF RESULTS

The geometry of Fig. 3A was examined for the following modes: $TM_{0,1}$, $TE_{0,1}$, TEM, $TM_{1,1}(EH_{1,1})$. The dimensions, dielectric profile values, and frequency used for each mode were

$$\begin{aligned}a &= 1.0 \text{ cm} \\b &= 1.5 \text{ cm} \\c &= 2.0 \text{ cm} \\\epsilon_{r1} &= 1.0, 2.0 \\\epsilon_{r2} &= 1.0\end{aligned}$$

There are two cases presented for each mode:

Case 1: $\epsilon_{r1} = \epsilon_{r2} = 1.0$

Case 2: $\epsilon_{r1} = 2.0, \epsilon_{r2} = 1.0$

Both cases were evaluated at 32 gigahertz (GHz). For clarity, region 1 will refer to the dielectric region of ϵ_{r1} , and region 2 will refer to the dielectric region of ϵ_{r2} .

The total number of points at which the dielectric profile was defined was 46. The points were equally spaced, except in the neighborhood of the discontinuity ($b = 1.5$ cm). Here, points were concentrated in an effort to increase the accuracy of the integration and when normalization and orthogonality were computed. In determining the optimum number of points to use, consideration had to be given to the cost,

time, and numerical accuracy desired. The number of points chosen, 46, gave good numerical accuracy while keeping the time and cost to a minimum. Appendix E lists the values of the individual points.

Before proceeding, the results for each mode are presented below (ϵ_{r2} is always equal to 1).

<u>Mode</u>	<u>ϵ_{rl}</u>	<u>k_z (meters⁻¹)</u>	<u>α</u>
$TM_{0,1}$	1.0	592.99	~
	2.0	681.37	~
$TE_{0,1}$	1.0	589.09	~
	2.0	819.66	~
TEM	1.0	670.89	~
	2.0	916.37	~
$TM_{1,1}$	1.0	589.84	-3.72 E-8
$EH_{1,1}$ mode 1	2.0	678.27	-7.33 E-2
$EH_{1,1}$ mode 2	2.0	815.32	-4.11

Sections 5.1 through 5.4 will compare/contrast the field component plots for the $TM_{0,1}$, $TE_{0,1}$, TEM, and $TM_{1,1}$ ($EH_{1,1}$) modes, respectively. Computation of orthogonality will be presented in Section 5.5. Two dispersion plots will then be presented and discussed in Section 5.6. Finally, Section 5.7 will show the effects on the propagation constant k_z as the dielectric ratio of ϵ_{rl} to ϵ_{r2} is varied.

5.1 TM_{0,1} Mode

The effect of the discontinuous dielectric profile at $r = b$ is readily apparent in Fig. 5 for E_r . Notice that the magnitude of E_r doubles (as required for an inner to outer dielectric ratio of two) along with the fact that the field lies primarily in region 2. As with the air filled case (Fig. 6), there is one zero crossing in each case.

The E_z component distribution has evolved from being almost symmetric (Fig. 7) to primarily concentrated in region 1 (Fig. 8). Note that E_z is continuous at $r = b$ (Fig. 8), but its first derivative with respect to r is discontinuous. The boundary condition that E_z be equal to zero at $r = a$ and $r = c$ is satisfied in both plots.

Figures 9 and 10 depict the H_ϕ component for cases 1 and 2, respectively. Case 2 (Fig. 9) shows H_ϕ continuous at $r = b$, with the overall field distribution primarily in region 1 (as with Fig. 10).

Poynting's vector shows that for case 2 (Fig. 11), the energy resides primarily in region 2, implying that most of the mode propagates in this region. This boldly contrasts the energy distribution for case 1 (Fig. 12), which is slightly larger for region 1.

TM 01 MODE AT 32.0 GHZ, ER1-2

RADIAL ELECTRIC E FIELD

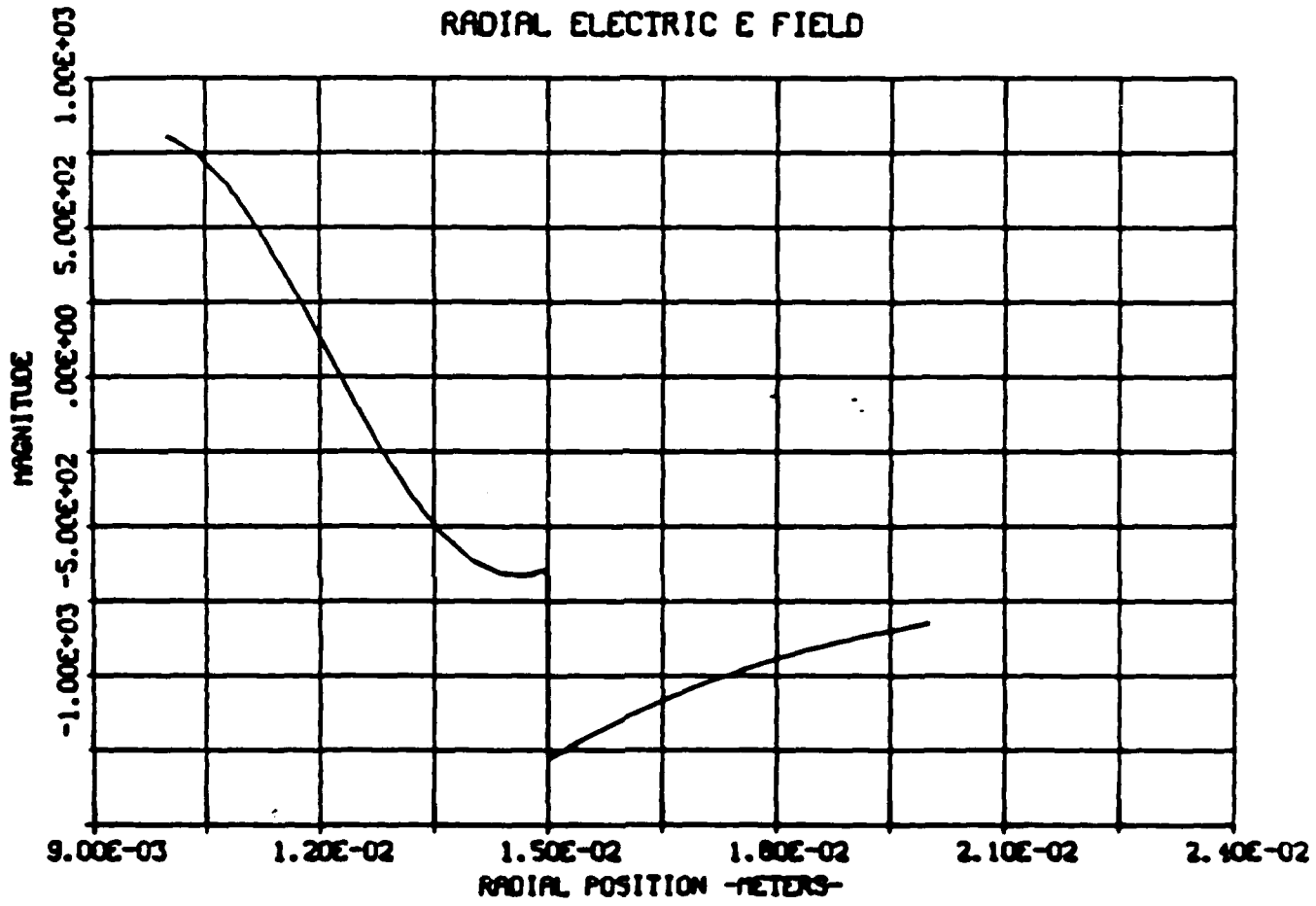


Fig. 5. $TM_{0,1}$ mode at 32 GHz, $ER1 = 1$; E_r component.

TM 01 MODE AT 32.0 GHZ, ER1-1

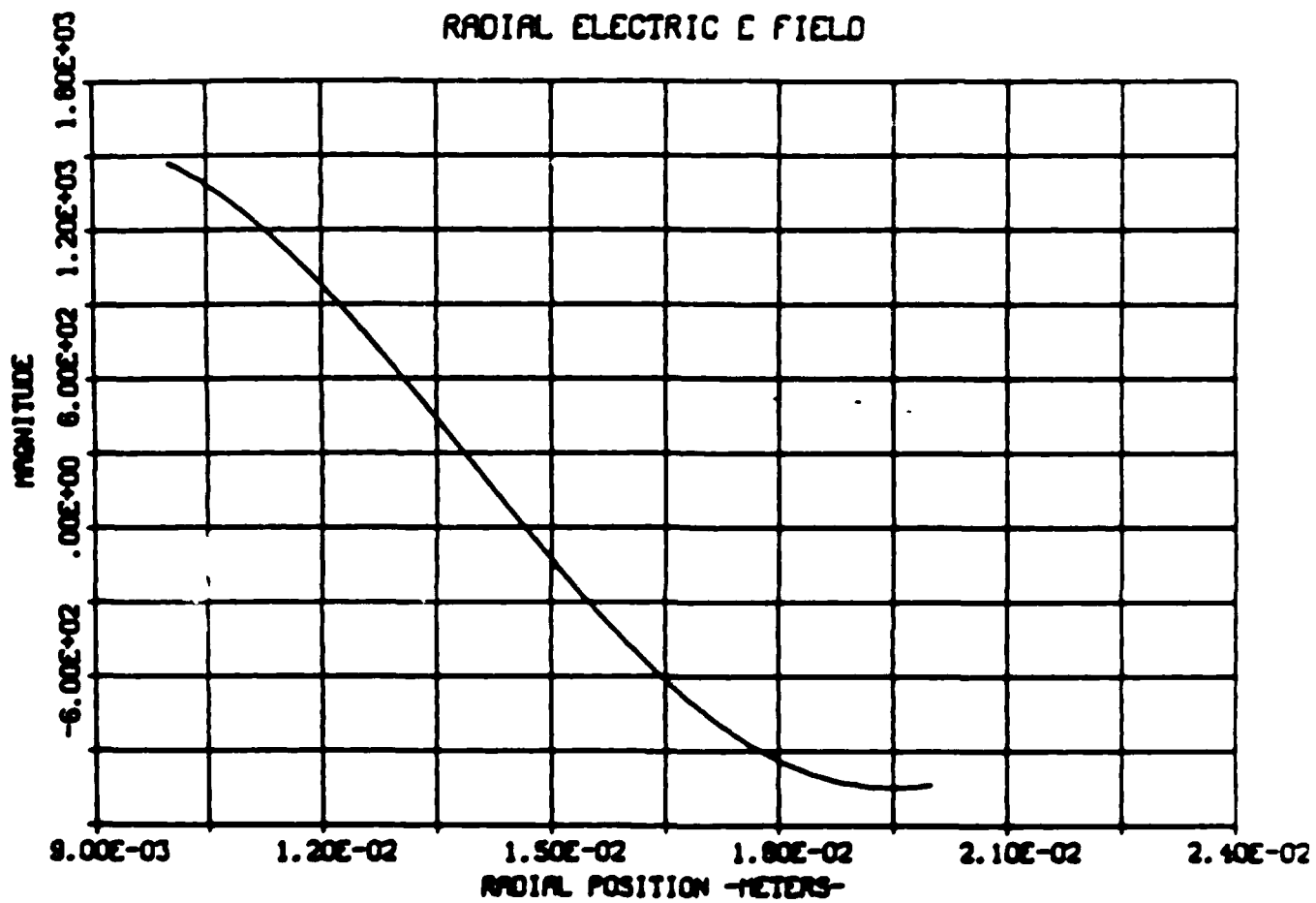


Fig. 6. TM_{0,1} mode at 32 GHz, ER1 = 1; E_r component.

TM 01 MODE AT 32.0 GHZ, ERI-1

AXIAL ELECTRIC E FIELD

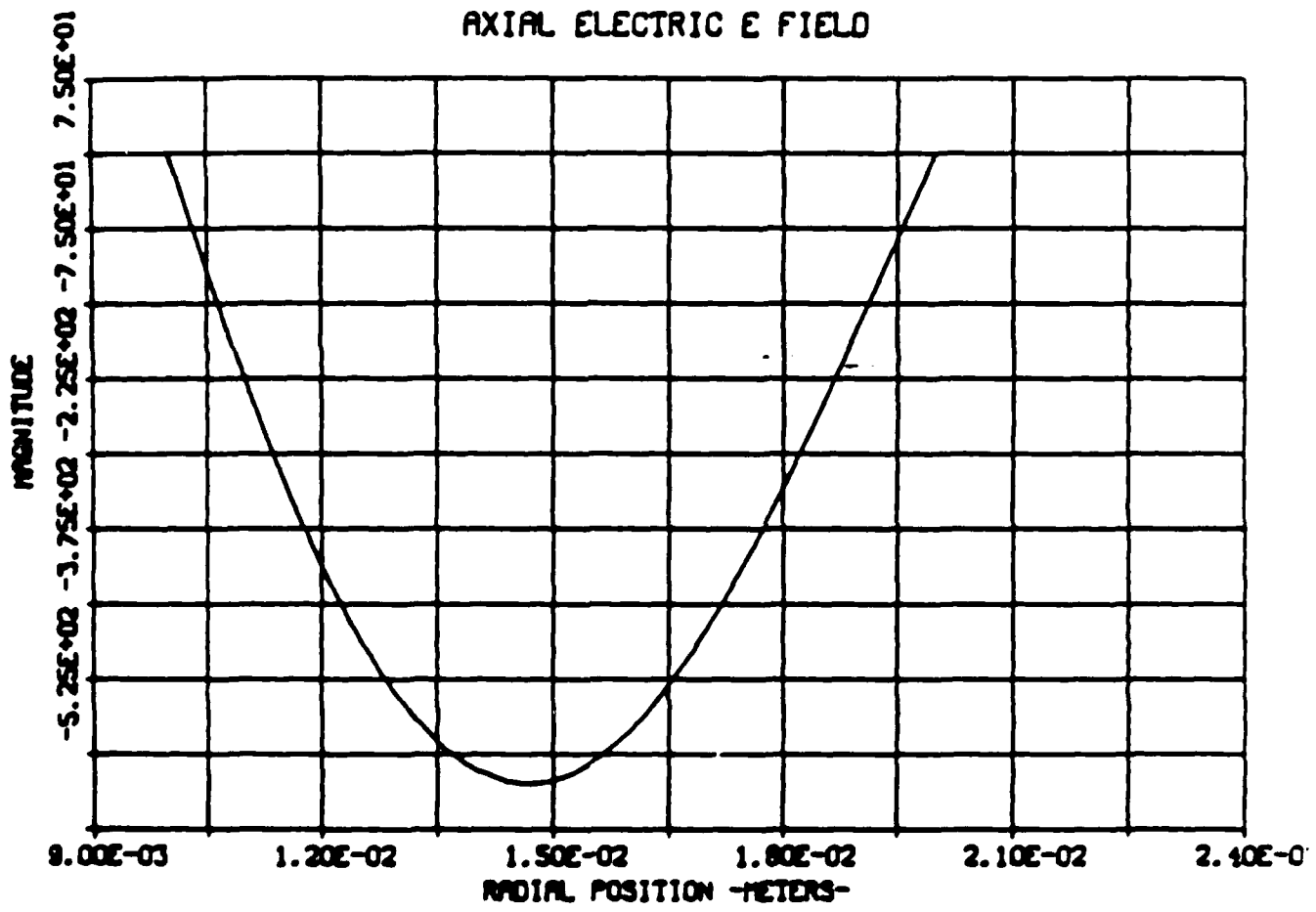


Fig. 7. $TM_{0,1}$ mode at 32 GHz, ERI = 1; E_r component.

TM 01 MODE AT 32.0 GHZ, ER1-2

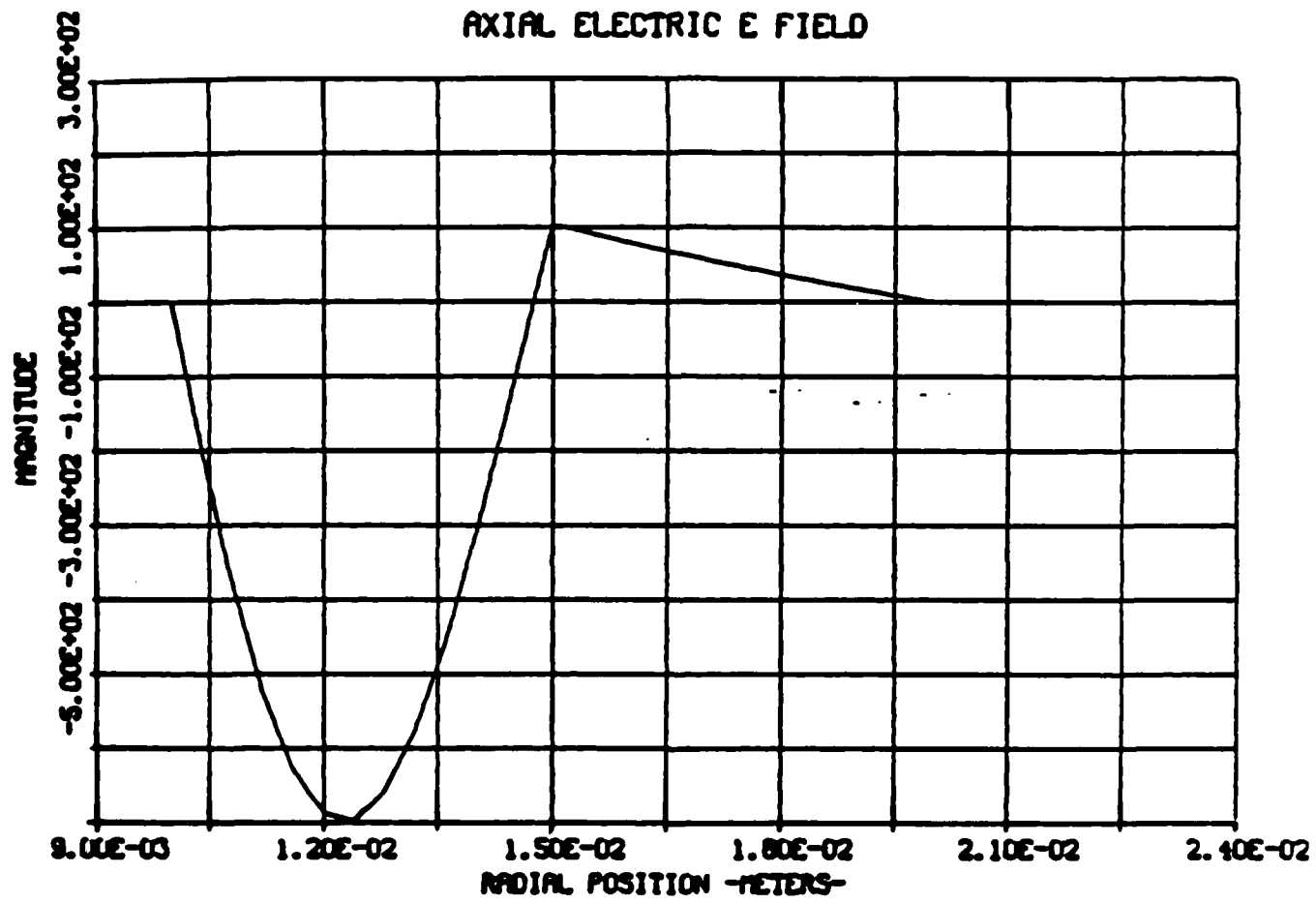


Fig. 8. $TM_{0,1}$ mode at 32 GHz, $ER1 = 1$; Poynting's vector $E_r H_\phi$.

TM 01 MODE AT 32.0 GHZ, ERI-2

AZIMUTHAL MAGNETIC H FIELD

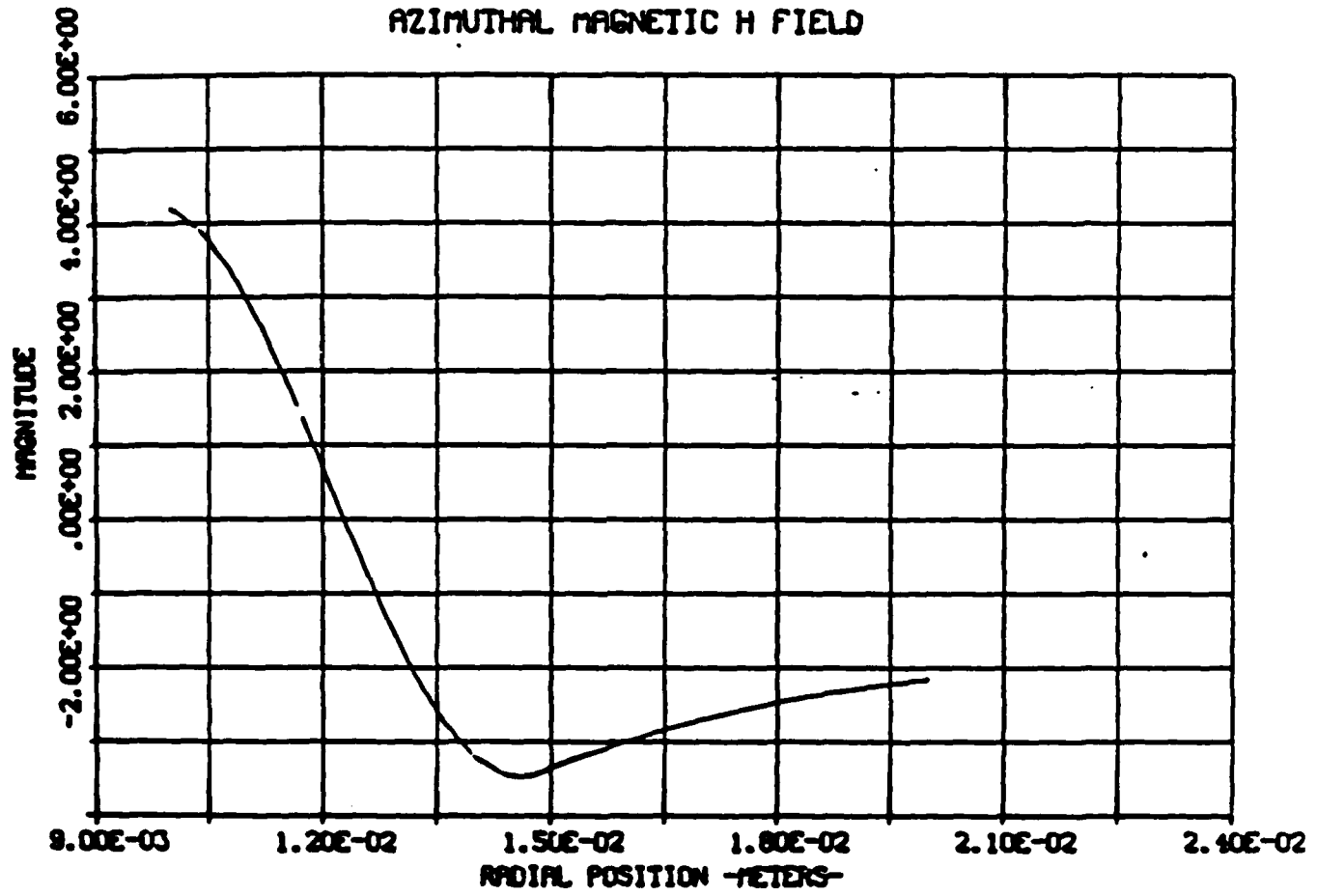


Fig. 9. $TM_{0,1}$ mode at 32 GHz, $ERI = 2$; E_r component.

TM 01 MODE AT 32.0 GHZ, ER1-1

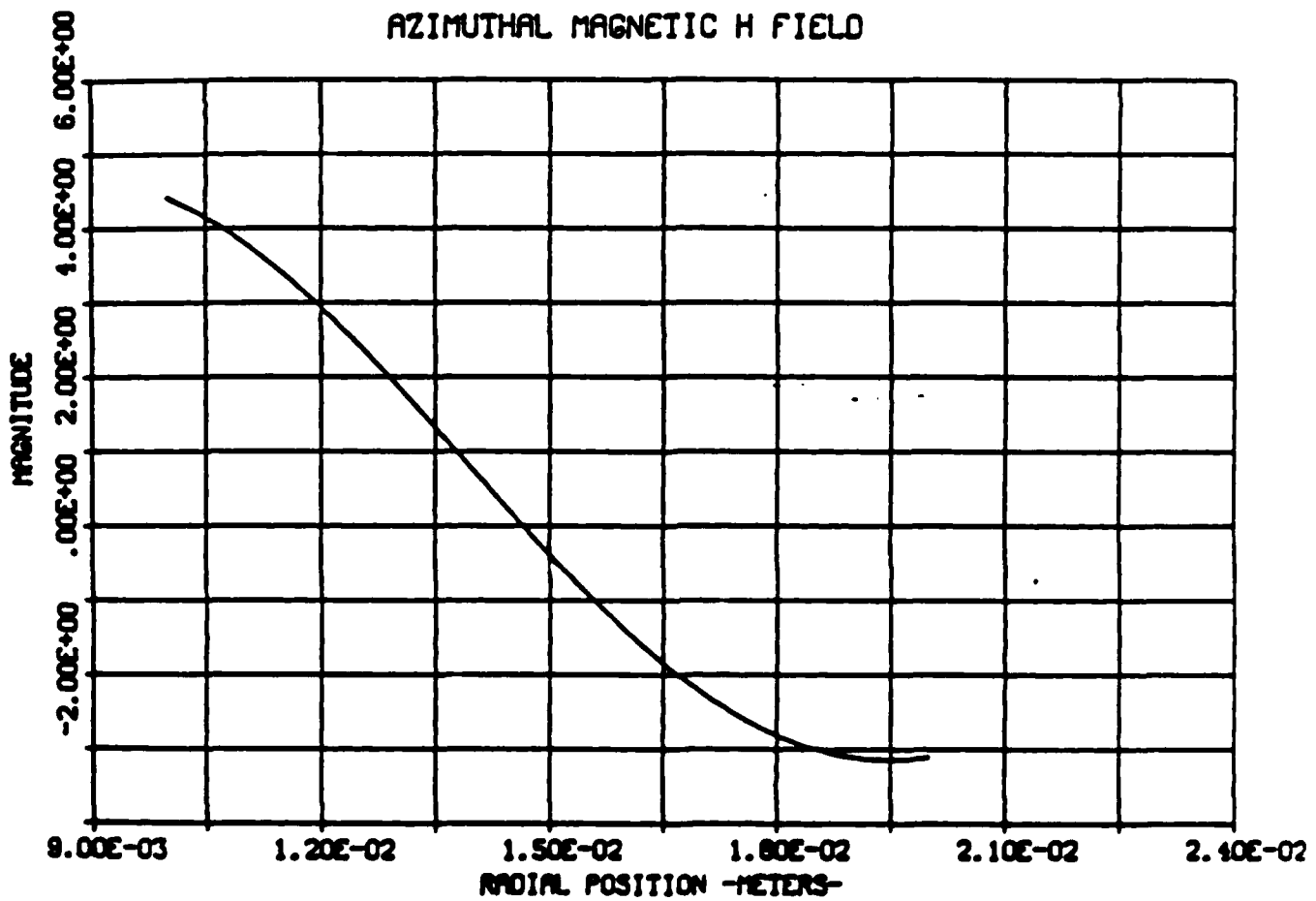


Fig. 10. $TM_{0,1}$ mode at 32 GHz, ER1 = 2; E_z component.

TM 01 MODE AT 32.0 GHZ, ERI-2

POYNITING'S VECTOR- ERI-2

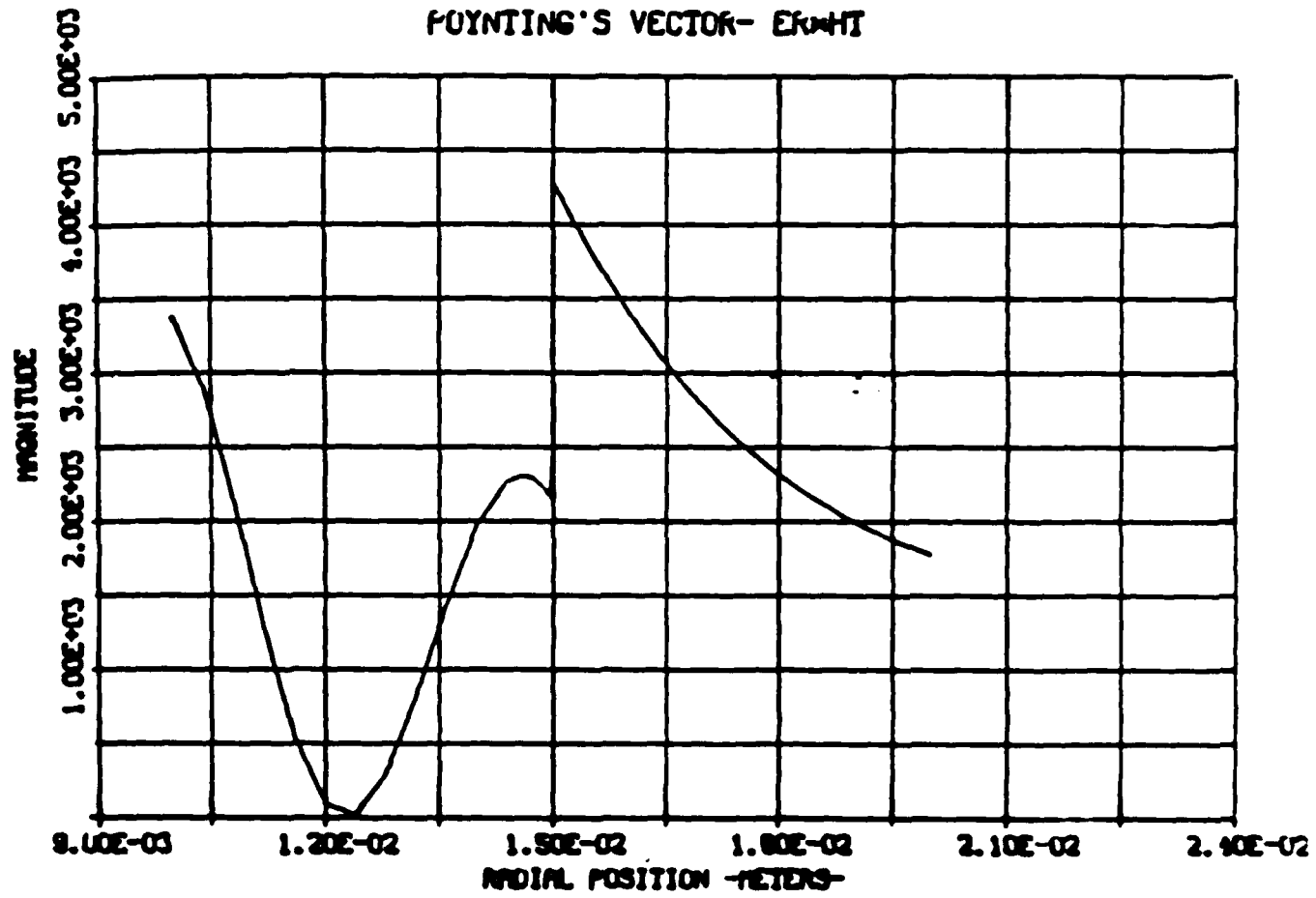


Fig. 11. TM_{0,1} mode at 32 GHz, ERI = 2; H_z component.

TM₀₁ MODE AT 32.0 GHZ, ER1-1

POYNITING'S VECTOR- ER1-1

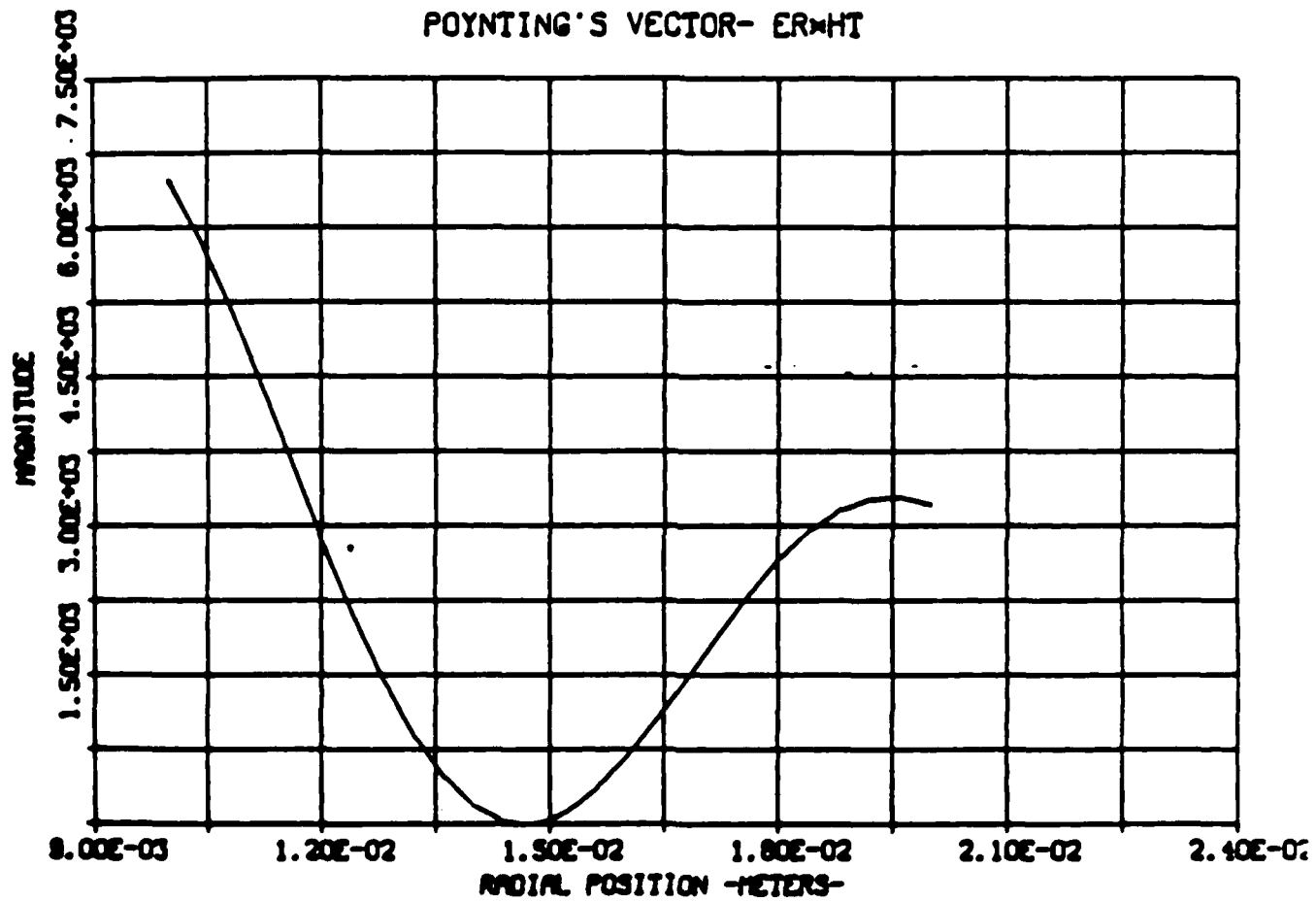


Fig. 12. TM_{0,1} mode at 32 GHz, ER1 = 2; Poynting's vector $E_r H_\phi$.

5.2 TE_{0,1} Mode

The E_ϕ component shows that the field has shifted primarily to region 1 (Fig. 13) from what was almost a symmetrical distribution (Fig. 14). In both cases, E_ϕ is equal to zero at $r = a$ and $r = c$, and is continuous at $r = b$.

The H_r component is similarly affected in that most of the field lies in region 1 (Fig. 15) in contrast to the air filled case (Fig. 16). The boundary condition that H_r be equal to zero at $r = a$ and $r = c$ is satisfied in both plots.

The H_z component for case 2 (Fig. 17) continues the trend toward concentrating in region 1. Although continuous at the dielectric discontinuity, the first derivative of H_z with respect to r is discontinuous. Also, there is one zero crossing, as with the air filled case (Fig. 18).

Poynting's vector for case 2 (Fig. 19) shows that the majority of the energy is in region 1 compared with the almost symmetrical distribution for case 1 (Fig. 20). Consequently, the $TE_{0,1}$ mode for the dielectric profile of case 2 propagates primarily in region 1.

TE 01 MODE AT 32.0 GHZ, ERI-2

AZIMUTHAL ELECTRIC E FIELD

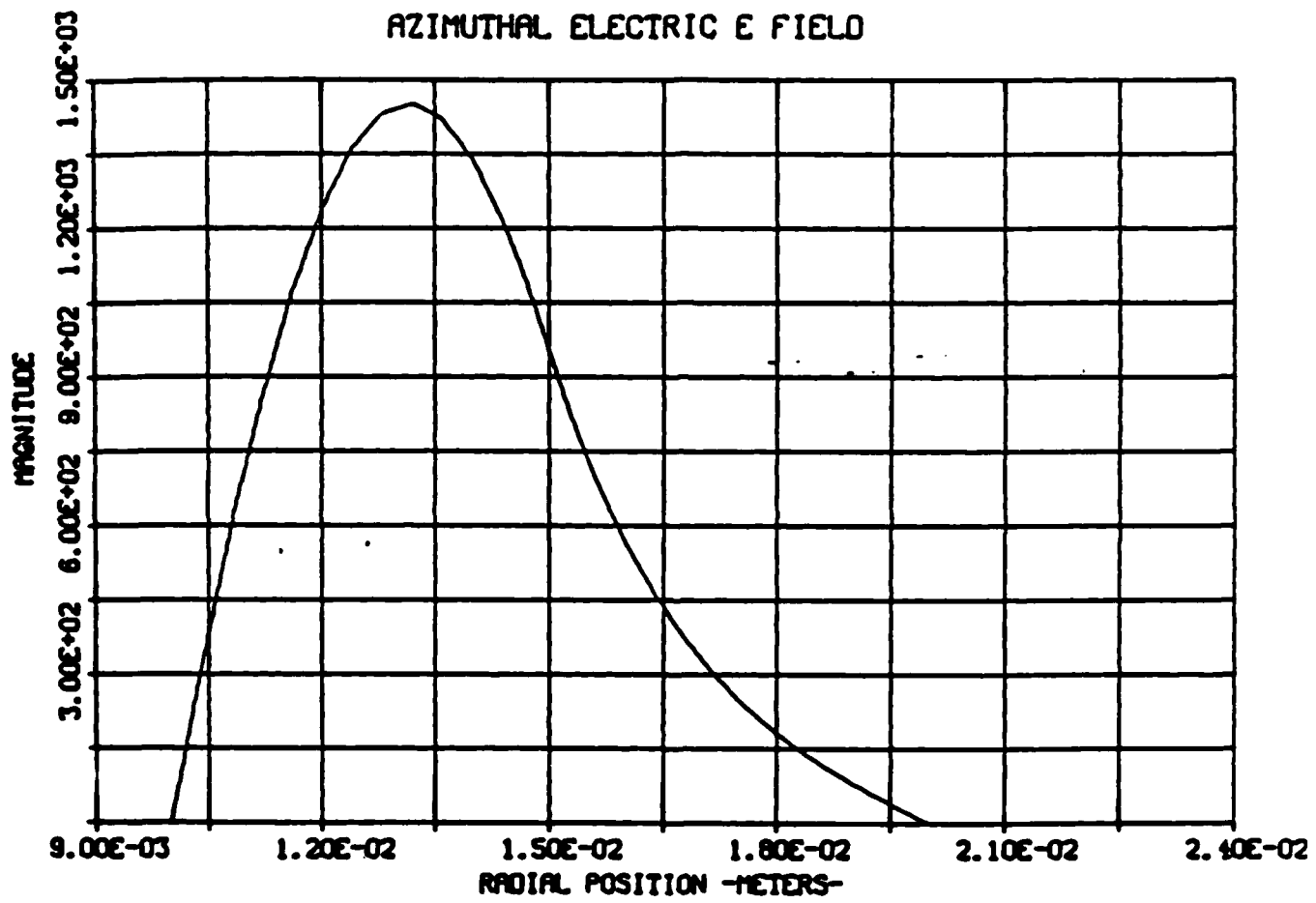


Fig. 13. $TE_{0,1}$ mode at 32 GHz, $ERI = 1$; E_ϕ component.

TE 01 MODE AT 32.0 GHZ, ER1-1

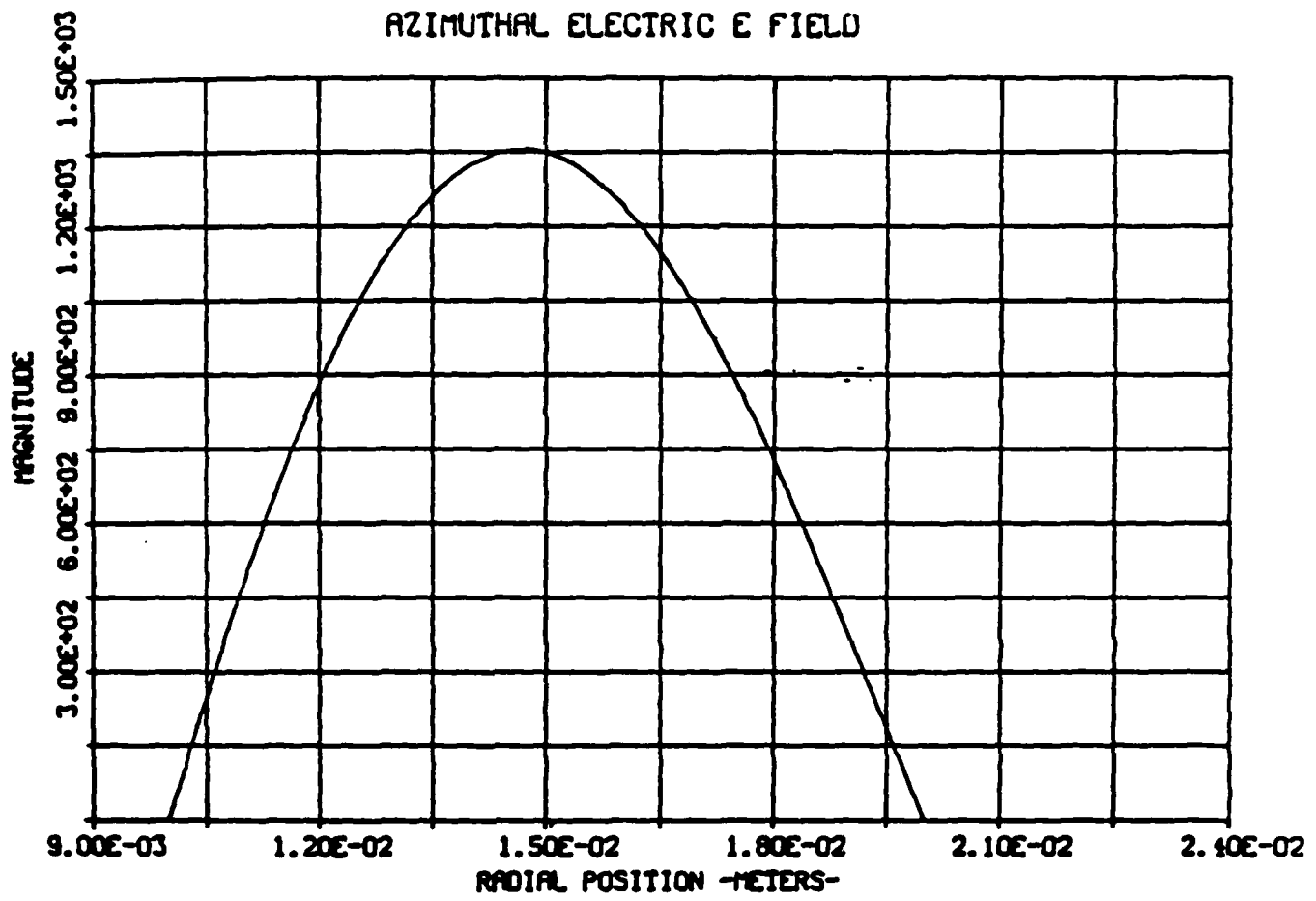


Fig. 14. $TE_{0,1}$ mode at 32 GHz, $ER1 = 1$; E_r component.

TE 01 MODE AT 32.0 GHZ, ER1-2

RADIAL MAGNETIC H FIELD

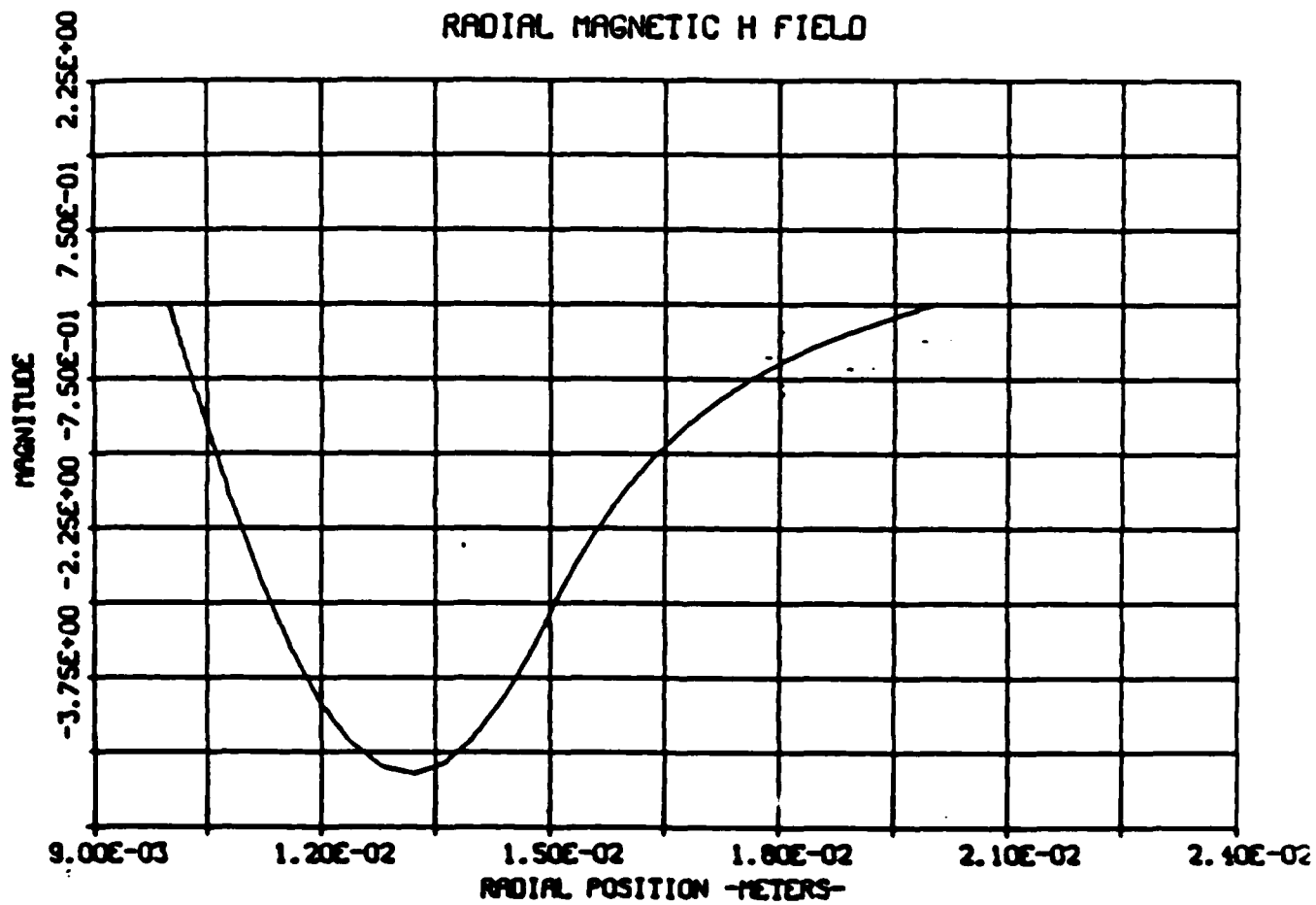


Fig. 15. $TE_{0,1}$ mode at 32 GHz, $ER1 = 1$; H_z component.

TE 01 MODE AT 32.0 GHZ, ER1-1

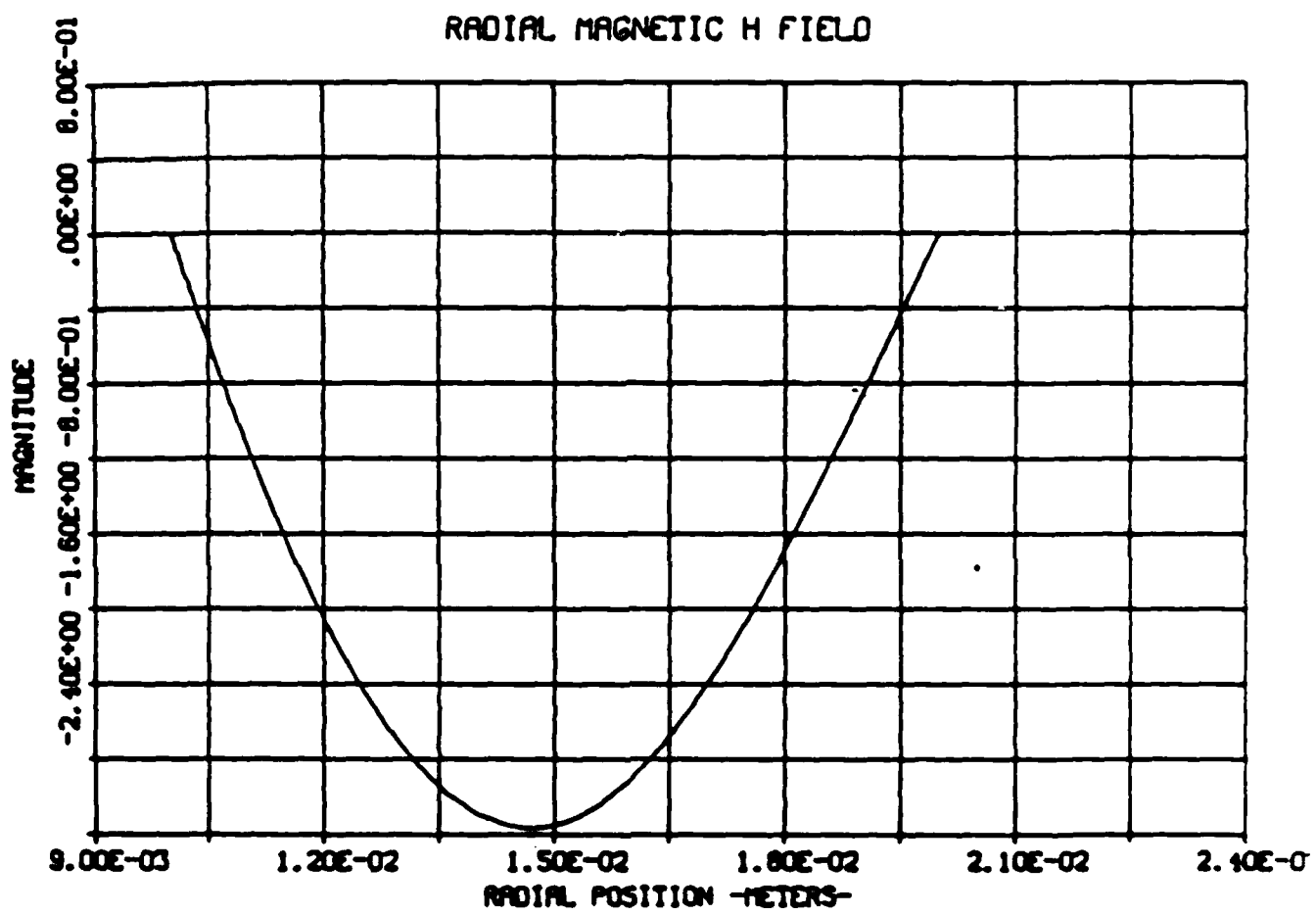


Fig. 16. TE_{0,1} mode at 32 GHz, ER1 = 1; Poynting's vector $E_r H_\phi$.

TE 01 MODE AT 32.0 GHZ, ER1-2

AXIAL MAGNETIC H FIELD

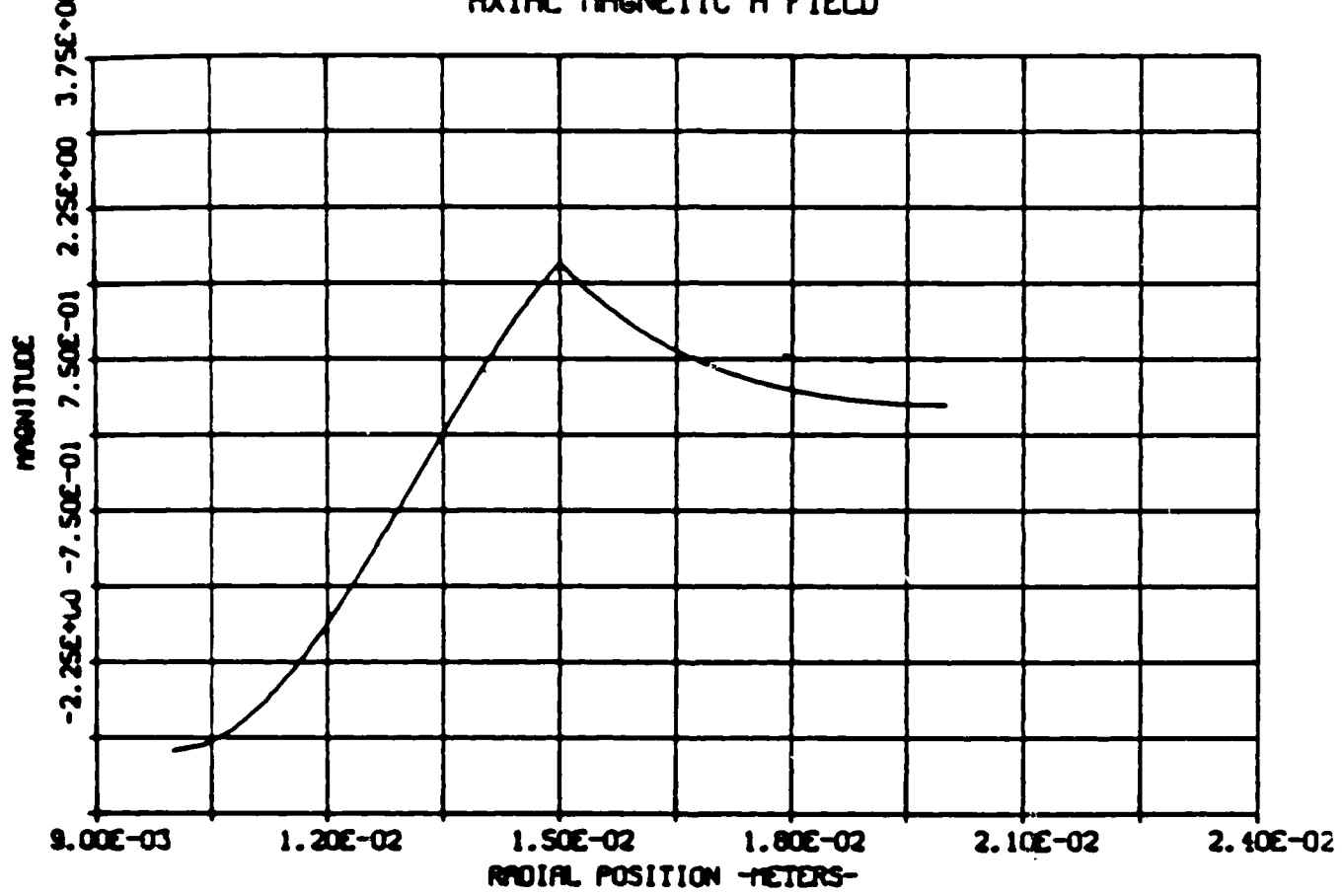


Fig. 17. $TE_{0,1}$ mode at 32 GHz, $ER1 = 2$; E_r component.

TE 01 MODE AT 32.0 GHZ, ER1-1

AXIAL MAGNETIC H FIELD

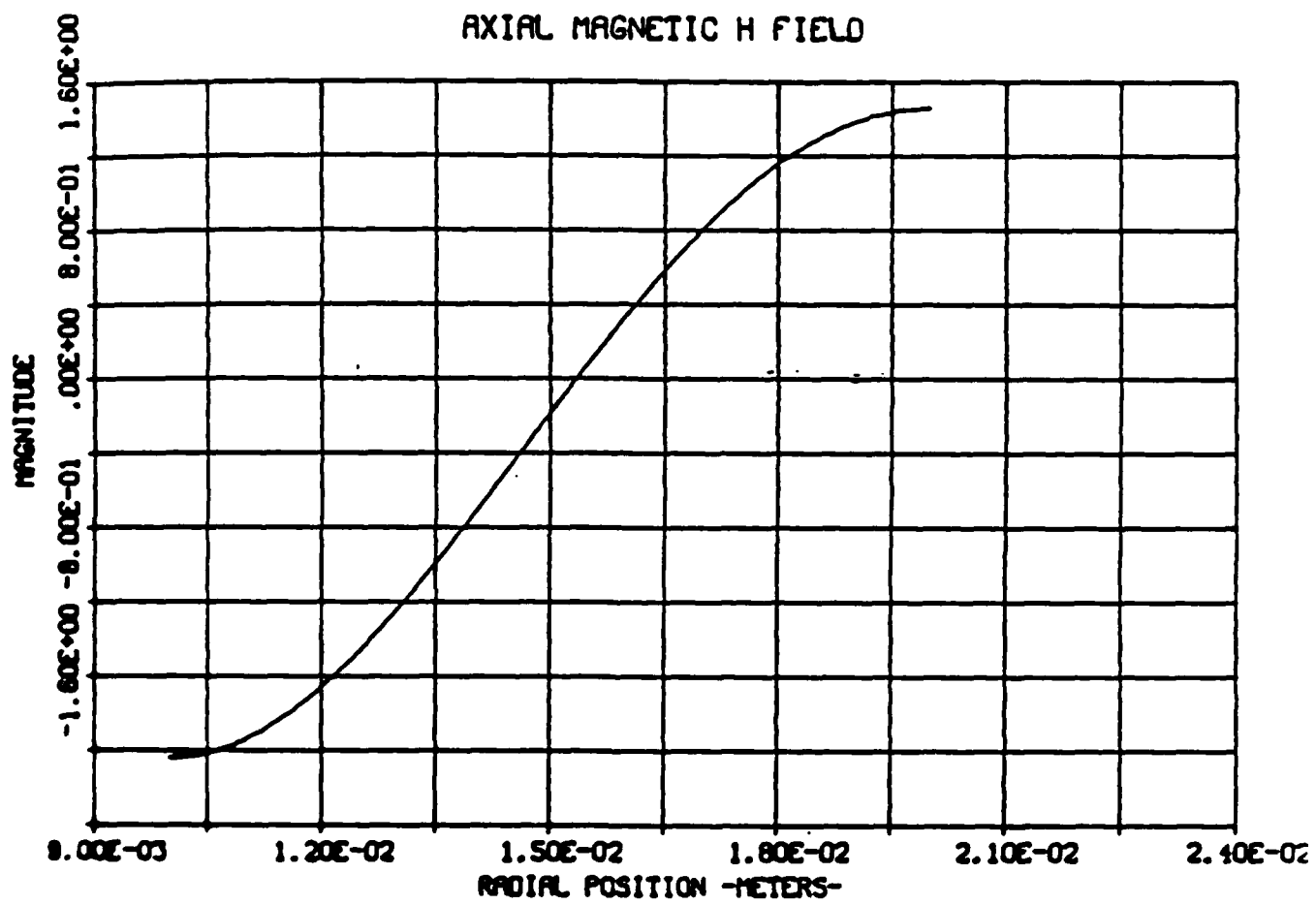


Fig. 18. $TE_{0,1}$ mode at 32 GHz, ER1 = 2; H_z component.

TE 01 MODE AT 32.0 GHZ, ER1-2

POYNITING'S VECTOR- ETMR

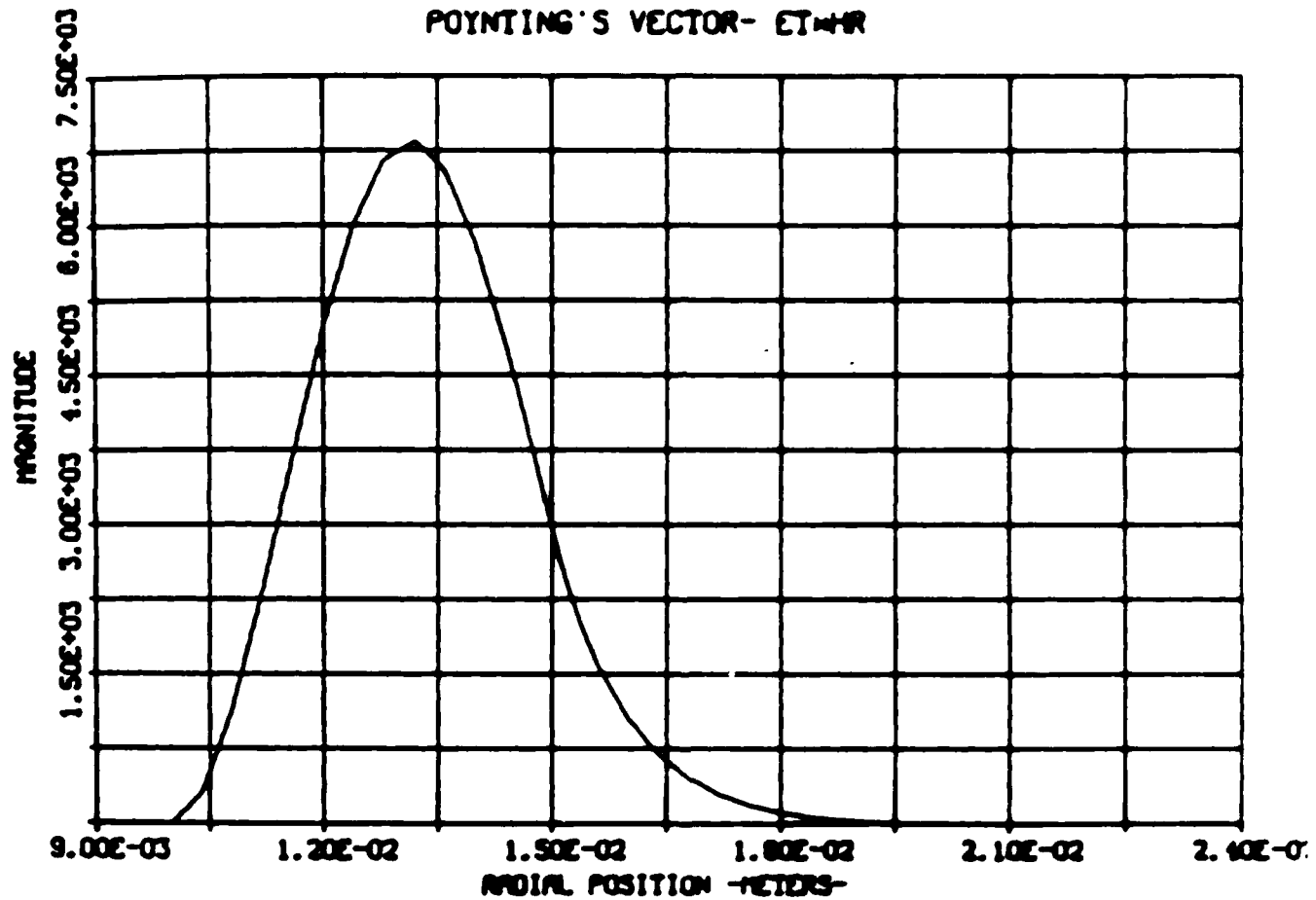


Fig. 19. TE_{0,1} mode at 32 GHz, ER1 = 2; H_z component.

IE 01 MODE AT 32.0 GHZ. ER1-1

POYNITING'S VECTOR- ET=HR

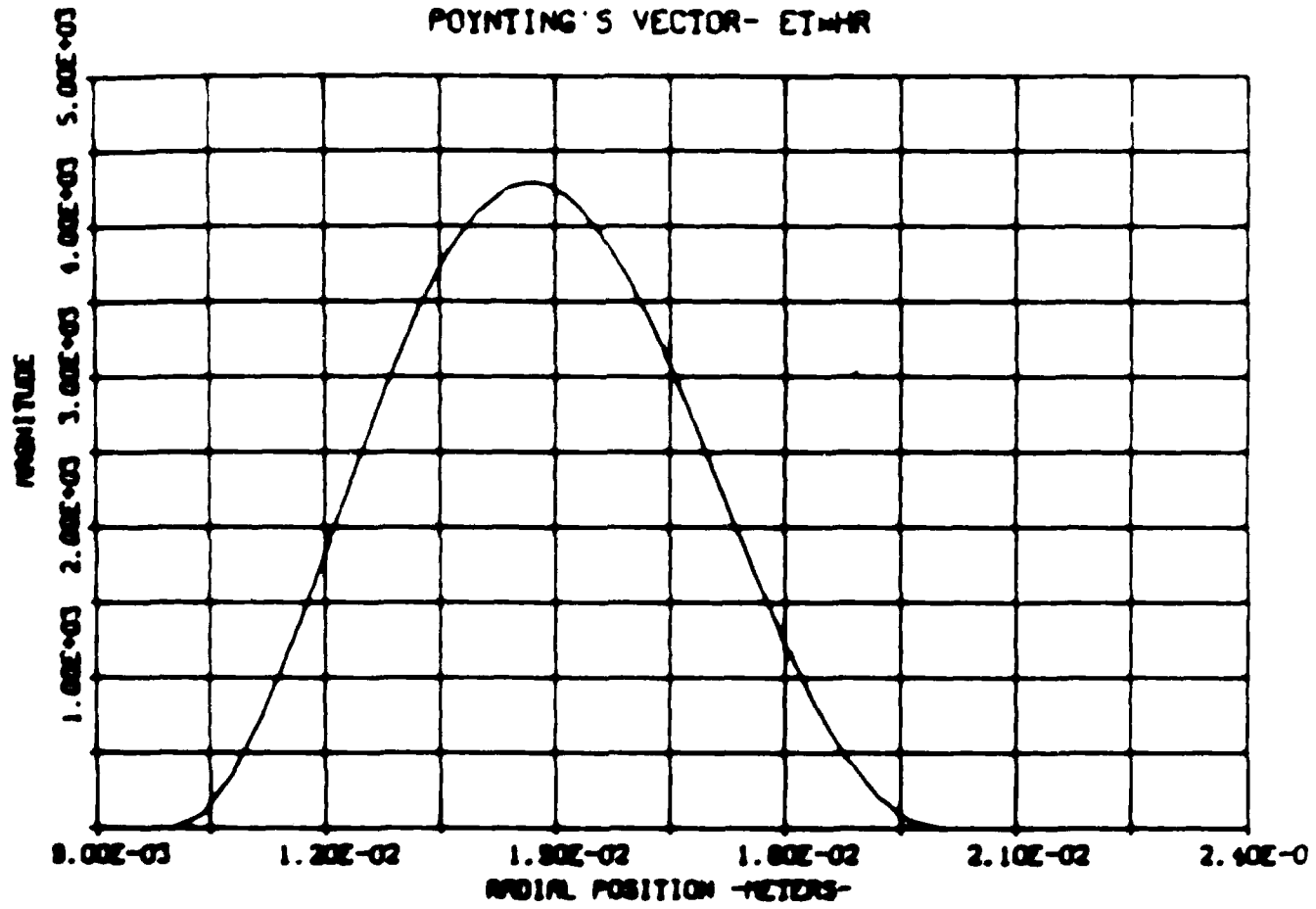


Fig. 20. $TE_{0,1}$ mode at 32 GHz, $ER1 = 2$; Poynting's vector $E_r H_r$.

5.3 TEM Mode

Comparing Figs. 21 (case 1) and 22 (case 2) for the E_r component reveals that a greater percentage of the field lies in region 1 for case 2. The appropriate discontinuous jump at $r = b$ is satisfied for case 2.

Theoretically, the TEM mode has no E_z (or H_z) component when $\epsilon_{r1} = \epsilon_{r2} = 1$. Figure 23 shows values for the air filled case which, although not exactly zero, are very small and reflect the accuracy of the program. But, the values for Fig. 24 show unquestioned existence of the E_z component when $\epsilon_{r1} = 2$. Here, a peak is reached at the dielectric interface ($r = b$) where the field is continuous, but its first derivative with respect to r is discontinuous. As required, E_z is zero at $r = a$ and $r = c$.

The H_r component shows an increased concentration in region 1 (Fig. 25) relative to that of the air filled case (Fig. 26). At $r = b$, H_r is continuous, although its first derivative with respect to r is discontinuous.

Poynting's vector shows how the mode has evolved into propagating almost entirely in region 1 (Fig. 27) compared to that of the air filled case (Fig. 28).

TEM MODE AT 32.0 GHZ, ERI=1

RADIAL ELECTRIC E FIELD

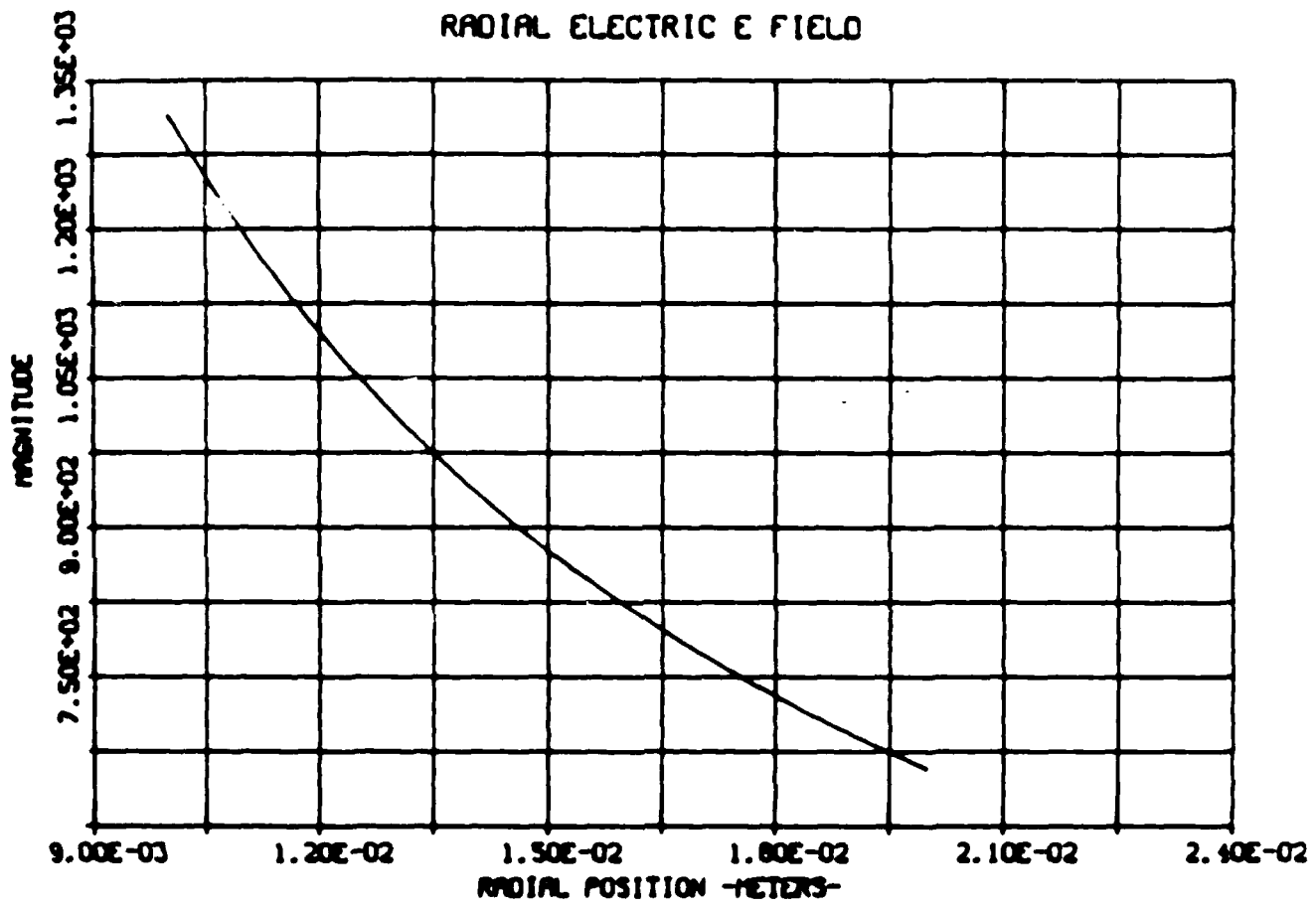


Fig. 21. TEM mode at 32 GHz, ERI = 1; E_r component.

TEM MODE AT 32.0 GHZ, ER1-2

RADIAL ELECTRIC E FIELD

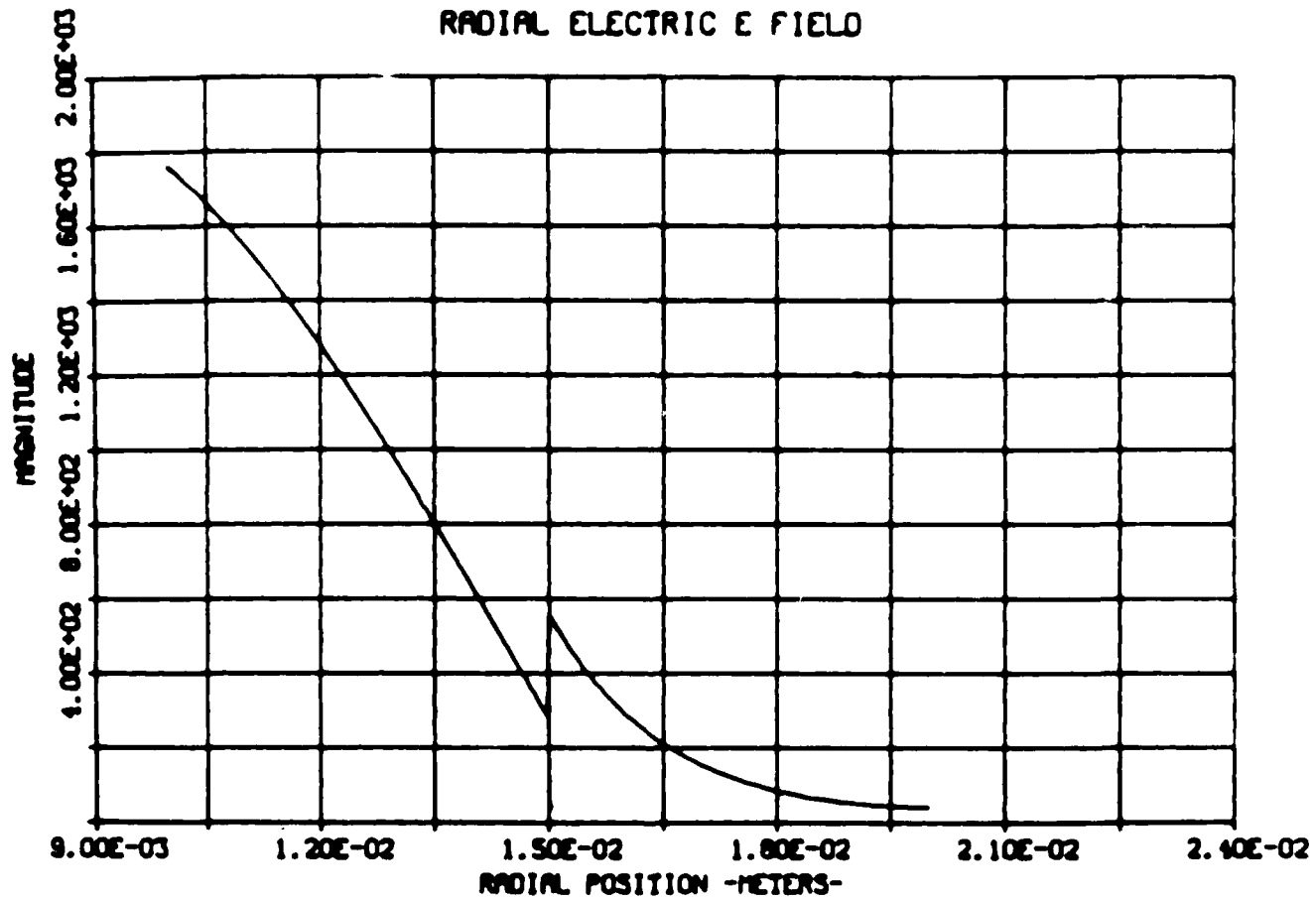


Fig. 22. TEM mode at 32 GHz. ER1 = 1; E_r component.

TEM MODE AT 32.0 GHz, ERI=1

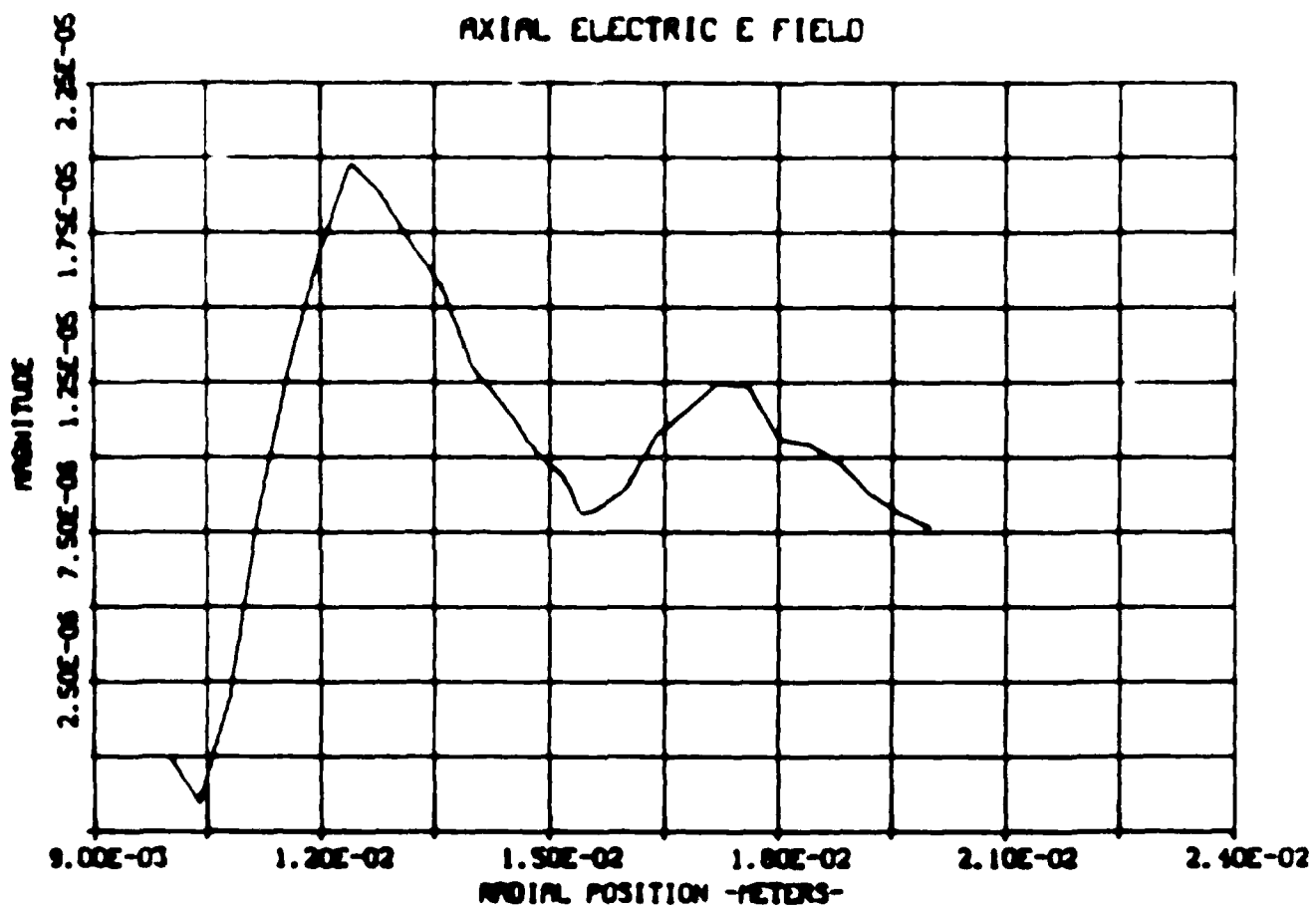


Fig. 23. TEM mode at 32 GHz, ERI = 1; H_ϕ component.

TEM MODE AT 32.0 GHZ, ER1-2

AXIAL ELECTRIC E FIELD

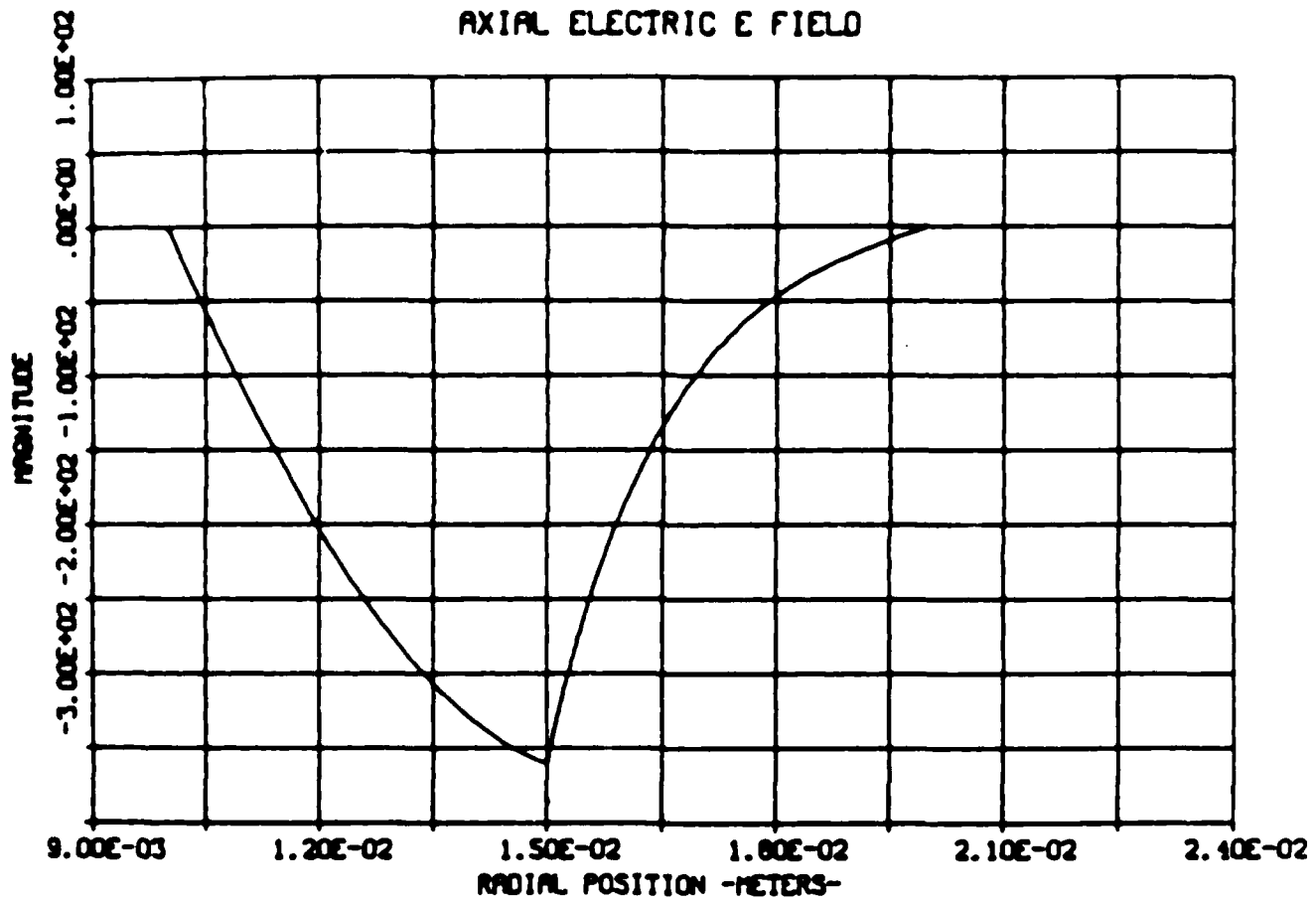


Fig. 24. TEM mode at 32 GHz, ER1 = 1; Poynting's vector $E_r H_\phi$.

TEM MODE AT 32.0 GHZ, ER1-2

AZIMUTHAL MAGNETIC H FIELD

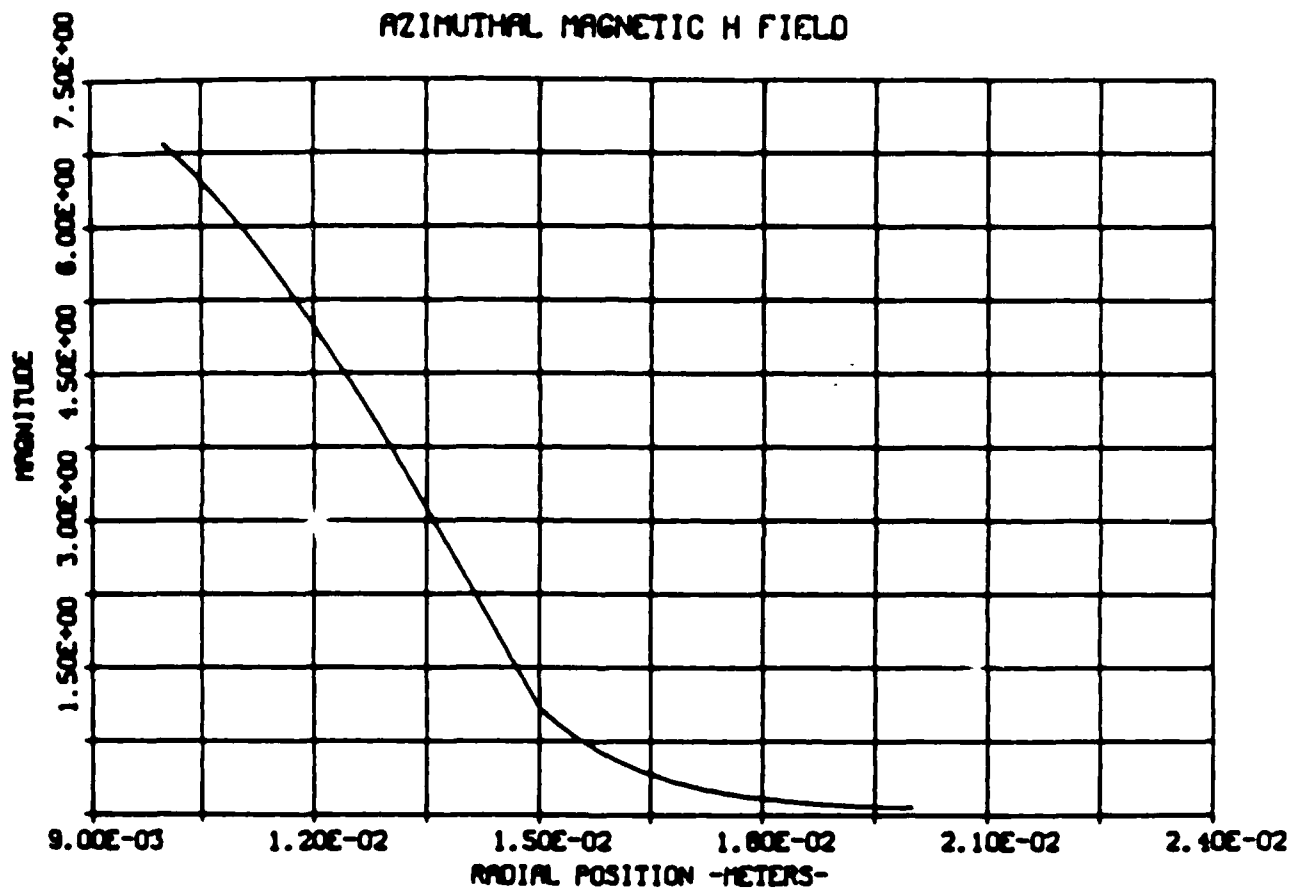


Fig. 25. TEM mode at 32 GHz, ER1 = 2; E_r component.

TEM MODE AT 32.0 GHz, ER1-1

AZIMUTHAL MAGNETIC H FIELD

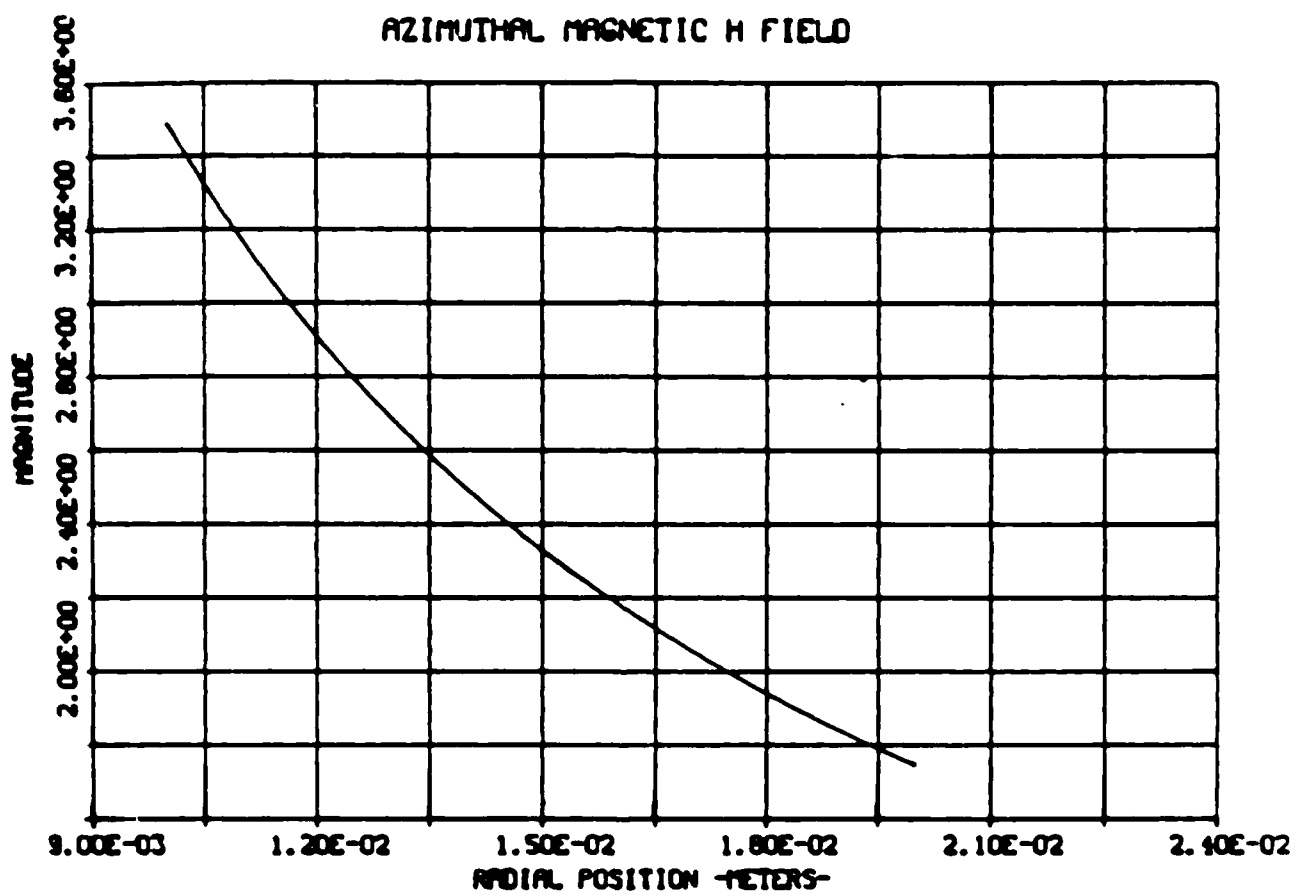


Fig. 26. TEM mode at 32 GHz, ER1 = 2; E_z component.

TEM MODE AT 32.0 GHZ, ER1-2

POYNITING'S VECTOR- ER=H

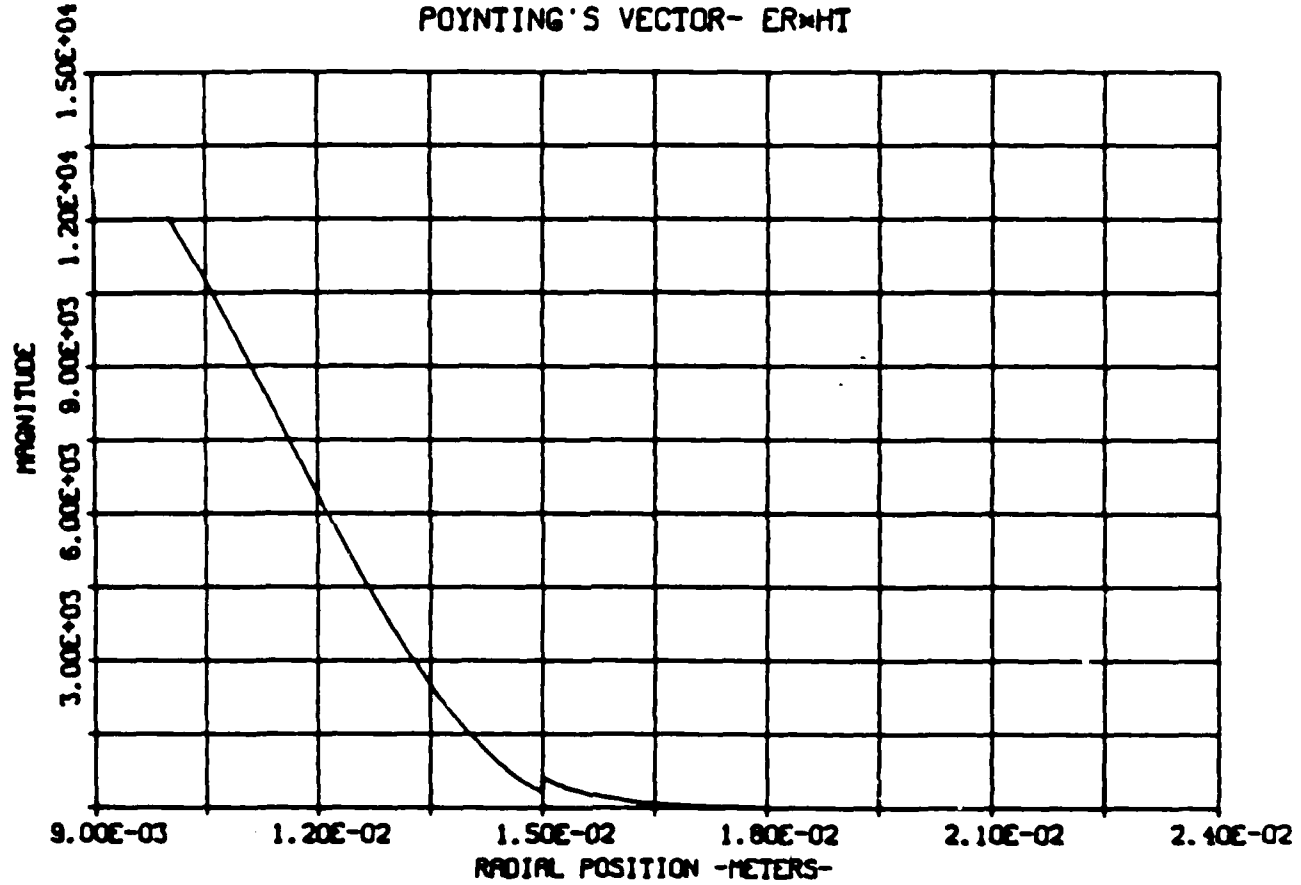


Fig. 27. TEM mode at 32 GHz, ER1 = 2; H_z component.

TEM MODE AT 32.0 GHZ, ER1-1

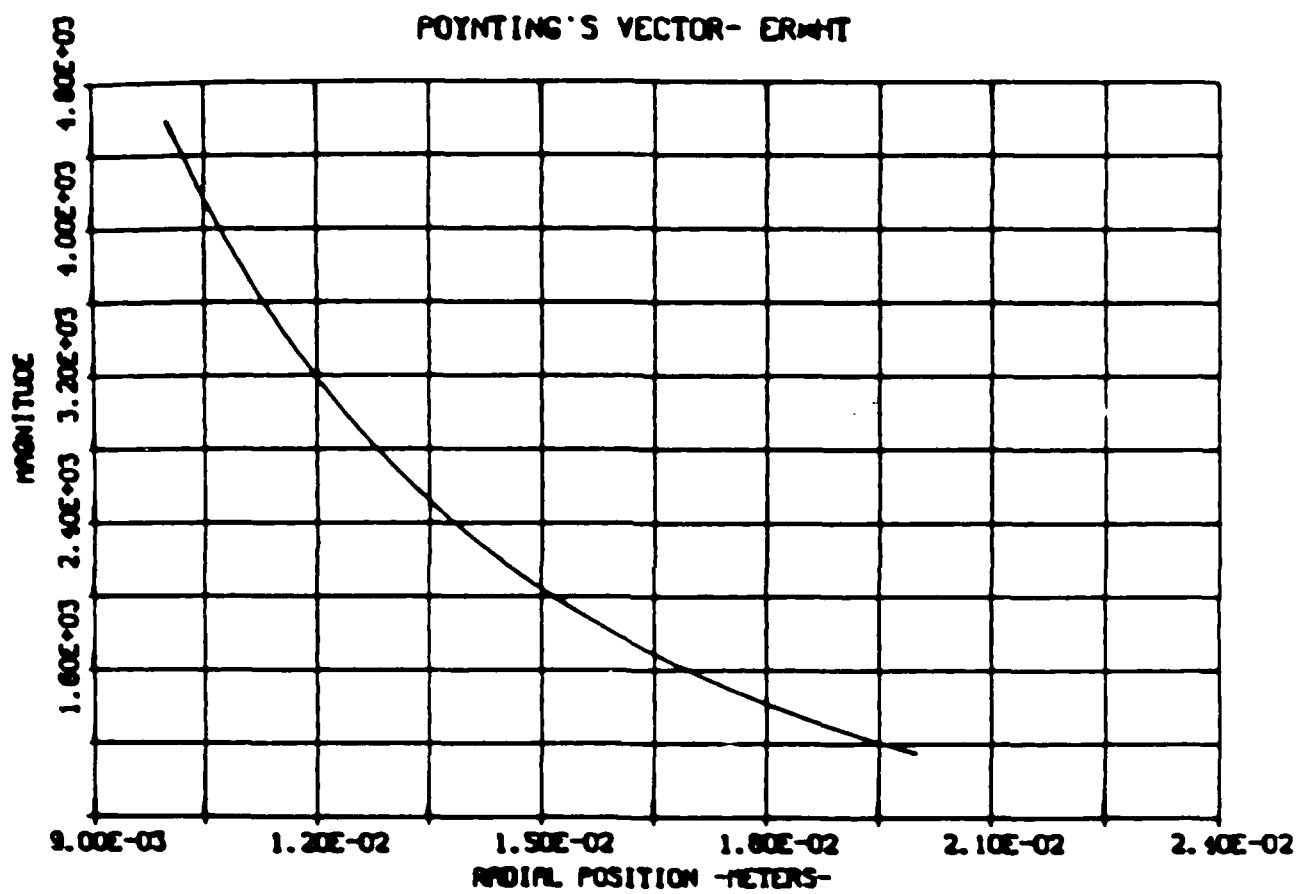


Fig. 28. TEM mode at 32 GHz, ER1 = 2; Poynting's vector $E_r H_\phi$.

5.4 $TM_{1,1}$ ($EH_{1,1}$) Mode

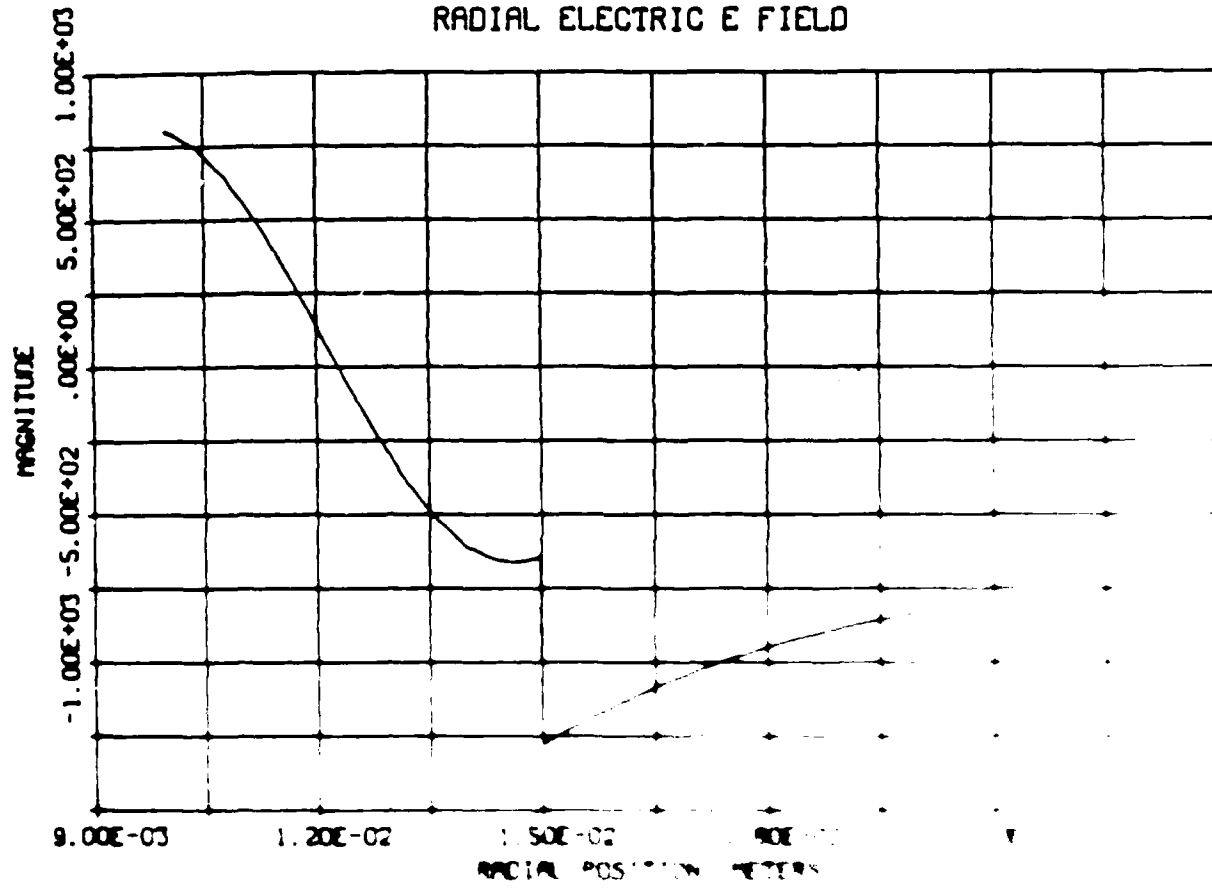
Here, there are two sets of answers when $\epsilon_{r1} = 2$ signifying a split of the $TM_{1,1}$ mode upon hybridization. The plots for the hybridized modes are labeled $EH_{1,1}$ mode 1 and $EH_{1,1}$ mode 2 corresponding to the k_z values of 678.27 and 815.32, respectively. In the discussion, we will simply refer to them as mode 1 and mode 2.

The E_r component for modes 1 and 2 (Figs. 29 and 30, respectively) undergoes the required jump at $r = b$ by doubling in magnitude. Both modes have one zero crossing, as with the $TM_{1,1}$ mode (Fig. 31). But, mode 1 has its field distribution concentrated in region 2, while mode 2 has its field almost entirely in region 1. Note that the E_r component for mode 1 is from one to two orders of magnitude larger than mode 2 over most of the radial cross section.

The azimuthal electric field, E_ϕ , for mode 1 (Fig. 32) has evolved into two positive peaks compared to the one positive peak for mode 2 (Fig. 33). Both modes 1 and 2 have their fields concentrated in region 1, as with the $TM_{1,1}$ mode (Fig. 34). In all the plots, E_ϕ is continuous at $r = b$ and is zero at $r = a$ and $r = c$. We further note that the E_ϕ component for mode 2 is one to two orders of magnitude larger than mode 1 over the radial cross section.

EH 11 MODE 1 AT 32.0 GHZ, ER1-2

RADIAL ELECTRIC E FIELD



RD-R182 775

ELECTROMAGNETIC DISPERSION OF A COAXIAL WAVEGUIDE WITH
AN ARBITRARY RADIUS (U) UTAH UNIV SALT LAKE CITY DEPT
OF ELECTRICAL ENGINEERING A M PUZELLA APR 87

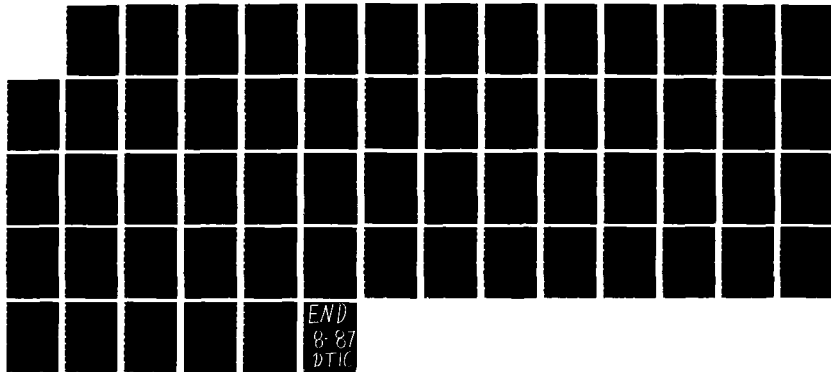
2/2

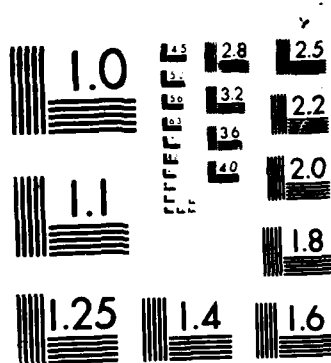
UNCLASSIFIED

UTEC-MD-86-043 RADC-TR-87-36

F/G 9/1

NL





MICROCOPY RESOLUTION TEST CHART
NATIONAL BUREAU OF STANDARDS 1963-A

EH 11 MODE 2 AT 32.0 GHZ, ER1-2

RADIAL ELECTRIC E FIELD

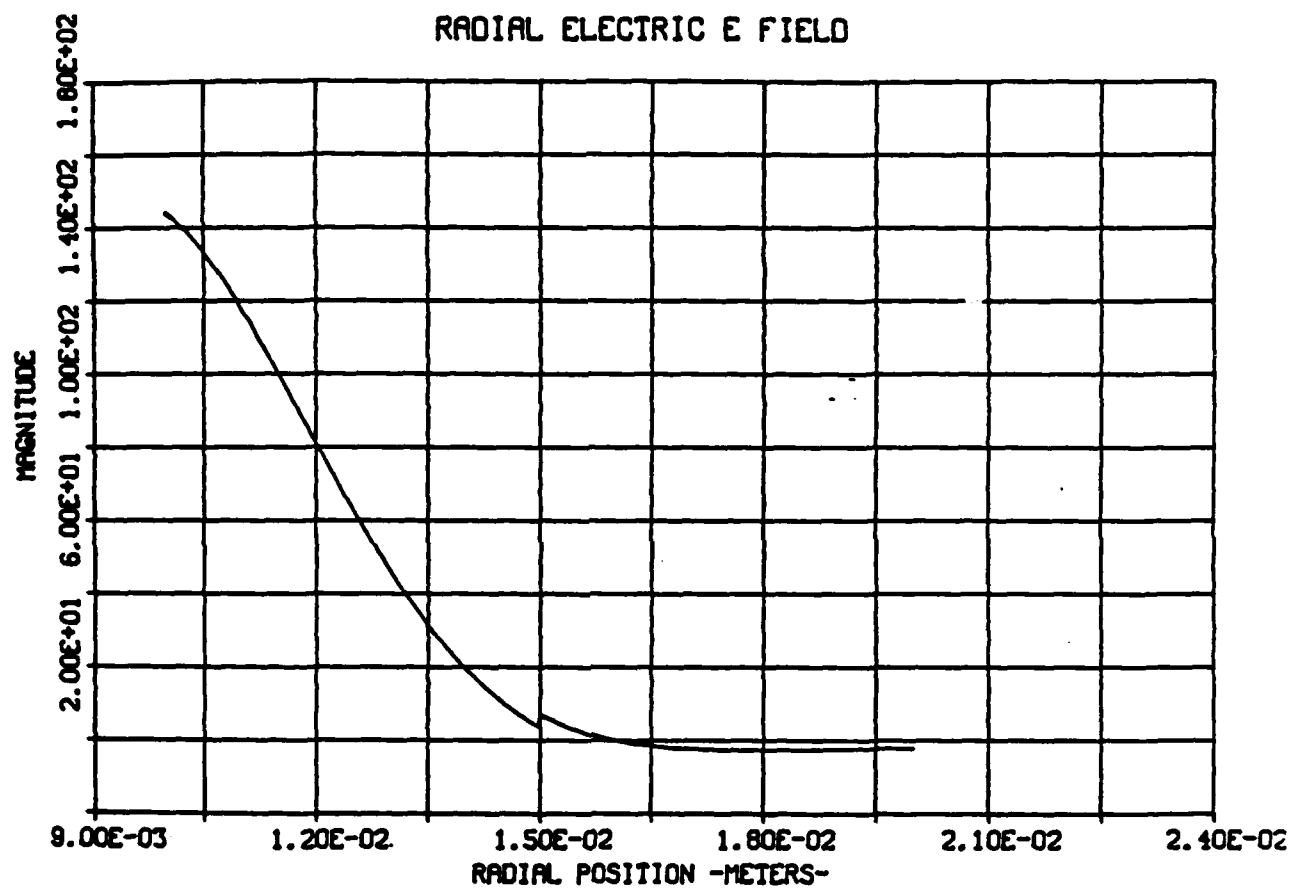


Fig. 30. $TM_{1,1}$ mode at 32 GHz, $ER1 = 1$; E_ϕ component.

TM 11 MODE AT 32.0 GHZ, ER1-1

RADIAL ELECTRIC E FIELD

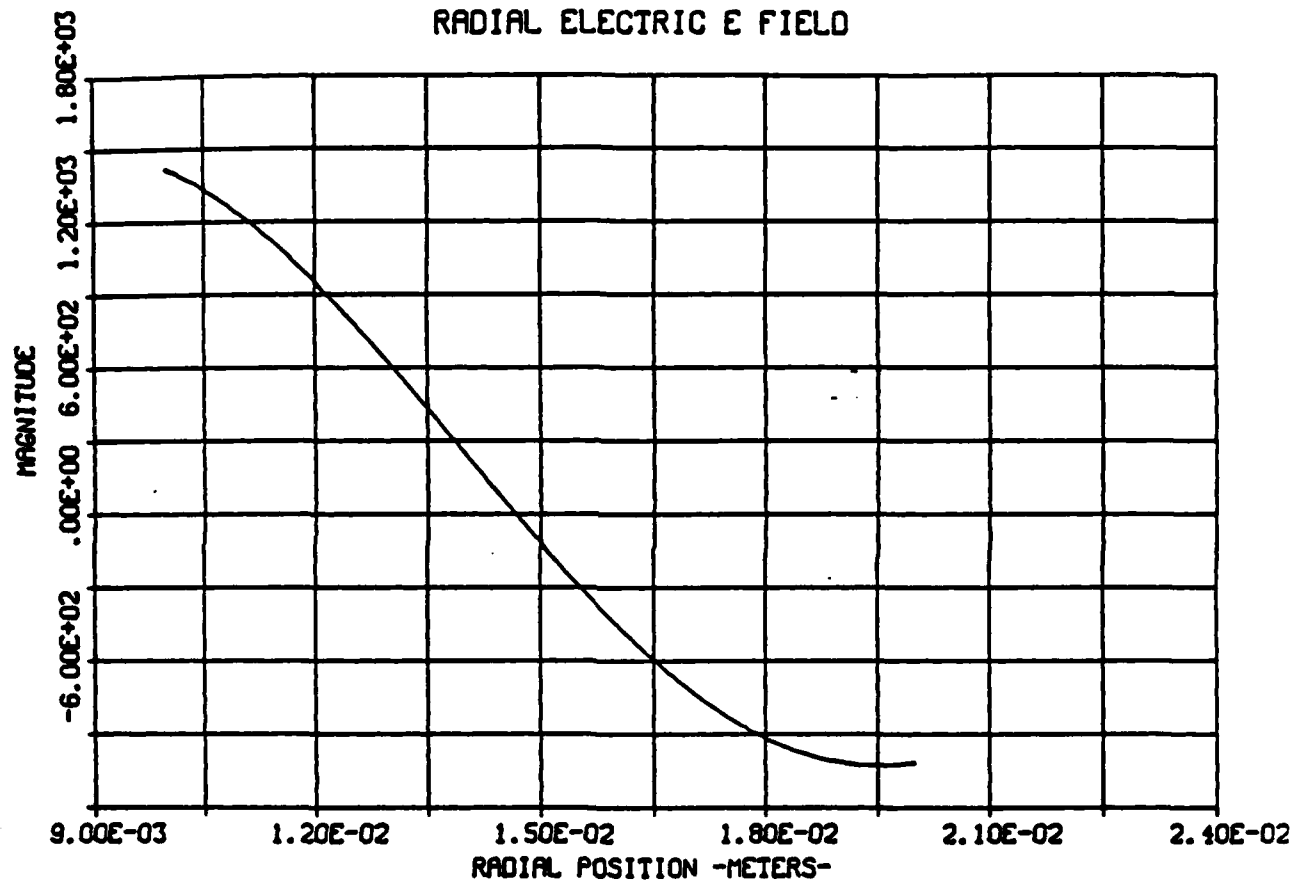


Fig. 31. $TM_{1,1}$ mode at 32 GHz. $ER1 = 1$; E_z component.

EH 11 MODE 1 AT 32.0 GHZ, ER1-2

AZIMUTHAL ELECTRIC E FIELD

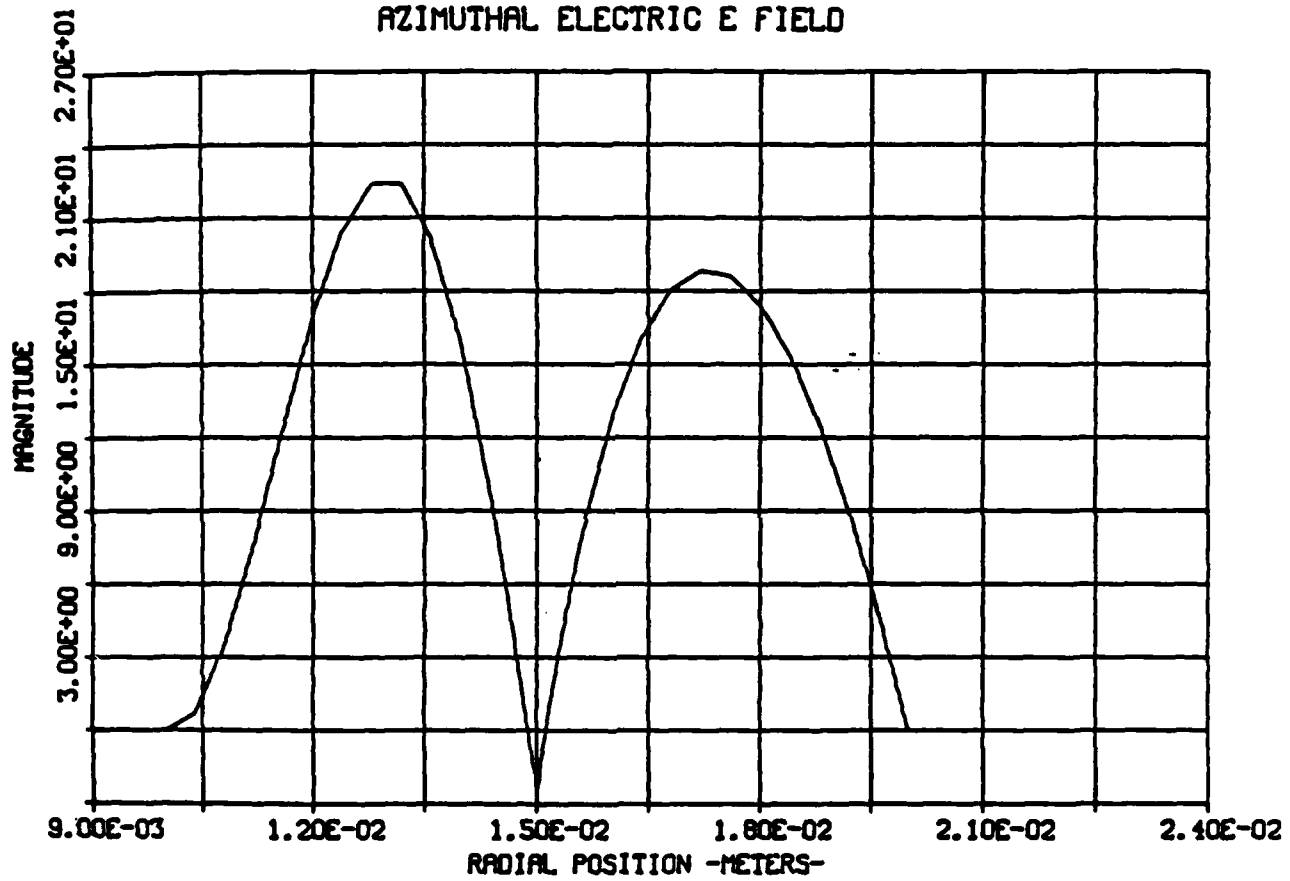


Fig. 32. $TM_{1,1}$ mode at 32 GHz, $ER1 = 1$; H_r component.

EH 11 MODE 2 AT 32.0 GHZ, ER1-2

AZIMUTHAL ELECTRIC E FIELD

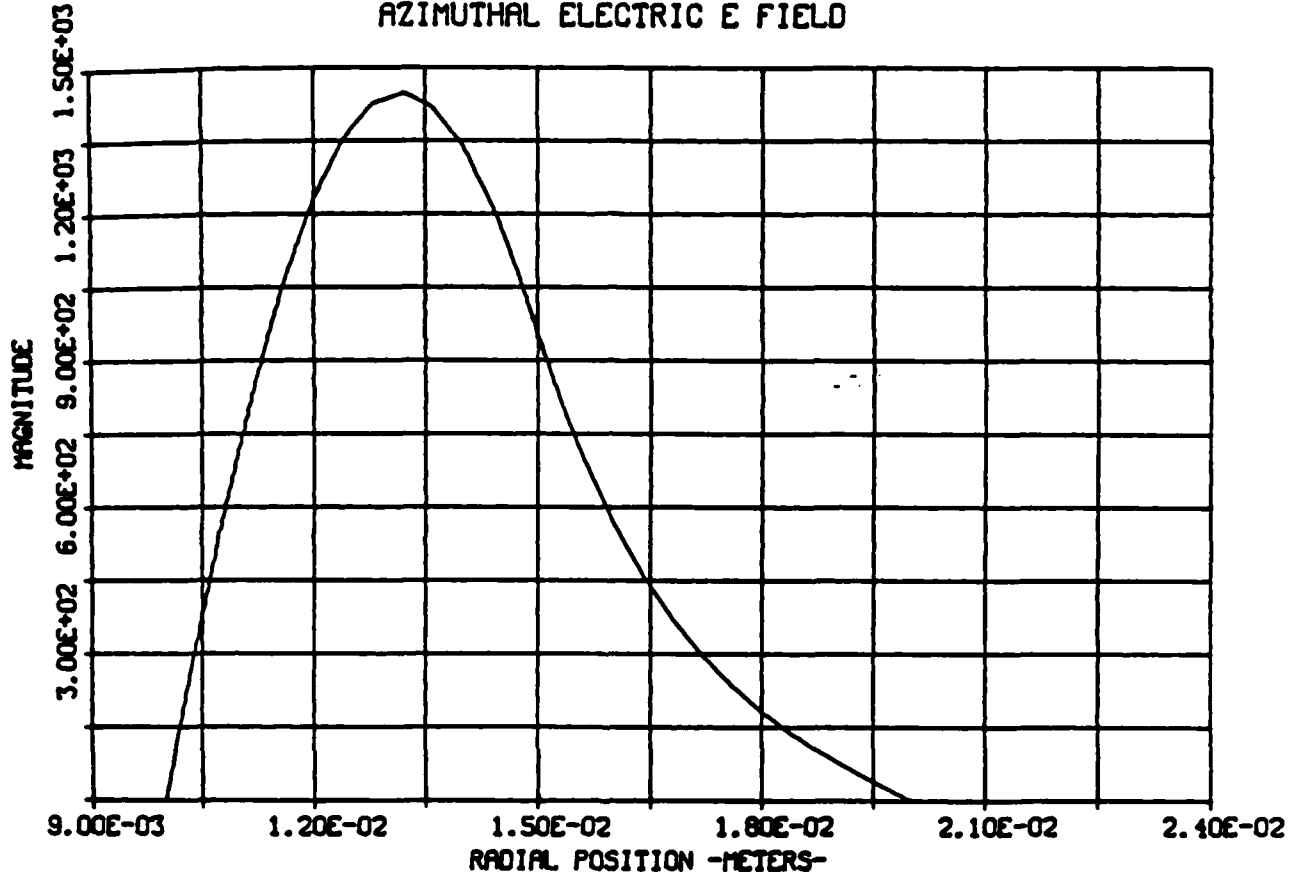


Fig. 33. $TM_{1,1}$ mode at 32 GHz, $ER1 = 1$; H_ϕ component.

TM 11 MODE AT 32.0 GHZ, ER1-1

AZIMUTHAL ELECTRIC E FIELD

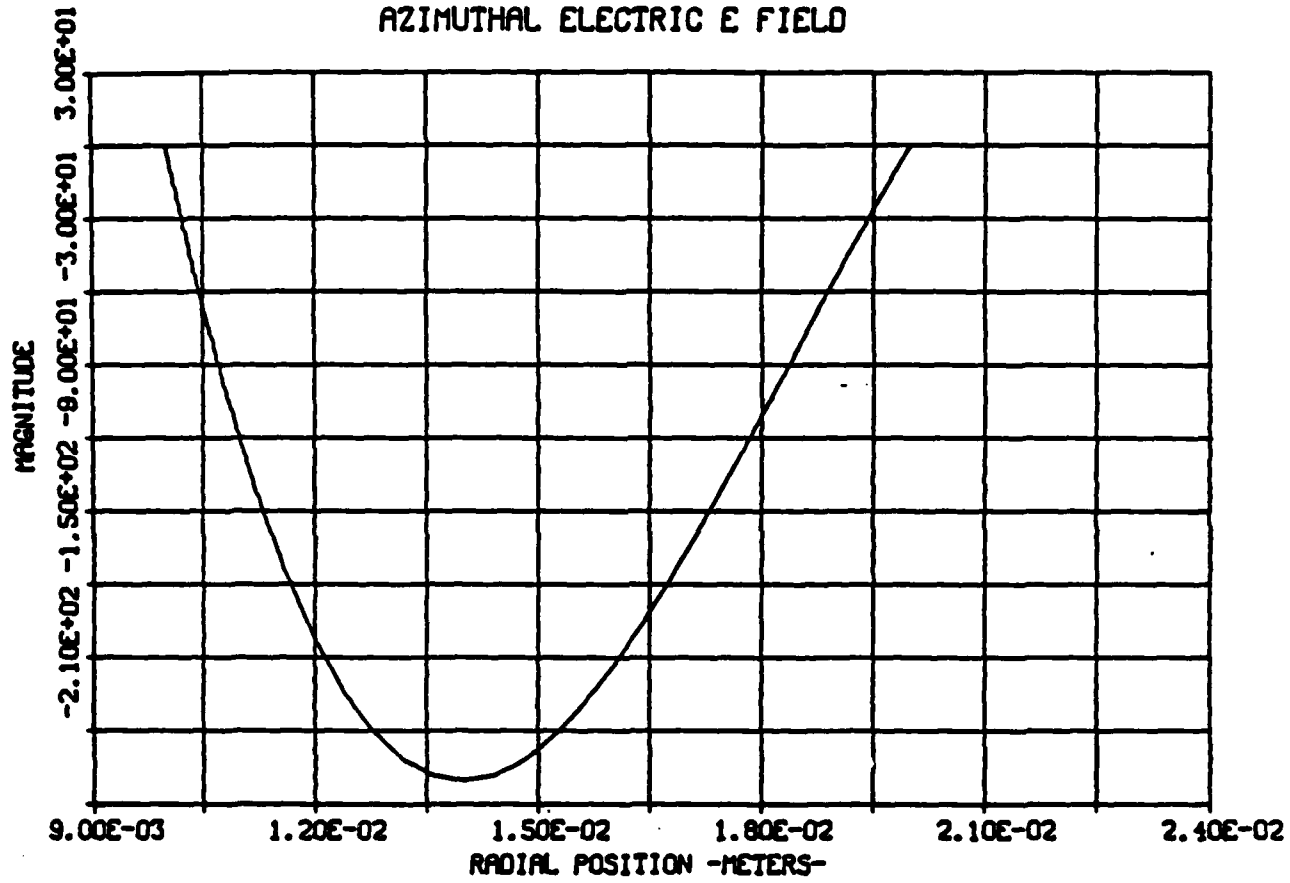


Fig. 34. $TM_{1,1}$ mode at 32 GHz, $ER1 = 1$; H_z component.

The E_z component shows that for both modes 1 and 2 (Figs. 35 and 36, respectively), the field resides primarily in region 1. Note that mode 1 goes through a zero crossing. Along with the $TM_{1,1}$ mode (Fig. 37), all three plots satisfy the boundary condition that E_z be equal to zero at $r = a$ and $r = c$ as well as being continuous at $r = b$. We again point out that mode 1 is an order of magnitude larger than mode 2 over the radial cross section. This is consistent with the fact that the magnitude of a (Eq. 49) for mode 1 is less than that for mode 2, resulting in E_z being larger for mode 1.

Figures 38, 39, and 40 show the H_r component for the $TM_{1,1}$ mode, mode 1 and mode 2, respectively. We note the field distribution having an increased concentration in region 1 for modes 1 (which goes through a zero) and 2. The H_r component for mode 2 is as much as two orders of magnitude larger than mode 1 over the radial cross section. At $r = a$ and $r = c$, H_r is equal to zero for all three modes, as required.

As with the H_r component, H_ϕ shows a majority of the field residing in region 1 for modes 1 and 2 (Figs. 41 and 42, respectively). Note that mode 2 does not have a zero crossing unlike mode 1 and the $TM_{1,1}$ mode (Fig. 43). All three modes are continuous at $r = b$. Here, the H_ϕ component for mode 1 is an order of magnitude larger than mode 2 over the radial cross section.

EH 11 MODE 1 AT 32.0 GHZ, ER1-2

AXIAL ELECTRIC E FIELD

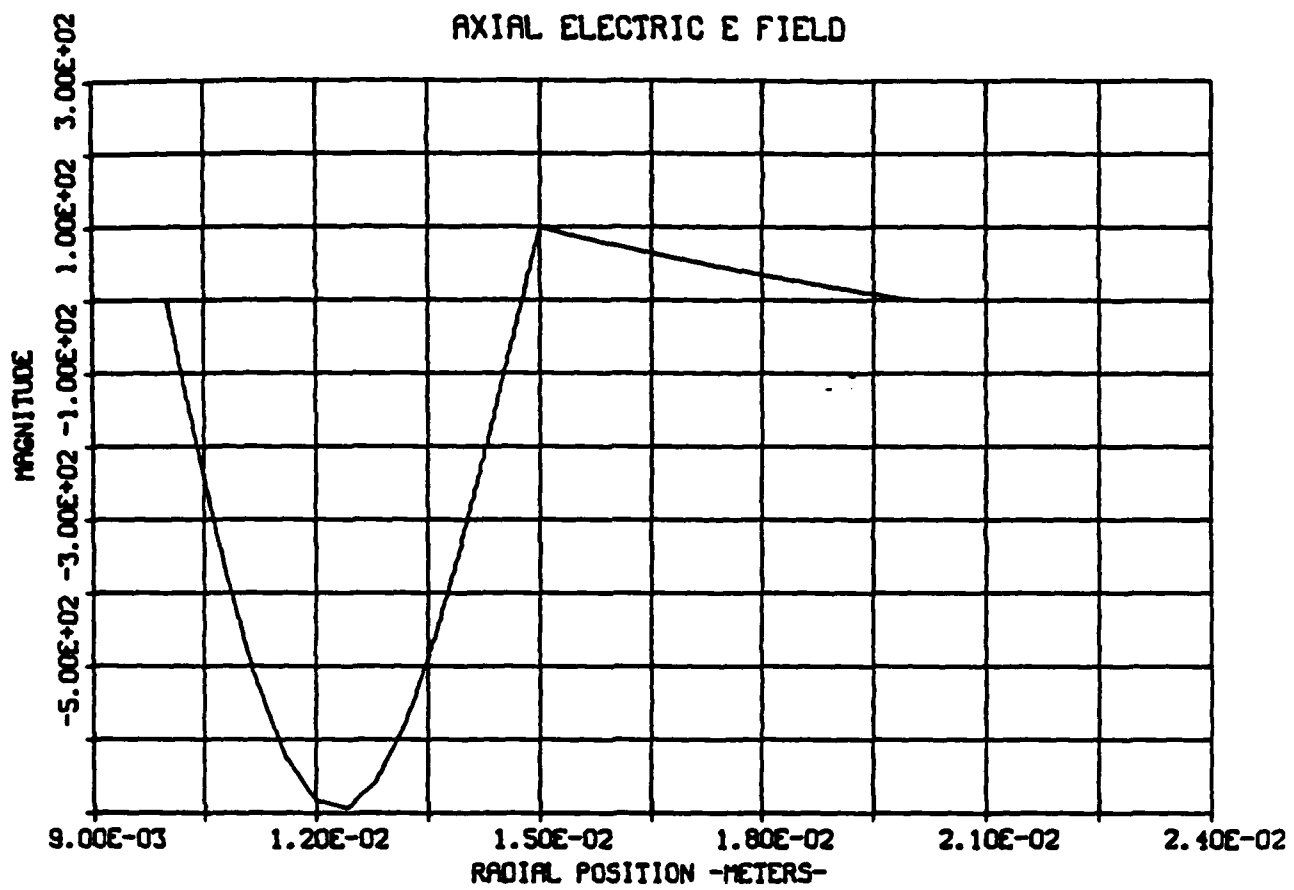


Fig. 35. $TM_{1,1}$ mode at 32 GHz, $ER1 = 1$; Poynting's vector $E_r H_\phi$.

EH 11 MODE 2 AT 32.0 GHZ, ER1-2

AXIAL ELECTRIC E FIELD

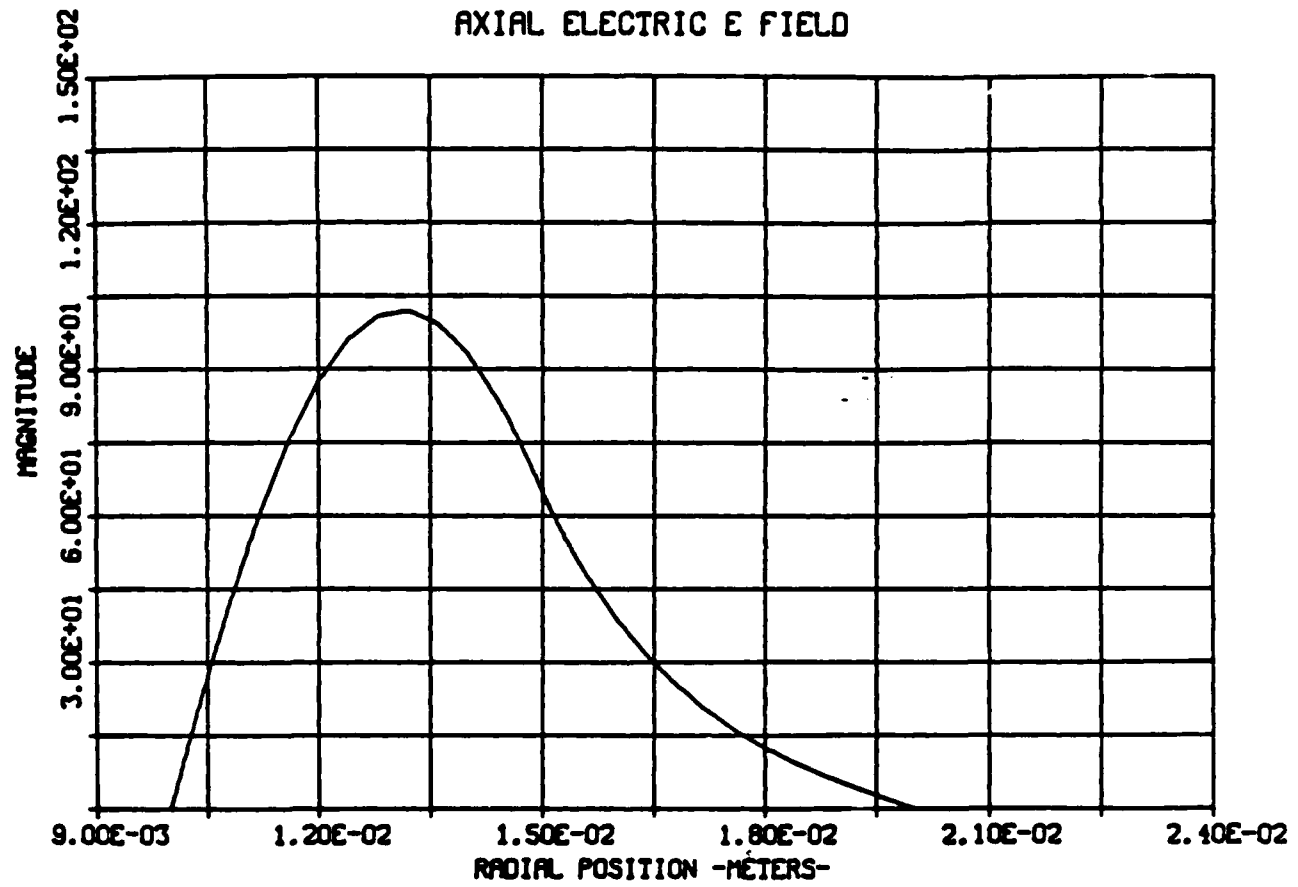


Fig. 36. $TM_{1,1}$ mode at 32 GHz, $ER1 = 1$; Poynting's vector E_H_T .

TM 11 MODE AT 32.0 GHZ, ER1-1

AXIAL ELECTRIC E FIELD

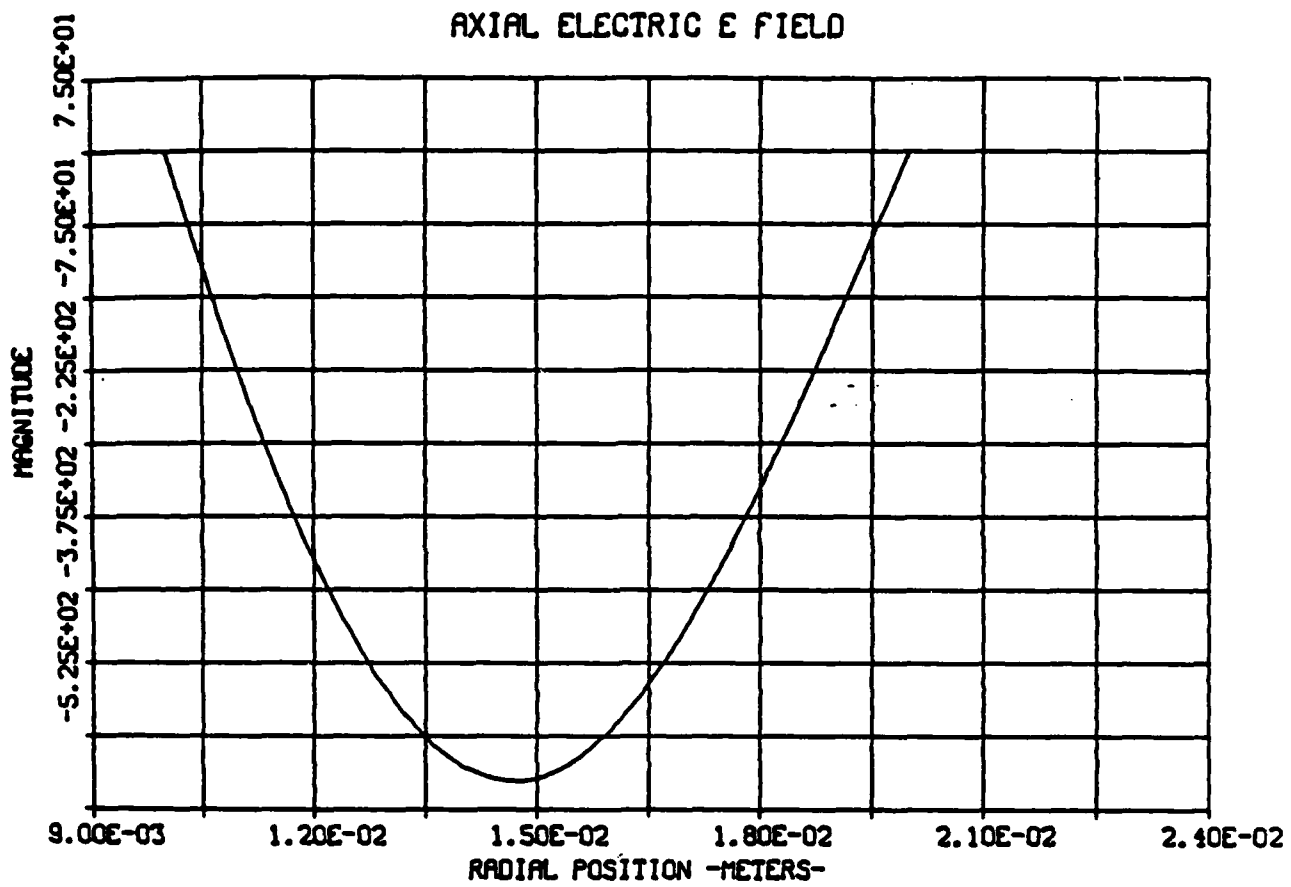


Fig. 37. EH_{1,1} mode 1 at 32 GHz, ER1 = 2; E_r component.

TM 11 MODE AT 32.0 GHZ, ER1-1

RADIAL MAGNETIC H FIELD

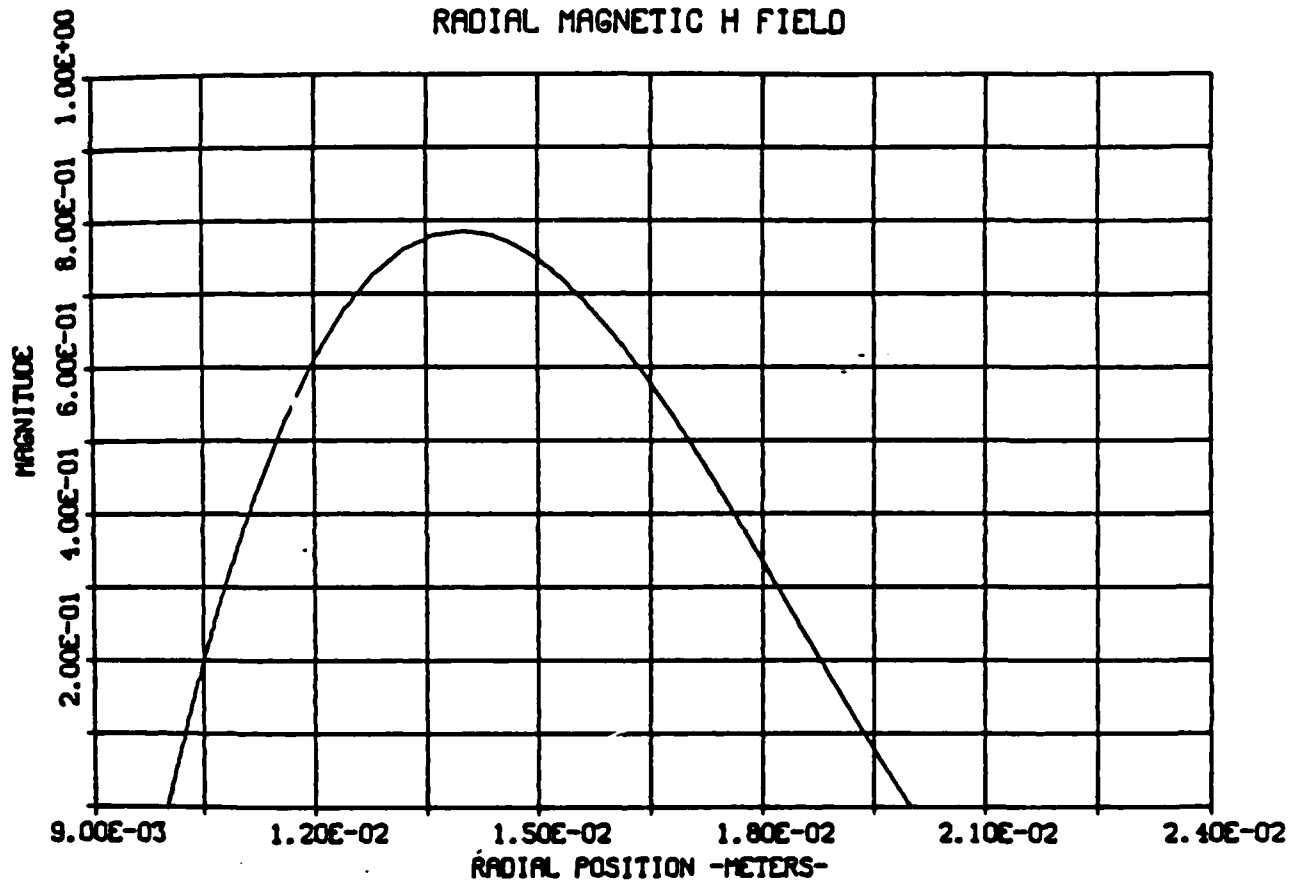


Fig. 38. EH_{1,1} mode 1 at 32 GHz, ER1 = 2; E_φ component.

EH 11 MODE 1 AT 32.0 GHZ, ER1-2

RADIAL MAGNETIC H FIELD

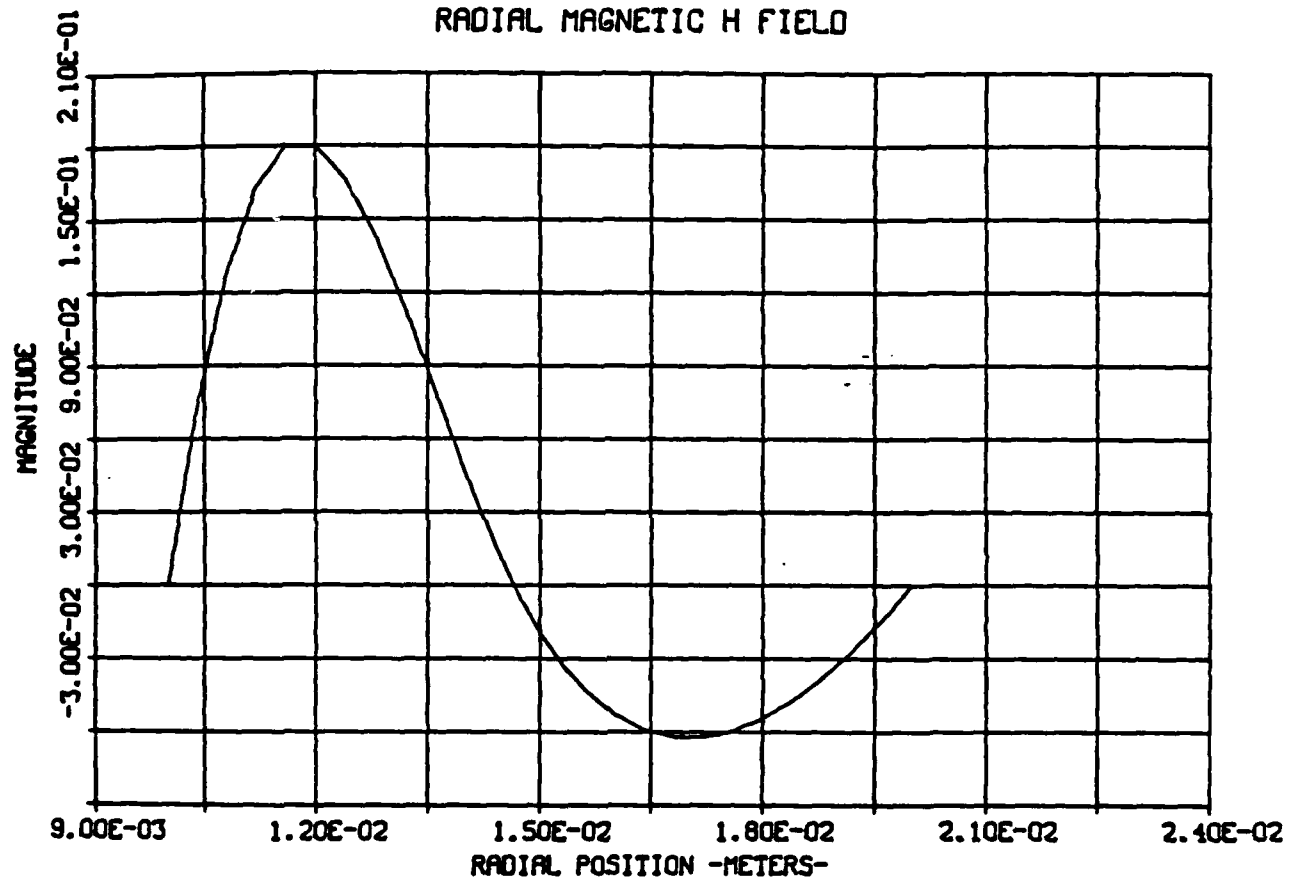


Fig. 39. $EH_{1,1}$ mode 1 at 32 GHz, $ER1 = 2$; E_z component.

EH 11 MODE 2 AT 32.0 GHZ, ER1-2

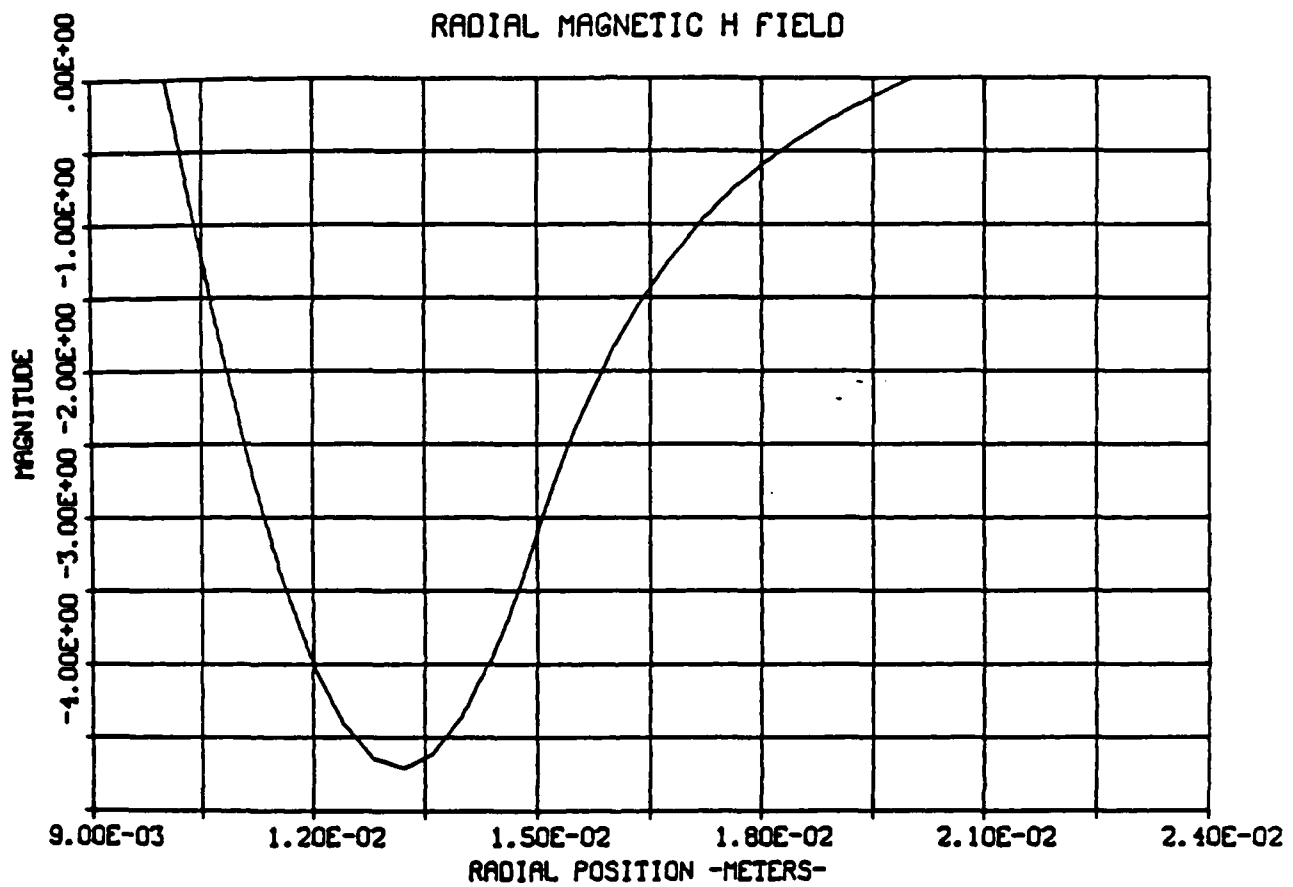


Fig. 40. EH_{1,1} mode 1 at 32 GHz, ER1 = 2; H_r component.

EH 11 MODE 1 AT 32.0 GHZ, ER1-2

AZIMUTHAL MAGNETIC H FIELD

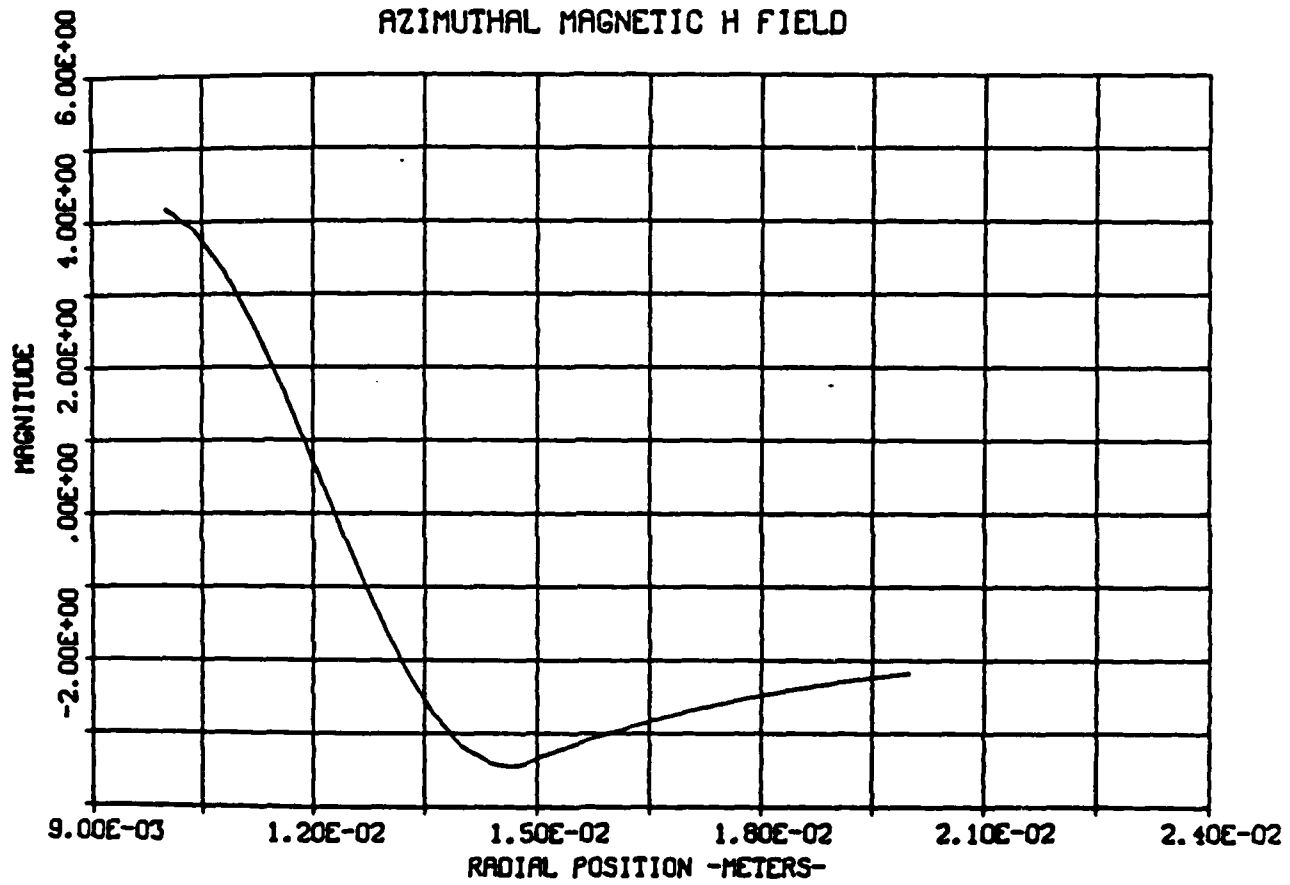


Fig. 41. $EH_{1,1}$ mode 1 at 32 GHz, ER1 = 2; H_ϕ component.

EH 11 MODE 2 AT 32.0 GHZ, ER1-2

AZIMUTHAL MAGNETIC H FIELD

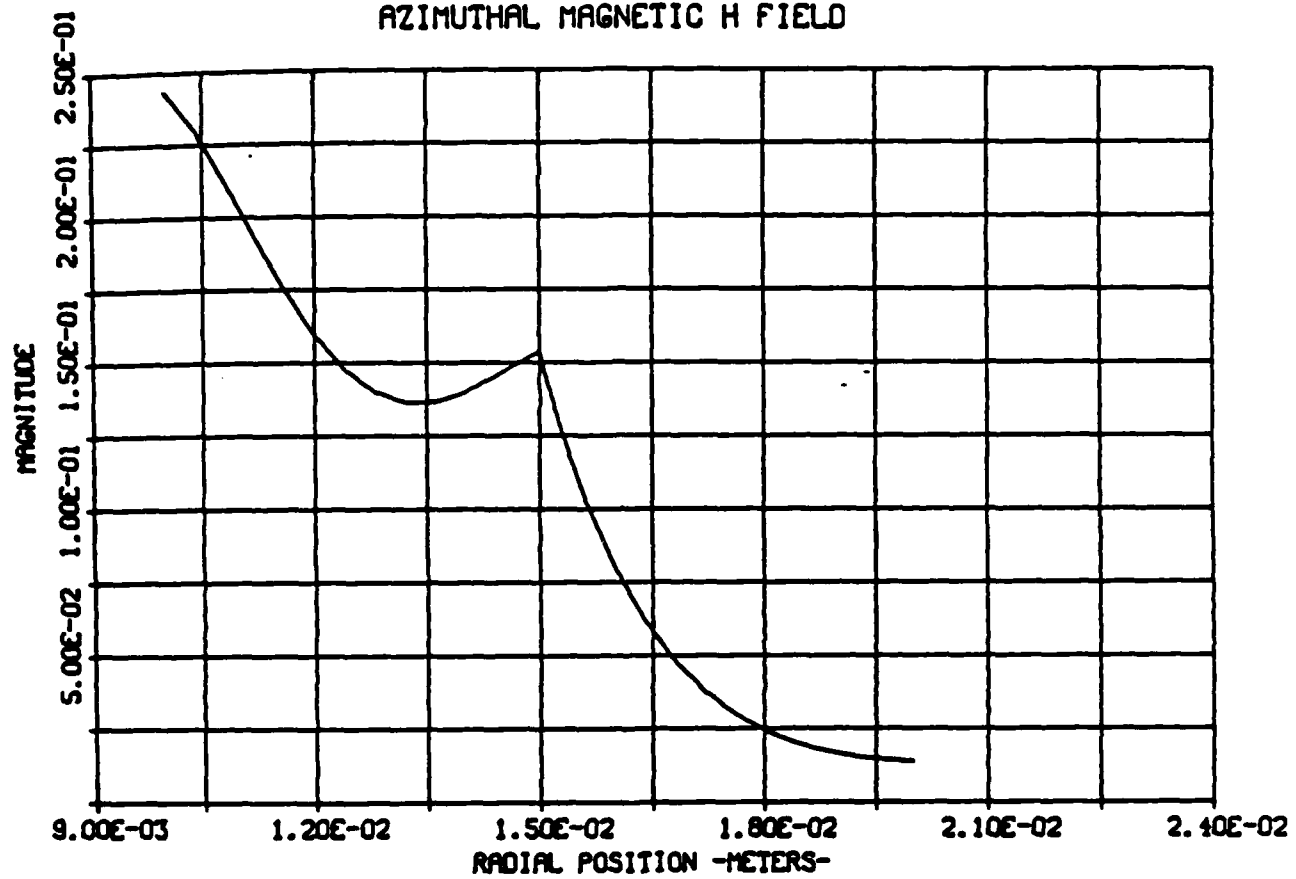


Fig. 42. $EH_{1,1}$ mode 1 at 32 GHz, $ER1 = 2$; H_z component.

TM 11 MODE AT 32.0 GHZ, ER1-1

AZIMUTHAL MAGNETIC H FIELD

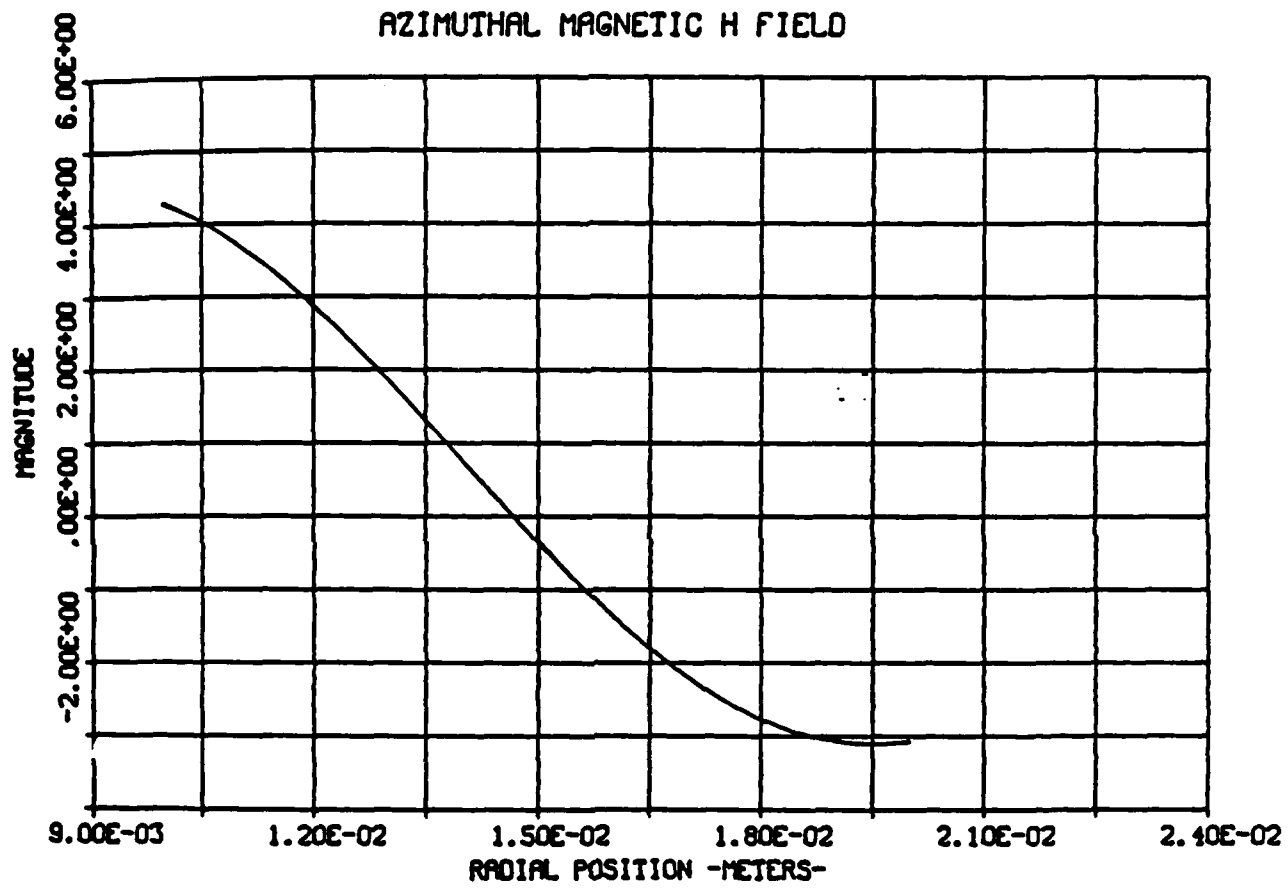


Fig. 43. EH_{1,1} mode 1 at 32 GHz, ER1 = 2; Poynting's vector E_rH_φ.

The fact that the magnitude of α is larger for mode 2 than for mode 1 is evidenced in the H_z component (Figs. 44 and 45, respectively). The field distributions are both concentrated in region 1, but the magnitude of H_z for mode 2 is larger. Along with the $TM_{1,1}$ mode (Fig. 46), all three modes have one zero crossing and are continuous at $r = b$.

Finally, the overall affects of the dielectric profile on modes 1 and 2 are summarized by examining the cosine ($E_r H_\phi$) and sine ($E_\phi H_r$) terms of Poynting's vector. The cosine term for the $TM_{1,1}$ mode (Fig. 47) shows initially that most of the energy lies in region 1. The sine term for the $TM_{1,1}$ mode (Fig. 48) shows a slightly greater concentration of energy in region 1. Similar to the $TM_{1,1}$ mode, the cosine term for mode 2 (Fig. 49) has an even larger fraction of energy residing in region 1, and its sine term (Fig. 50) has almost all of its energy in region 1. However, mode 1 shows behavior that contrasts that of the $TM_{1,1}$ mode and mode 2. Figure 51 for mode 1 shows that the majority of the cosine energy term resides in region 2. The sine term of mode 1 (Fig. 52) has its energy primarily in the peak of region 1, but the magnitude is negative.

EH 11 MODE 2 AT 32.0 GHZ, ER1-2

AXIAL MAGNETIC H FIELD

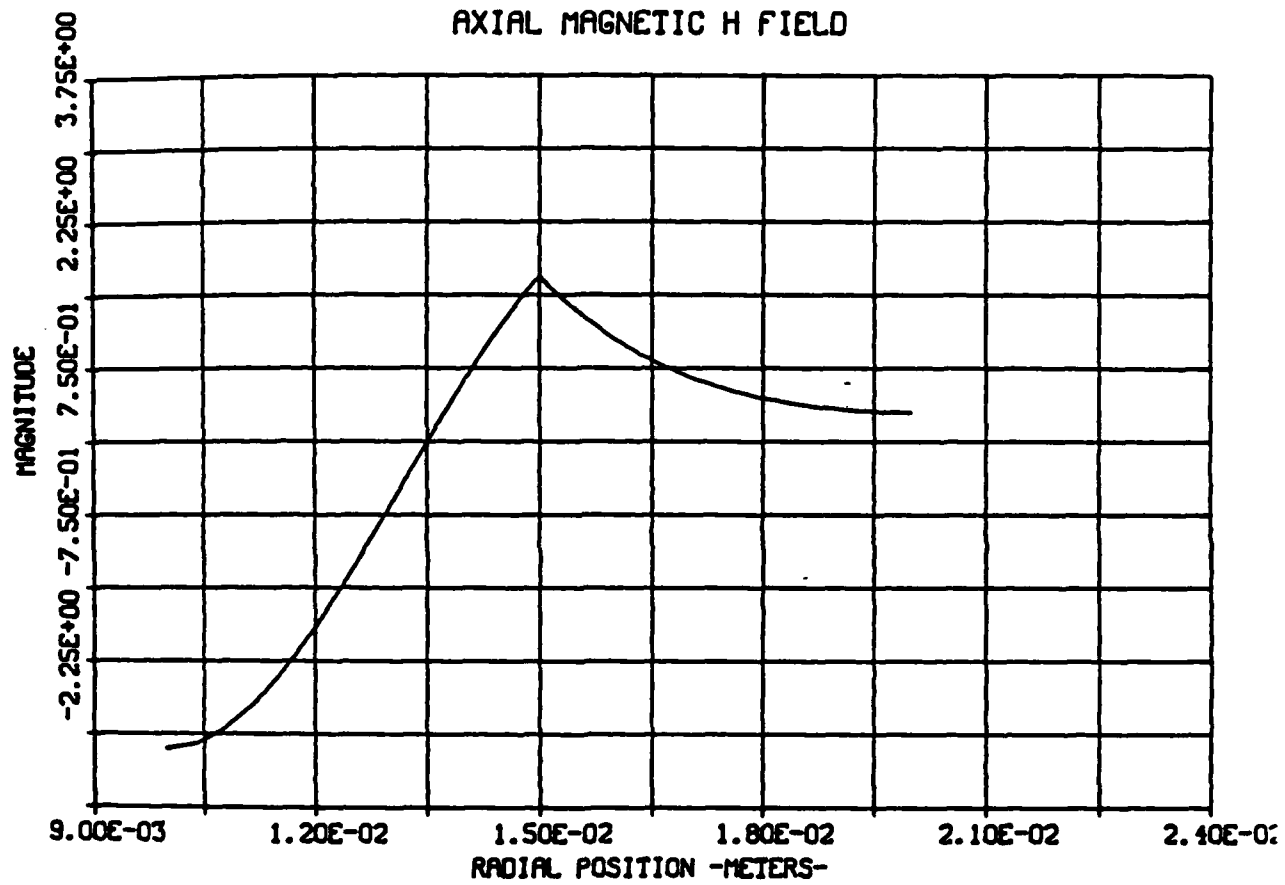


Fig. 44. EH_{1,1} mode 1 at 32 GHz, ER1 = 2; Poynting's vector $E_\phi H_r$.

EH 11 MODE 1 AT 32.0 GHZ, ER1-2

AXIAL MAGNETIC H FIELD

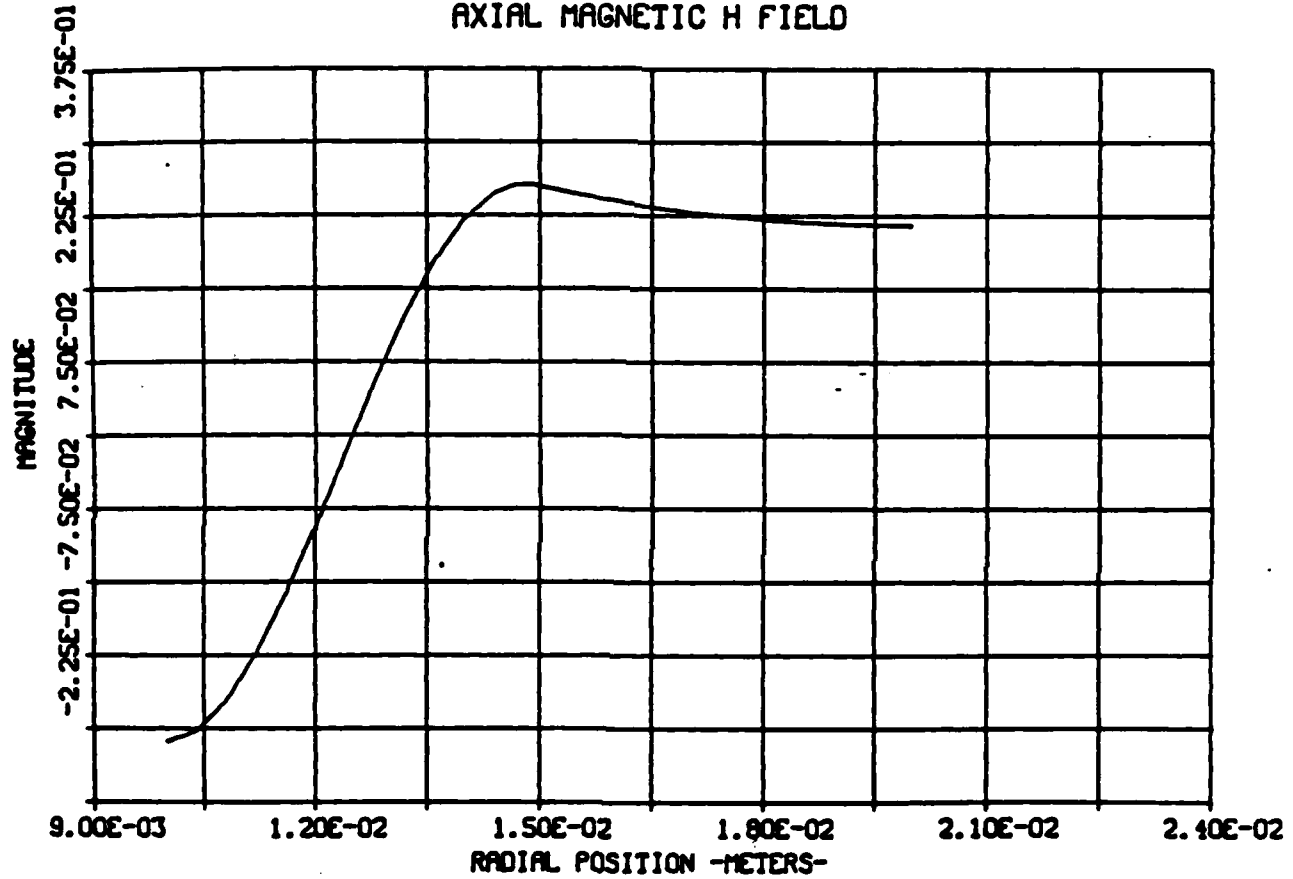


Fig. 45. EH_{1,1} mode 2 at 32 GHz, ER1 = 2; E_r component.

TM 11 MODE AT 32.0 GHZ, ER1-1

AXIAL MAGNETIC H FIELD

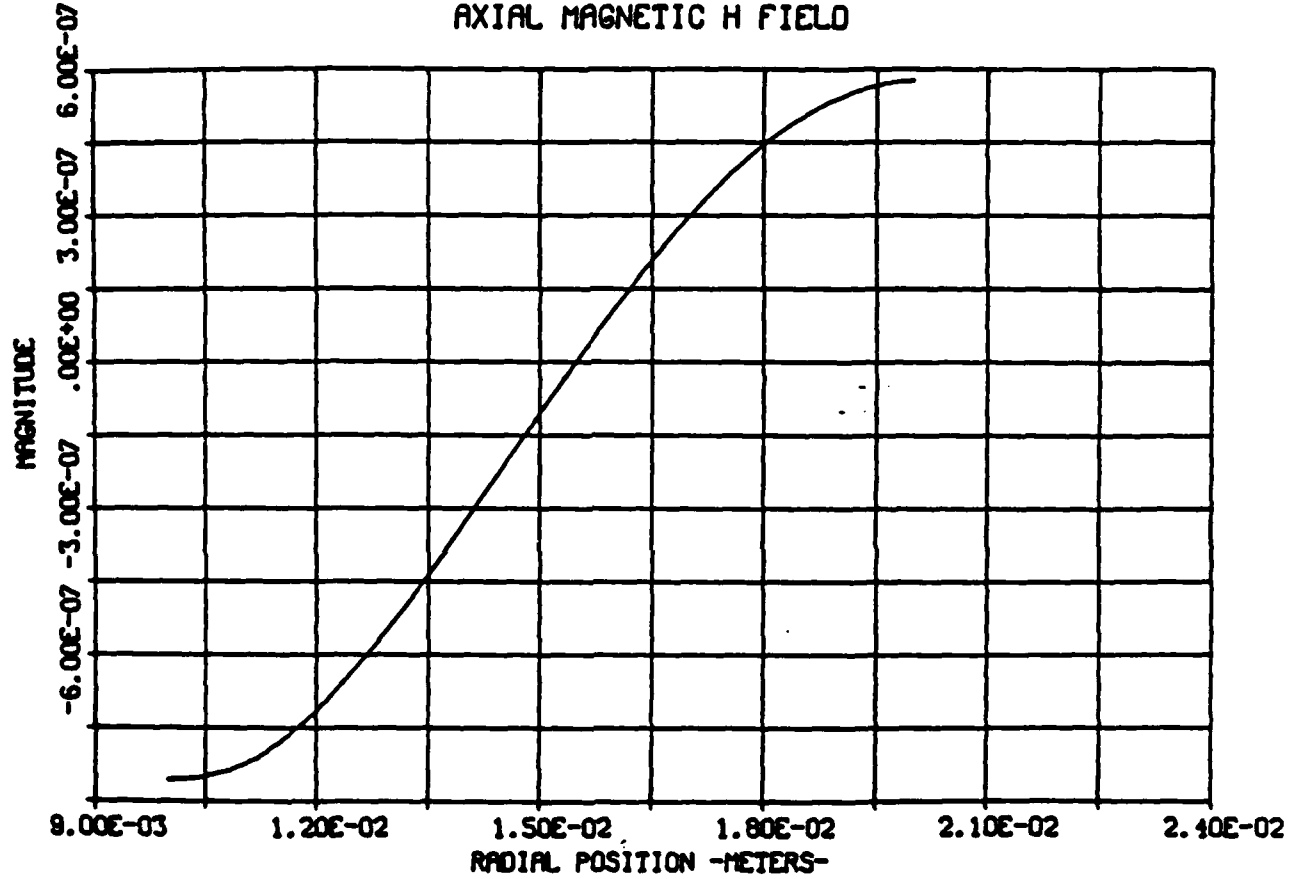


Fig. 46. $EH_{1,1}$ mode 2 at 32 GHz, ER1 = 2; E_ϕ component.

IM 11 MODE AT 32.0 GHZ, ER1-1

POYNITING'S VECTOR- ER1HT

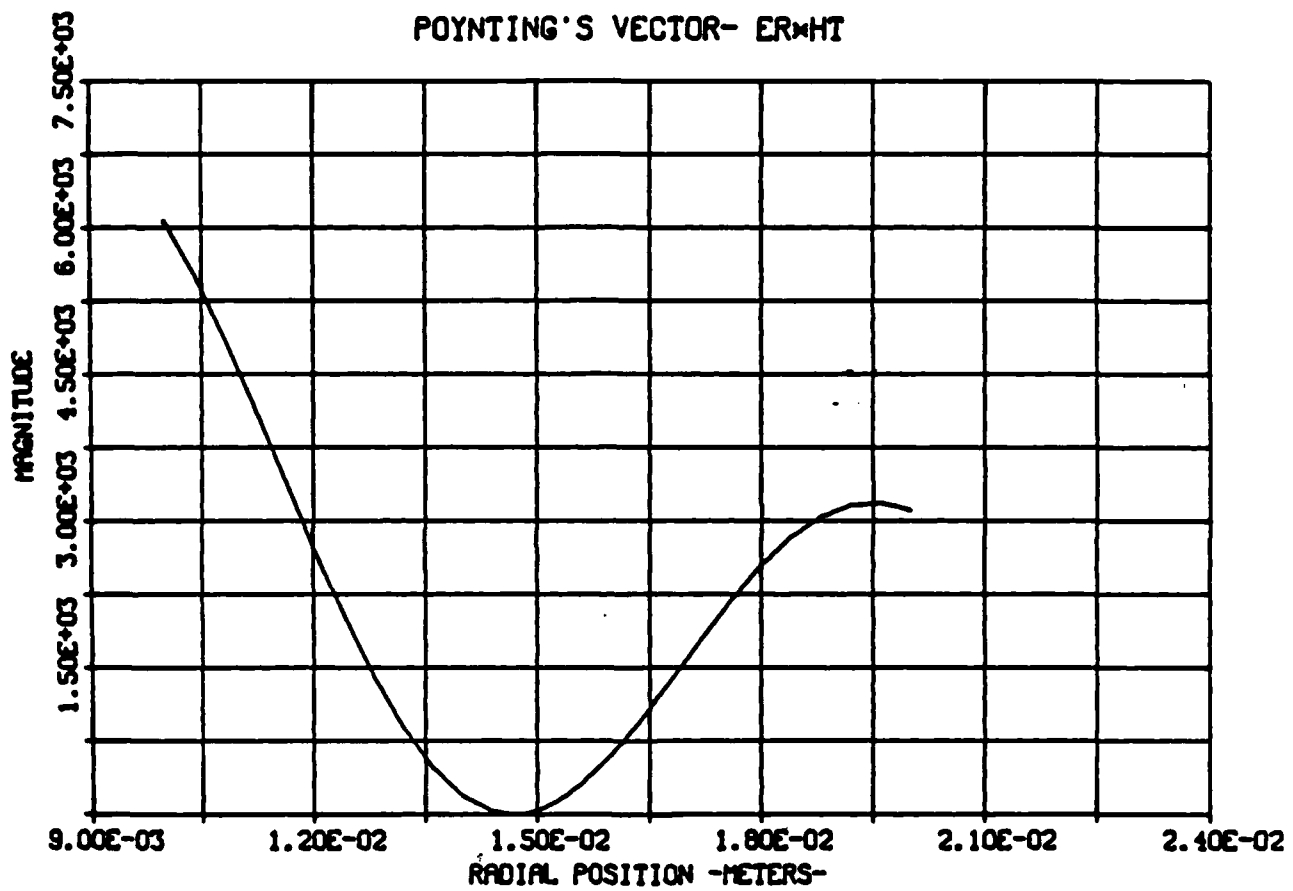


Fig. 47. $EH_{1,1}$ mode 2 at 32 GHz, $ER1 = 2$; E_z component.

TM 11 MODE AT 32.0 GHZ, ER1-1

POYNITING'S VECTOR- ETMR

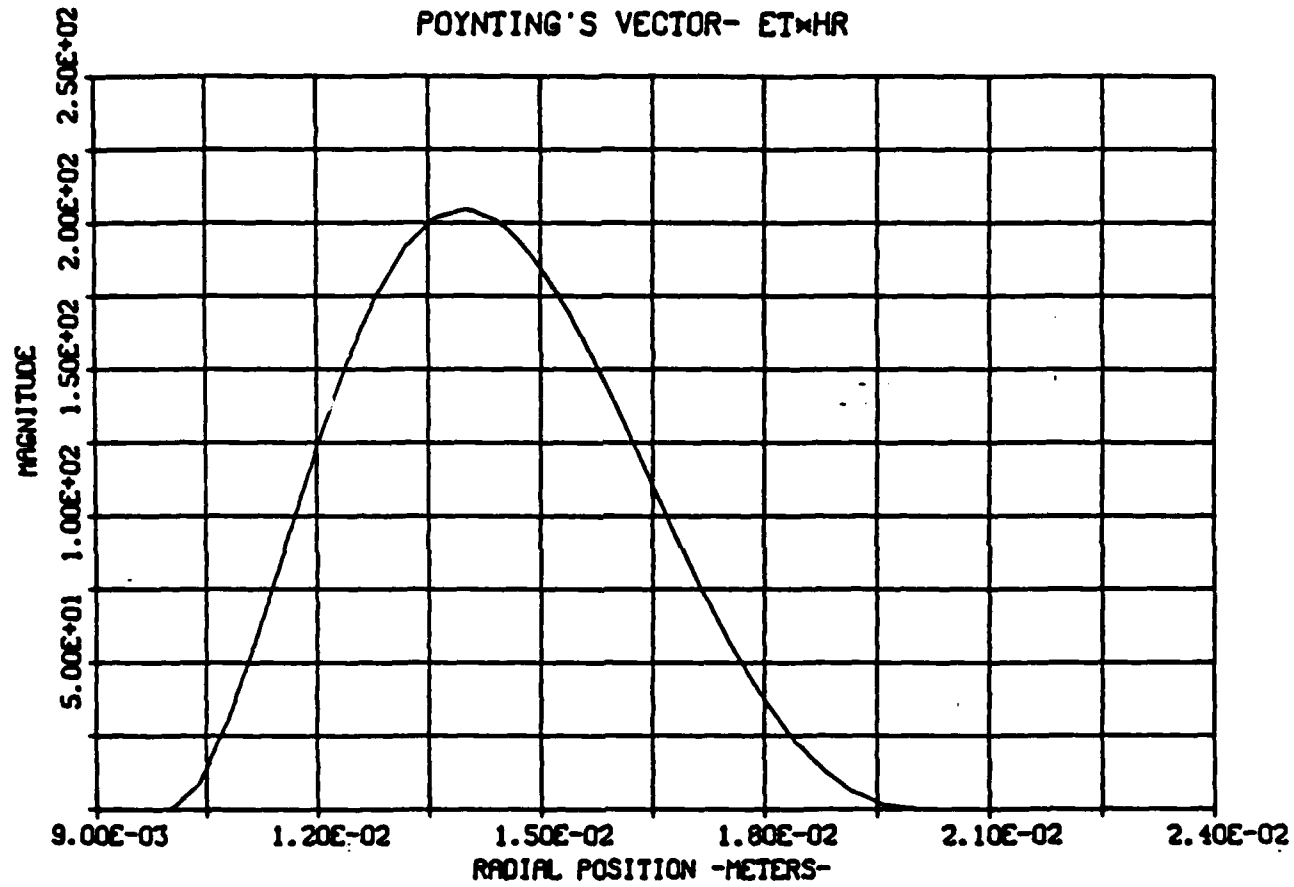


Fig. 48. $EH_{1,1}$ mode 2 at 32 GHz, ER1 = 2; H_r component.

EH 11 MODE 2 AT 32.0 GHZ, ER1-2

POYNITING'S VECTOR- ER₁HT

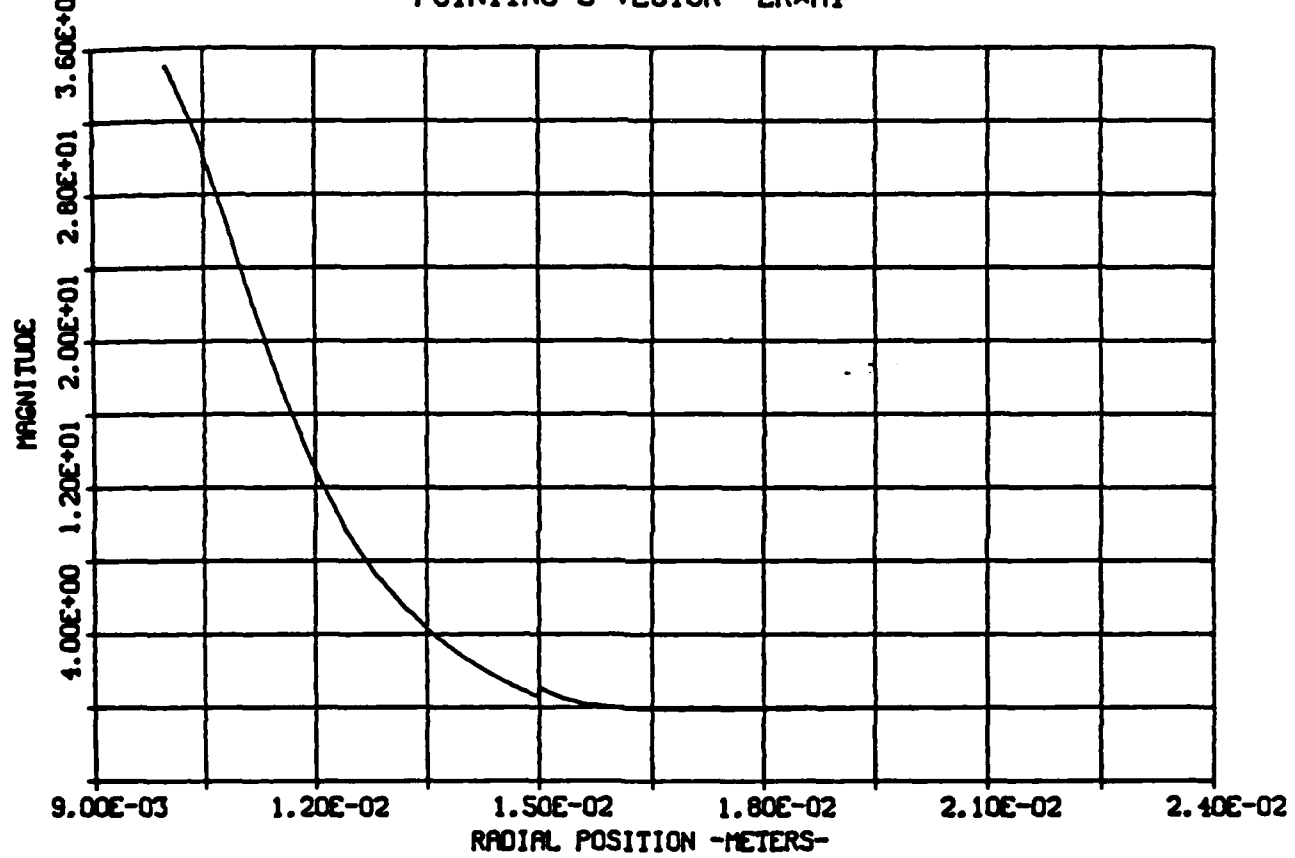


Fig. 49. EH_{1,1} mode 2 at 32 GHz, ER1 = 2; H_φ component.

EH 11 MODE 2 AT 32.0 GHZ, ER1-2

POYNITING'S VECTOR- ET \times HR

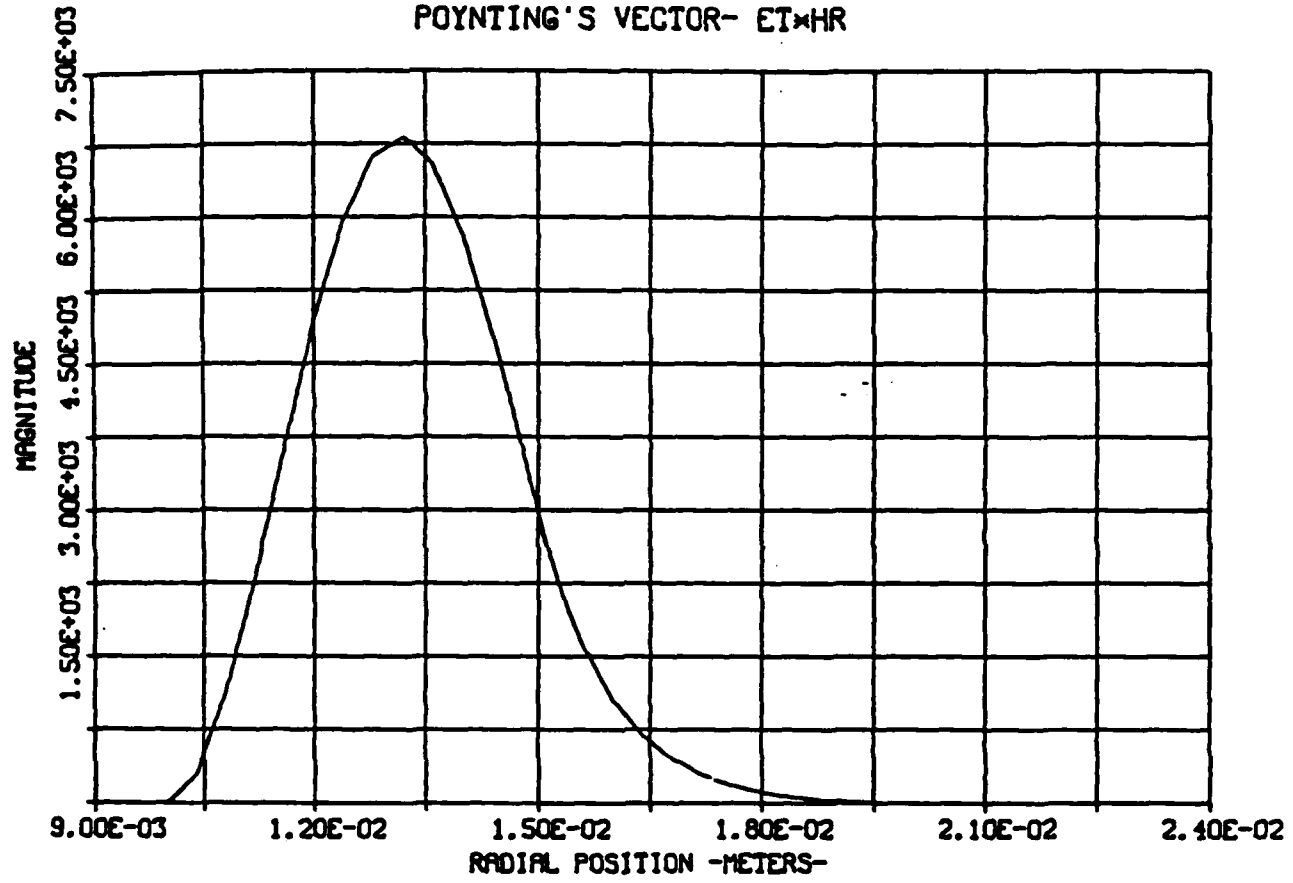


Fig. 50. EH_{1,1} mode 2 at 32 GHz, ER1 = 2; H_z component.

EH 11 MODE 1 AT 32.0 GHZ, ER1-2

POYNITING'S VECTOR- ER1-2

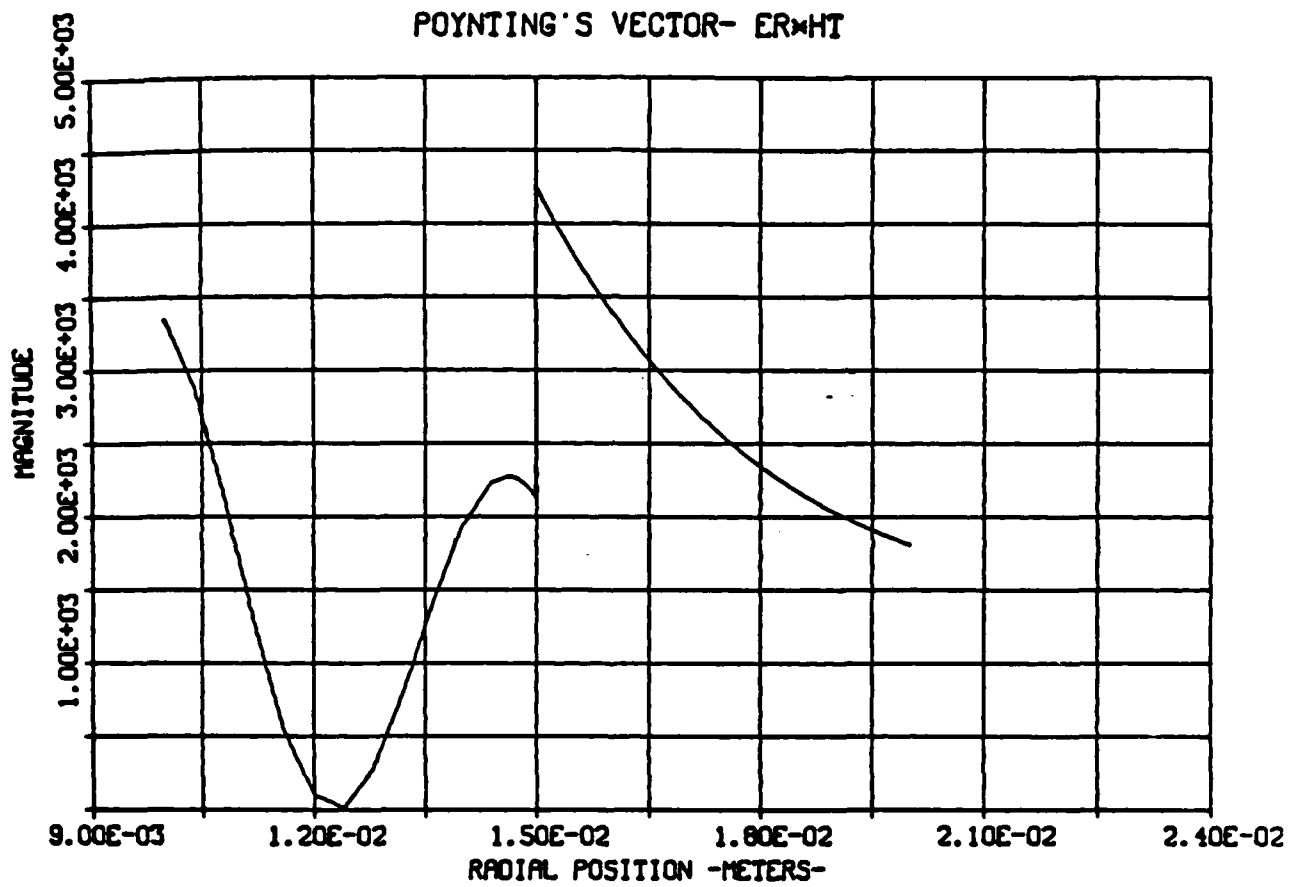


Fig. 51. EH_{1,1} mode 2 at 32 GHz. ER1 = 2; Poynting's vector $E_r H_\phi$.

EH 11 MODE 1 AT 32.0 GHZ, ER1-2

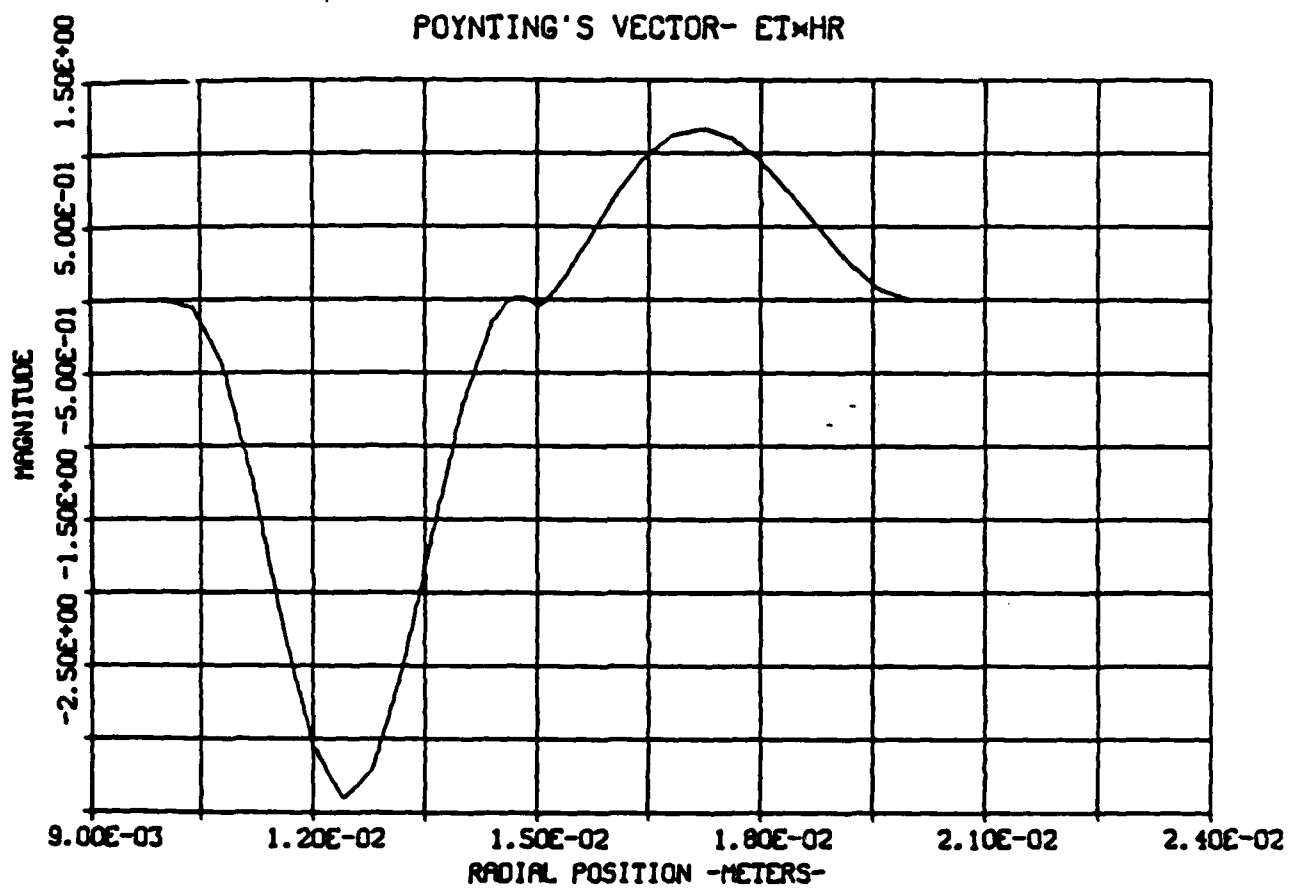


Fig. 52. EH_{1,1} mode 2 at 32 GHz, ER1 = 2; Poynting's vector E_H .

From examining the field component plots and the sine and cosine Poynting vector components (which combine to represent the total net flow of energy), we note that the $TM_{1,1}$ mode and mode 2 have similar characteristics. While mode 1 is also similar to the $TM_{1,1}$ mode in some respects, its energy distribution is quite different. Since sine and cosine are functions which are 90 degrees out of phase, there will be (for a given cross-sectional plane) points in the azimuth where cosine is zero and sine is not. Although the majority of energy for mode 1 propagates in region 2 in the $+z$ direction, there are locations in the cross-sectional plane where there is a net flow of energy ($\sim 1.0 E-4$) in the $-z$ direction (as a result of the sine-cosine relationship). This behavior is analogous to the "back eddys" created from water flowing through a pipe containing obstacles. Unlike mode 1, the energy for the $TM_{1,1}$ mode and mode 2 propagates primarily in region 1 in the $+z$ direction.

5.5 Evaluation of Orthogonality

Sections 5.1 through 5.4 presented the values for k_z , α (where appropriate), and field plots for the given modes. With every mode, k_z for the dielectric profile of $\epsilon_{r1} = 2 (\epsilon_{r1} - 1)$ was larger than that for the air filled case. This is consistent with Eq. 97 of Section 4.2. From Section 5.4, the magnitude of α showed that significant hybridization had occurred for modes 1 and 2. The fact that α for the $TM_{1,1}$ mode was finite (but very small) reflects the numerical accuracy of the program. The boundary conditions at $r = a$ and $r = c$ for the tangential electric field and normal magnetic field components were satisfied for

all the modes examined. The boundary condition that E_r jump by a factor of two (ratio of ϵ_{r1} to ϵ_{r2}) at $r = b$ for case 2 was also satisfied. Poynting's vector has shown for each mode that a discontinuous dielectric profile shifts the majority of energy to one of the two regions. Thus, as previously noted, the mode propagates primarily in one region. One further aspect that must be examined is whether the modes in question are orthogonal.

Orthogonality was computed between the following pairs of modes: TEM and $TM_{0,1}$; $TE_{0,1}$ and $TE_{0,2}$ (chosen for convenience); $EH_{1,1}$ mode 1, and $EH_{1,1}$ mode 2. The results of Eq. 68 (Section 3.5) for each pair are presented under columns 2 through 5 where the mode before the backlash contributes the E_r and E_ϕ components and the mode following the backlash contributes the H_ϕ and H_r components:

TEM and $TM_{0,1}$

<u>ϵ_{r1}</u>	<u>TEM/TEM</u>	<u>TEM/$TM_{0,1}$</u>	<u>$TM_{0,1}$/TEM</u>	<u>$TM_{0,1}/TM_{0,1}$</u>
1.0	1.0	1.22 E-7	1.08 E-7	1.0
2.0	1.0	5.36 E-6	3.56 E-6	1.0

$TE_{0,1}$ and $TE_{0,2}$

<u>ϵ_{r1}</u>	<u>$TE_{0,1}/TE_{0,1}$</u>	<u>$TE_{0,1}/TE_{0,2}$</u>	<u>$TE_{0,2}/TE_{0,1}$</u>	<u>$TE_{0,2}/TE_{0,2}$</u>
1.0	1.0	3.32 E-7	8.62 E-7	1.0
2.0	1.0	-2.47 E-6	-4.39 E-6	1.0

EH_{1,1} Mode and EH_{1,1} Mode 2

<u>ϵ_{rl}</u>	<u>Mode 1/Mode 1</u>	<u>Mode 1/Mode 2</u>	<u>Mode 2/Mode 1</u>	<u>Mode 2/Mode 2</u>
2.0	1.0	2.87 E-6	1.94 E-6	1.0

Theoretically, if two modes are orthogonal, then Eq. 68 is exactly equal to zero. The results show that for each mode pair, the computed values of orthogonality are very small for both values of ϵ_{rl} . Furthermore, columns 2 and 5 (which represent computation of self orthogonality) have the value of 1 for each case of ϵ_{rl} , as expected. In light of these results, we conclude that the modes TM_{0,1}, TE_{0,1}, TEM, EH_{1,1} mode 1, and EH_{1,1} mode 2 are valid.

5.6 Dispersion Plots

Two dispersion plots, ω versus k_z , are presented in this section for the following conditions:

$$\epsilon_{rl} = 2, \epsilon_{rl} = 1$$

Frequency range : 1.0-34.0 GHz

Figure 53 is a plot of the TM_{0,1}, TE_{0,1}, and TEM modes, and Fig. 54 is a plot of the modes EH_{1,1} mode 1 and EH_{1,1} mode 2. In each plot, the y axis (ω) has been normalized by dividing by the speed of light in vacuum (c_0) and multiplying by the radius of the dielectric interface, b ($b = 1.5$ cm). Upon multiplying the x axis (k_z) by b results in both axes being dimensionless and of the same order of magnitude. Thus, the

DISPERSION OF STEPPED DIELECTRIC PROFILE

TEM, TM₀₁, TE₀₁ MODES

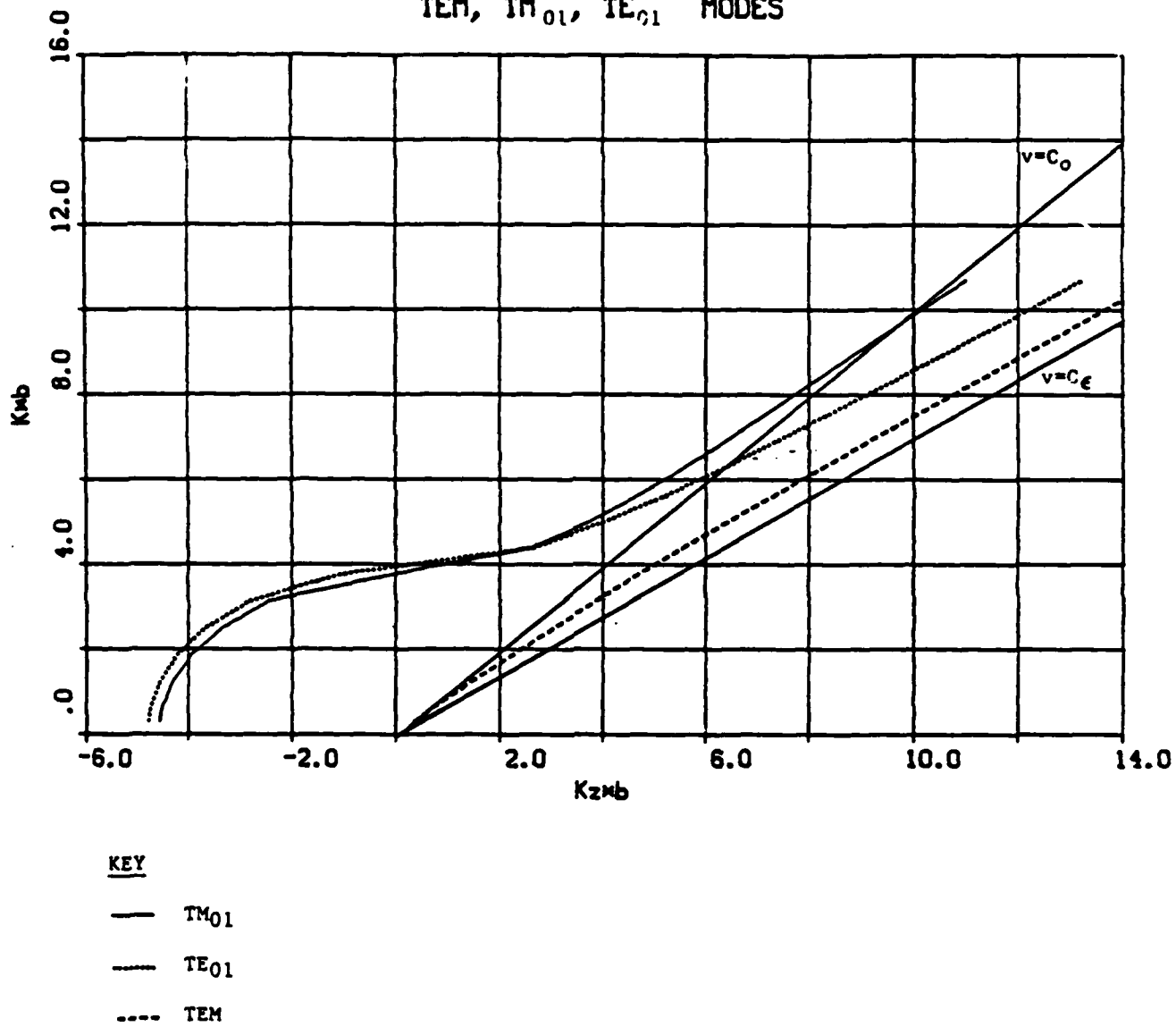
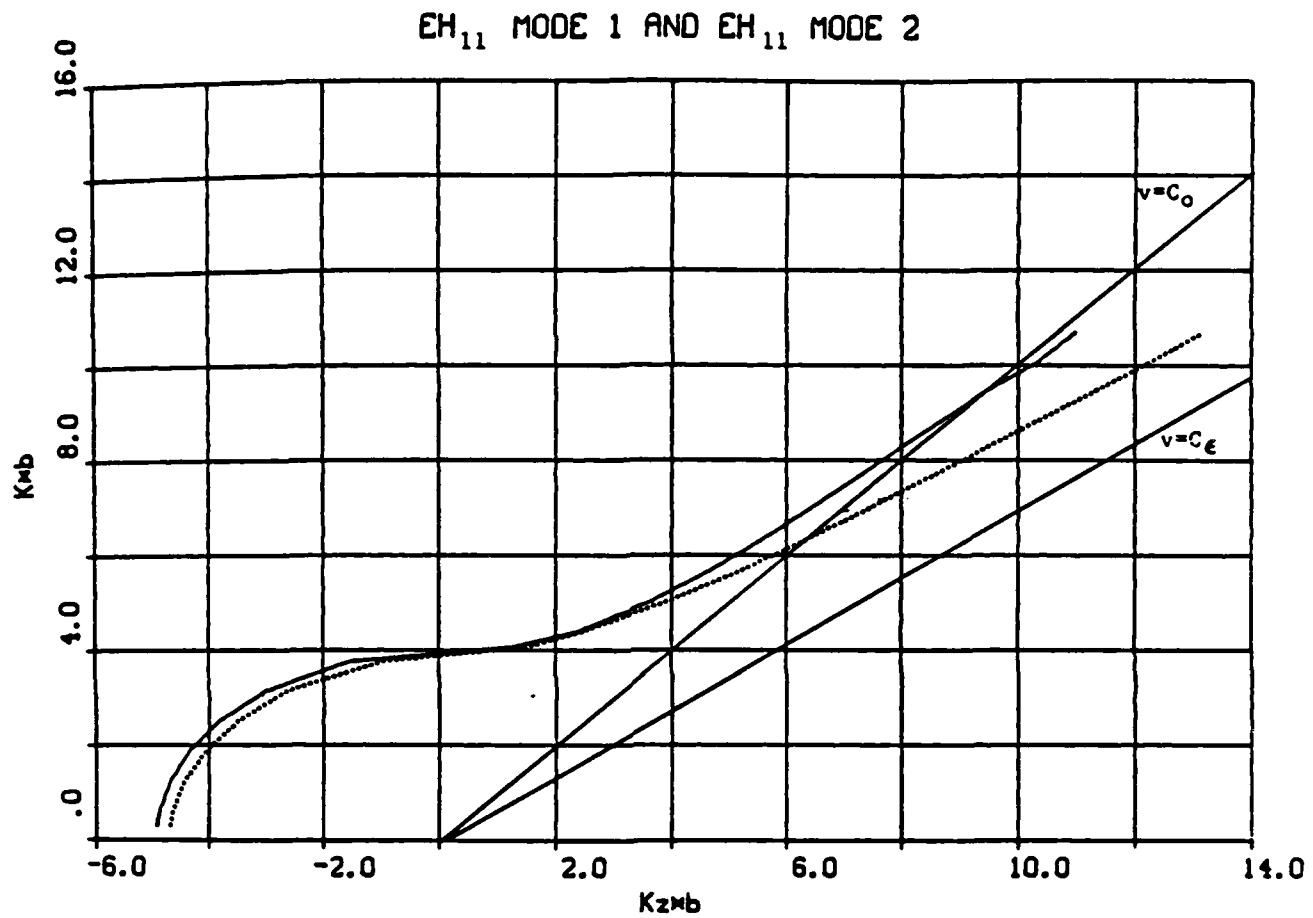


Fig. 53. Dispersion for a stepped dielectric:
TM_{0,1}, TE_{0,1}, and TEM modes.

DISPERSION OF STEPPED DIELECTRIC PROFILE



KEY

- EH_{1,1} MODE 1
- EH_{1,1} MODE 2

Fig. 54. Dispersion for a stepped dielectric:
EH_{1,1} mode 1, EH_{1,1} mode 2.

x and y axes are labeled $k_z b$ and $k b$ (where $k = \omega c_0^{-1}$), respectively. A negative value of $k_z b$ represents the propagation constant when it is cutoff (imaginary).

Beyond a certain frequency for a given mode, both plots reveal propagation between the two velocity of light curves $v = c_0$ and $v = c_\epsilon$ (for the dielectric profile of $\epsilon_{r1} = \epsilon_{r2} = 2$). For the mode in question, this implies that the fraction of the total energy which propagates in region 2 is a slow wave mode (below $v = c_0$) and the remaining energy which propagates in region 1 is a fast wave mode (above $v = c_\epsilon$). Thus, the mode propagates with an overall k_z that lies between the k_z for the air filled region (region 2, $v = c_0$) and the k_z for region 2 ($\epsilon_{r1} = 2, v = c_\epsilon$). This is precisely Eq. 97 presented in Section 4.2. Hence, the dispersion plots reinforce the validity of the modes examined for the dielectric profile of $\epsilon_{r1} = 2$ and $\epsilon_{r2} = 1$.

A connection can be made between the asymmetric behavior of the mode as the frequency goes to infinity with the distribution of the energy from the analysis of Poynting's vector. For a mode that is concentrated in the dielectric ($TE_{0,1}$, TEM , $EH_{1,1}$ mode 2), the dispersion should approach the $v = c_\epsilon$ line. Conversely, for a mode that is concentrated in the vacuum region ($TM_{0,1}$, $EH_{1,1}$ mode 1), the dispersion should approach the $v = c_0$ line. This appears to be the trend for the data in Figs. 53 and 54.

5.7 Effect of the Dielectric Profile on k_z

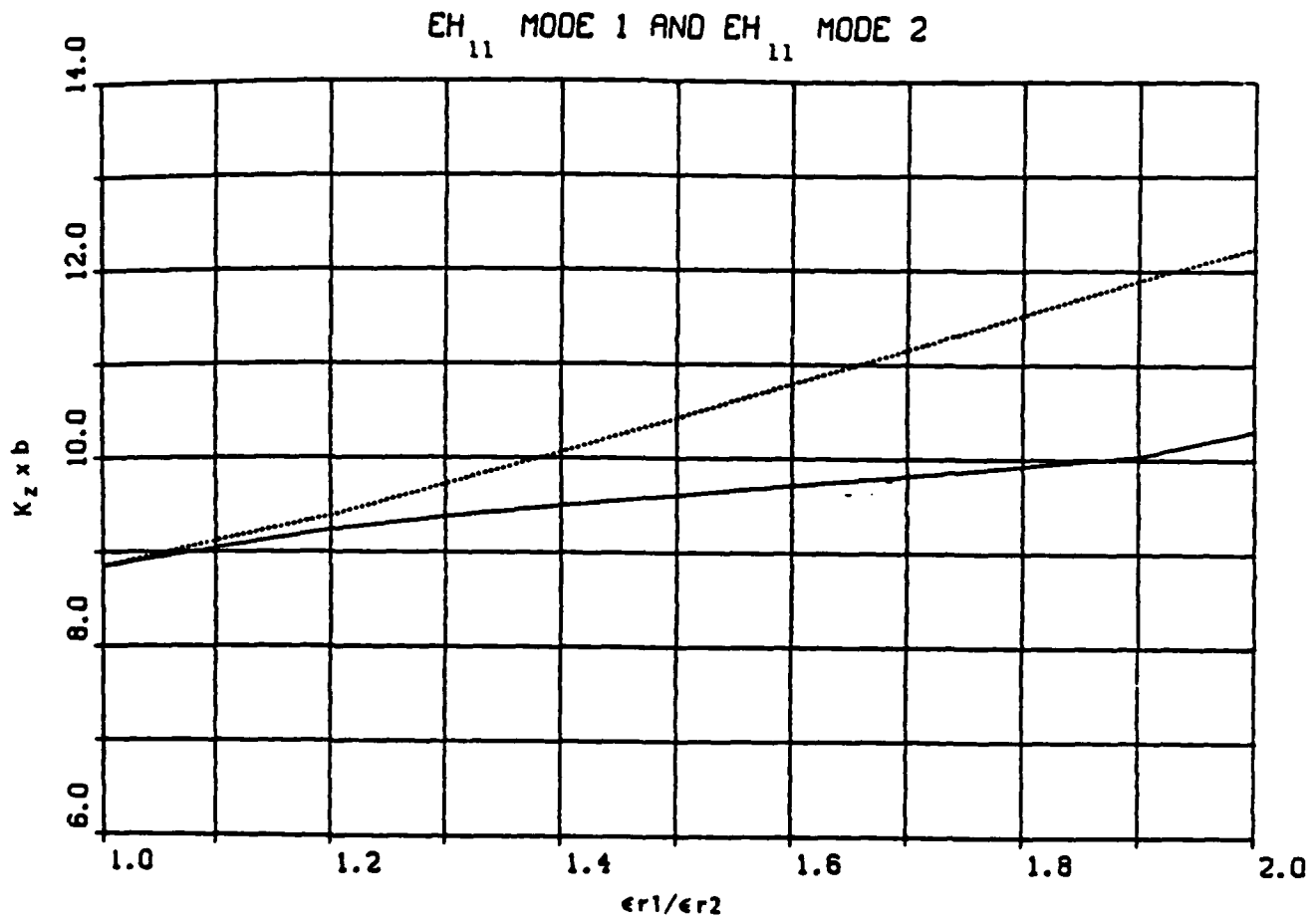
The effect on the propagation constant k_z by varying the dielectric ratio of ϵ_{r1} to ϵ_{r2} from one to two at 32 gigahertz, is examined in this section. As in Figs. 53 and 54, k_z is normalized by multiplying by b .

Figure 55 shows how modes 1 and 2 split as the dielectric ratio increases. Although the modes are orthogonal to one another at each value of the dielectric ratio, there is generally a slow increase in the magnitude of the computed values as the ratio becomes larger.

$\epsilon_{r1}/\epsilon_{r2}$	Mode 1/Mode 1	Mode 1/Mode 2	Mode 2/Mode 1	Mode 2/Mode 2
1.2	1.0	-5.10 E-8	-2.80 E-8	1.0
1.3	1.0	2.51 E-8	4.61 E-8	1.0
1.4	1.0	3.58 E-8	4.51 E-8	1.0
1.5	1.0	9.50 E-8	1.04 E-8	1.0
1.6	1.0	1.20 E-7	1.32 E-7	1.0
1.7	1.0	1.14 E-7	1.45 E-7	1.0
1.8	1.0	1.82 E-7	2.35 E-7	1.0
1.9	1.0	1.86 E-7	2.53 E-7	1.0
2.0	1.0	2.87 E-6	1.94 E-6	1.0

This degradation is principally due to the "ringing" which becomes larger at the dielectric discontinuity. The consequence is an increase in the errors of the solutions which, in turn, affects the orthogonality computations.

K_z VERSUS $\epsilon_{r1}/\epsilon_{r2}$



KEY

- $EH_{1,1}$ MODE 1
- $EH_{1,1}$ MODE 2

Fig. 55. K_z versus $\epsilon_{r1}/\epsilon_{r2}$.

VI. CONCLUSION

6.1 Advantages and Drawbacks

The direct integration approach formulated in Chapter 3 has various advantages over the traditional modal expansion. First, the TEM mode can be examined for a discontinuous dielectric profile (as was done for Fig. 3A). The second order differential equation systems for the $m \neq 0$ and $m = 0$ modes (Eqs. 47 and 48, respectively) were derived independently of the dielectric profile. As a result, each differential equation system can evaluate a general dielectric profile (which could be a combination of stepped and linearly graded sections). This characteristic is quite unlike the modal expansion approach where the size of the dispersion determinant varies as the square of the number of steps, and therefore the determinant grows in complexity and size in accordance with the complexity of the profile. Unlike the dispersion determinant, Eqs. 47 and 48 involve no Bessel functions. Hence, the computer program does not have to evaluate Bessel function expansions, therefore allowing the investigation of modes that are near cutoff (nonpropagating). The success of this technique is illustrated by the solutions obtained in Chapter 5.

As noted in Section 4.3, the $m \neq 0$ modes ($TE_{m,n}$ and $TM_{m,n}$ modes) had a tendency to "walk" to an undesired solution for k_z and α if the initial guesses were relatively poor. Also, the time involved in finding a solution to an $m \neq 0$ mode was a factor of five or more slower than the $m = 0$ modes.

6.2 Future Goals and Applications

The formulation in Chapter 3 was derived with the permeability of the dielectric to be that of air (μ_0). A natural extension would be to incorporate a permeability profile $\mu(r)$. Also of interest would be the addition of a complex permittivity $\epsilon^*(r)$ to the formulation and investigating the complex propagation constant k_z for various lossy dielectric profiles. Finally, work needs to be done on the zero finding logic to improve the speed of convergence of k_z for α for the $m \neq 0$ modes.

REFERENCES

1. R. F. Harrington, Time Harmonic Electromagnetic Fields, McGraw-Hill Book Company, New York, 1961.
2. E. J. Rothwell, "A Study of Slow-Wave Propagation in a Loss Dielectric/Ferrite Lined Waveguide," AFTER Thesis, April 1982.
3. J. D. Jackson, Classical Electrodynamics, 2nd edition, 1962; John Wiley and Sons, New York, 1975.
4. C. de Boor, "A Practical Guide to Splines, Vol. 27, Springer-Verlag New York, Inc., New York, 1978.
5. IMSL, Customer Relations, Sixth Floor, NBC Building, 7500 Bellaire Boulevard, Houston, Texas 77036-5085.
6. Numerical Algorithms Group LTD, 1101 - 31st Street, Suite 100, Downers Grove, Illinois 60515.

APPENDIX A
NUMERICAL SUBROUTINES

The following subroutines were provided by the IMSL⁵ and NAG⁶ libraries, which are collections of mathematical and statistical subroutines written in FORTRAN. Following the name of each routine will be the library from which it was taken.

The routine DGEAR is used to integrate the second order differential equation systems (Eqs. 47 and 48). The zero finding in the shooting method is performed by ZREAL1 and E04JBF. Evaluating the integral (Eq. 68) of the solutions to perform normalization and the orthogonality tests is carried out by DCADRE. The routines ICSEVU and DCSEVU are used as utilities to generate and evaluate spline approximations to the given dielectric profile and the final solutions to the field components.

A.1 DGEAR (IMSL)

This routine is used to integrate Eqs. 47 and 48 in the "shooting method." The solution to a system of first order ordinary differential equations of the form $y' = f(x, y)$ with initial conditions can be solved by DGEAR. The basic methods taken in obtaining solutions are of the implicit linear multistep type. There are two classes of such methods available to the user. The first is the implicit Adam's methods (up to order twelve), and the second is the backward differentiation formula methods (up to order five) also known as Gear's stiff methods. We used the second method. With either case, an algebraic system of equations

must be solved at each step where a variety of corrector iteration methods are available for use.

To evaluate the first order differential equation system, DGEAR must call on two subroutines provided by the user. The first subroutine, DERIV, defines and evaluates the first order differential equation system Y'_1, Y'_2, \dots, Y'_n given N (the number of first order differential equations), x (the values at which to evaluate the equations, and Y_1, Y_2, \dots, Y_n (the integration variables). The second subroutine, PARDRV, defines and evaluates the Jacobian matrix of partial derivatives.

A.2 ZREAL1 (IMSL)

The routine ZREAL1 is used to find the zero for the $TM_{0,n}$, and $TE_{0,n}$ type modes. This routine finds the N real zeros of a single argument, real function subprogram $F(\mathbf{x})$ which is supplied by the user. Upon supplying \mathbf{x} with N initial guesses X_1, X_2, \dots, X_n , the subroutine uses Muller's method to locate the N real zeros of $F(\mathbf{x})$. The solutions to $F(\mathbf{x}) = 0$ are returned in \mathbf{x} .

A.3 E04JBF (NAG)

The routine E04JBF is used to find the minimums (k_z and α) for $TM_{m,n}$ ($EH_{m,n}$) and $TE_{m,n}$ ($HE_{m,n}$) type modes. This routine employs a comprehensive quasi-Newton algorithm for finding:

1. An unconstrained minimum of a function of several variables.
2. A minimum of a function of several variables subject to fixed upper and/or lower bounds on the variables. No derivatives

are required, but the user may specify continuous first and second derivatives (the routine will usually work when there are occasional discontinuities).

A function of N variables $F(x_1, x_2, \dots, x_n)$ is minimized subject to the constraint,

$$L_j \leq x_j \leq U_j$$

for $j = 1, 2, \dots, N$, where L_j is the lower bound and U_j the upper bound. The user must specify a starting point and an external function subroutine FUNCT to calculate the value of $F(\mathbf{x})$ at any point \mathbf{x} in N dimensional space, where $\mathbf{x} = (x_1, x_2, \dots, x_n)$. The function subroutine FUNCT defines and evaluates the function which is minimized,

$$FC = F(XC(1), XC(2), \dots, XC(n))$$

where XC is an array of dimension N, which contains the current point of evaluation. Special variables that need to be defined are:

STEPMAX -- specifies an estimate of the Euclidean distance between the solution and starting point

FEST -- specifies an estimate of the function value at the minimum

IBOUND -- specifies whether the problem was constrained or bounded

BL -- array of dimension N containing the fixed lower bounds

$$L_j$$

BU -- array of dimension N containing the fixed lower bounds

U_j

The user must also supply the subroutine MONIT with proper parameter list. If desired, MONIT can be used to monitor the minimization process. Subroutine EO4HBF (from the NAG library), which computes the finite difference intervals for input to EO4JBF, was modified. Normally, using machine accuracy in its computations, the accuracy of EO4HBF was altered to that used in subroutine DGEAR.

A.4 DCADRE (IMSL)

The routine DCADRE is used to integrate the solutions to Eqs. 47 and 48 to normalize the field components and to check orthogonality. Numerical integration of a function using cautious adaptive Romberg extrapolation is performed. In many instances, DCADRE can handle jump discontinuities. The user must supply a single argument, real function subprogram F(X).

A.5 ICSCCU, ICSEVU, DCSEVU (IMSL)

The routines ICSCCU, ICSEVU, and DCSEVU are presented together, since they are all involved in the cubic spline interpolation of a given set of points. The interpolatory approximation to a set of points by a cubic spline is performed by ICSCCU. The endpoint conditions are determined automatically. Input to the routine requires the number of points N, a set of points x_j , where $x_i < x_{i+1}$ for $i = 1, 2, \dots, N$, and a corresponding set of y_j (functional) values for $i = 1, 2, \dots, N$. Evaluation of the spline coefficients generated by ICSCCU is performed

by ICSEVU. Input to this routine requires the set of spline coefficients and points where the spline coefficients are to be evaluated. Evaluation of the first and/or second derivatives of a cubic spline is performed by DCSEVU. Input to this routine requires the interpolated spline coefficients and the points at which the first and/or second derivative should be evaluated.

APPENDIX B

NAMELISTS

The following namelist definitions are input variable files that the user specifies before the program is executed. Before proceeding, we define the index variables used in the arrays:

I -- radial position

J -- mode

K -- mode

L -- frequency

NLORTHO -- orthogonality control

<u>Variable Name</u>	<u>Default</u>	<u>Function</u>
LORTHO	FALSE	Subroutine ORTHO activated
LTEST(J,K)	FALSE	Compute orthogonality between modes J, K

NLFRE -- frequency data control

FRQLOW	8.0 E+9	Frequency at low end of desired band
FRHIGH	12.0 E+9	Frequency at high end of desired band
NFRE	1	Number of frequencies at which to evaluate desired modes

NLGEO -- geometry and dielectric control

RIN	1.0 E-2	Inner conductor radius (meters)
RMID	1.5 E-2	Radius of inner dielectric region (meters)
NPTST	---	Number of points at which the radial profile is defined

DRELT(1)	---	Value of relative dielectric permittivity at <i>i</i> th radial position
XPAT(1)	---	Radial position of <i>i</i> th point (meters)
LTAPER	FALSE	Generate a linearly tapered dielectric profile

NLMOD -- mode control

MC1MX	1	Number of modes to be evaluated
MC2(J)	1	Azimuthal eigenvalue for $TE_{m,n}$ and $TM_{m,n}$ modes
LTM(J)	TRUE	compute k_z and fields for $TM_{0,n}$ and TEM modes
LTE(J)	FALSE	Compute k_z and fields for $TE_{0,n}$ modes
LMX(J)	FALSE	Compute k_z and fields for $TE_{m,n}$ and $TM_{m,n}$ modes
RKZG(J)	---	Initial guess for k_z
RATIOG(J)	---	Initial guess for α

NLPLT -- printing and plotting control

LPPLOT	FALSE	Generate field plots for the print file COAD7P
LPRINT	TRUE	Generate output data for COAD7P
LDPLLOT	FALSE	Generate field plots in subroutine DPLOT
LDFL	FALSE	<i>i</i> th field component output plot generated
LDER	FALSE	Field component 1; E_r
LDET	FALSE	Field component 2; E_ϕ
LDEZ	FALSE	Field component 3; E_z
LDDR	FALSE	Field component 4; D_r
LDDT	FALSE	Field component 5; D_ϕ
LDDZ	FALSE	Field component 6; D_z

LDBR	FALSE	Field component 7; B_r
LDBT	FALSE	Field component 8; B_ϕ
LDBZ	FALSE	Field component 9; B_z
LDHR	FALSE	Field component 10; H_r
LDHT	FALSE	Field component 11; H_ϕ
LDHz	FALSE	Field component 12; H_z
LDPC	FALSE	Generate plot of the Poynting vector term $E_r H_\phi$
LDPS	FALSE	Generate plot of the Poynting vector term $E_\phi H_r$

NLDGR -- DGEAR control variables

HTP	1.0 E-6	Next step size in x (independent variable)
TOLT	1.0 E-8	Relative error bound
INDXT	1	Indicates the type of call to the subroutines called by DGEAR
MITERT	1	Iteration method indicator

NLZRE -- ZREAL1 control variables

EPS	1.0 E-5	Convergence criterion: a root, X(1), is acceptable if $ABS(F(X(1))) < EPS$
NSIG	2	Convergence criterion: a root is accepted if two successive approximations to a given root agree in the first NSIG digits
ITMAX	100	Maximum number of iterations

NLE04 -- E04JBF control variables

MAXCAL	560	Number of function iterations
XTOL	1.0 E-5	Accuracy to which the solution is desired

FEST	0.0	Estimate of the function value at the minimum
STEPMX	1.0 E+5	Estimate of the Euclidean distance between the solution and the starting point
BL(1,J)	-1000	Fixed lower bound for k_z
BL(2,J)	-100	Fixed lower bound for α
BU(1,J)	1000	Fixed upper bound for k_z
BU(2,J)	100	Fixed upper bound for α

NLCAD -- DCADRE control variables

AERR	1.0 E-5	Absolute error of the zero
ERROR	1.0 E-5	Estimated bound on the absolute error of the zero

APPENDIX C
INTERPOLATION OF A DISCONTINUOUS FUNCTION

As mentioned in Section 4.2, a discontinuous dielectric profile will generate a "ringing" in the neighborhood of the jump if the standard spline approach is used. The approach described below is a modification for a discontinuous function.

Let the range of the function be $[a, b]$, with the given values at x_i , $1 < i < N$, and $x_1 = a$ and $x_N = b$. Let the values of the function at x_i be equal to Y_i . The standard spline coefficients for the interval $[x_i, x_{i+1}]$ are defined as a_i , b_i , c_i , and d_i , where the interpolated function for x in the interval is given by

$$Y = a_i + b_i u + c_i u^2 + d_i u^3 \quad (C.1)$$

where $u = x - x_i$. Since the splines normally are continuous across the interval $[x_{i-1}, x_i]$, $[x_i, x_{i+1}]$, the following must hold:

$$a_{i-1} + b_{i-1}(x_i - x_{i-1}) + c_{i-1}(x_i - x_{i-1})^2 + d_{i-1}(x_i - x_{i-1})^3 = a_i \quad (C.2)$$

Therefore, a discontinuity may be introduced across an interval junction by modifying the a_i term only.

Introduce a discontinuity across the interval junction by defining Y_i as the value at the open end of the left interval and T_i as the value at the closed end of the right interval. Also, only let T_i be defined

for i contained in I , the set of interval junctions that are discontinuous. Next, define a new set of function values Z_i by

$$Z_i = Y_i - \sum_{\substack{j \in I \\ j > i}} (T_j - Y_j) \quad (C.3)$$

By construction, this set of points is "smooth," since the discontinuities have all been subtracted off. The standard spline coefficients are then calculated for these values. Finally, the discontinuity is reintroduced by modifying the constant terms a_i to A_i ,

$$A_i = a_i - \sum_{\substack{j \in I \\ j > i}} (T_j - Y_j) \quad (C.4)$$

Using this modified set of spline coefficients (A_i, b_i, c_i, d_i) will generate the correct step discontinuity across the interval junctions and a smooth value for the function inside the intervals.

APPENDIX D
VARIABLE DEFINITIONS

The variables used in the main program and subroutines are presented. For compactness, variables which are used throughout the program will be defined only in the section where they first appear. The variables listed for the subroutines are local. Section D.7 will define the variables set by the program and used in the calling argument of the IMSL and NAG routines. Before proceeding, we define the index variables used in the arrays,

I -- radial position
J -- mode
K -- mode
L -- frequency

D.1 Main Program (COAD7R)

Titles and Headers -- used for output file purposes

<u>Variable</u>	<u>Name</u>	<u>Function</u>	<u>Type</u>	<u>Units</u>
CFTIT		Title for hard copy field plots	Character	---
CMESS		Label for hard copy field plots	Character	---
CVERS		Title used in the output print file COAD7P	Character	---
DATE		Current date for in COAD7P	---	---
TIME		Current time of printing for in COAD7P	---	---

<u>Variable Name</u>	<u>Function</u>	<u>Type</u>	<u>Units</u>
Constants -- physical and numerical constants			
PI02	$\pi/2$	Real	---
EPS0	ϵ_0 (permittivity of air)	Real	Farad meter ⁻¹
U0	μ_0 (permeability of air)	Real	Henry meter ⁻¹
VLIGHT	c_0 (speed of light in vacuum)	Real	Meters s ⁻¹

Program Flow Control

K	Mode index	Integer	---
L	Frequency index	Integer	---
FREQ	Current value of the frequency	Real	GHz
DELFREQ	Frequency step	Real	GHz
SRKZ(K)	Sign of the final value of k_z for the kth mode	Real	---

Dielectric Profile -- The following variables and arrays define and aid the processing of the dielectric profile

NJUMPS	Total number of discontinuities in the dielectric profile	Integer	---
NPTS	Actual number of points (NPTST-NJUMPS) at which the dielectric profile is defined	Integer	---
XPA(1)	Radial positions at which dielectric profile is defined; length that of XPAT(1)-NJUMPS	Real	---
DRELA(1)	Defines dielectric profile, length is that of DRELT-NJUMPS	Real	---
DRELN(1)	$DRELN(1) = \log_e (DRELN(1))$	Real	---
DRELJ(1)	Value of the "jump" at the ith discontinuity in the dielectric	Real	---

<u>Variable Name</u>	<u>Function</u>	<u>Type</u>	<u>Units</u>
DRATIO(1)	Ratio of DRELA (I + 1) to DRELA (1) at the ith discontinuity in the dielectric	Real	---
AJUMP(1)	Radial position of the ith discontinuity in the dielectric	Real	Meters
IJUMP(1)	Index of the radial position of ith discontinuity in the dielectric	Real	---
DRELD(1)	"Smoothed" dielectric profile; DRELD(1) = DRELT(1) = DRELJ(1)	Real	---
DRELDS(1,3)	Spline coefficients for DRELDS at ith radial position	Real	---
DRELNS(1,3)	Spline coefficients for DRELNS at ith radial position	Real	---

Shooting Parameters -- Shooting parameters and related variables computed by the program

ROOTS(K)	k_z for kth mode	Complex	Meter^{-1}
RATIOA(K)	α for kth mode	Real	---
RMIN(K)	Final value of minimum in E04JBF for kth mode	Real	---
ORTHOG(L,J,K)	Computed value of orthogonality between modes J and K at frequency L	Real	---

Integration Variables -- The integration variables below are defined in Section 3.6

YVAR(1)	Y_1	Real	---
YVAR(2)	Y_2	Real	---
YVAR(3)	Y_3	Real	---
YVAR(4)	Y_4	Real	---
YPRIME(1)	Y'_1	Real	---

<u>Variable Name</u>	<u>Function</u>	<u>Type</u>	<u>Units</u>
YPRIME(2)	Y'_2	Real	---
YPRIME(3)	Y'_3	Real	---
YPRIME(4)	Y'_4	Real	---

Field Components -- Field values as a function of r and related arrays used in processing the field components

ER(I,L,K)	E_r at the i th radial point for frequency L and mode K	Real	Volts meter $^{-1}$
ET(I,L,K)	E_ϕ at the i th radial point for frequency L and mode K	Real	Volts meter $^{-1}$
EZ(I,L,K)	E_z at the i th radial point for frequency L and mode K	Real	Volts meter $^{-1}$
DR(I,L,K)	D_r at the i th radial point for frequency L and mode K	Real	Coulombs meter $^{-2}$
DT(I,L,K)	D_ϕ at the i th radial point for frequency L and mode K	Real	Coulombs meter $^{-2}$
DZ(I,L,K)	D_z at the i th radial point for frequency L and mode K	Real	Coulombs meter $^{-2}$
BR(I,L,K)	B_r at the i th radial point for frequency L and mode K	Real	Weber meter $^{-2}$
BT(I,L,K)	B_ϕ at the i th radial point for frequency L and mode K	Real	Weber meter $^{-2}$
BZ(I,L,K)	B_z at the i th radial point for frequency L and mode K	Real	Weber meter $^{-2}$
HR(I,L,K)	H_r at the i th radial point for frequency L and mode K	Real	Amperes meter $^{-1}$
HT(I,L,K)	H_ϕ at the i th radial point for frequency L and mode K	Real	Amperes meter $^{-1}$
HZ(I,L,K)	H_z at the i th radial point for frequency L and mode K	Real	Amperes meter $^{-1}$

<u>Variable Name</u>	<u>Function</u>	<u>Type</u>	<u>Units</u>
PC(I,L,K)	Value of the Poynting vector component $E_r * H_\phi$ at the i th radial point for frequency L and mode K	Real	Watts
PS(I,L,K)	Value of the Poynting vector component $E_\phi * H_r$ at the i th radial point for frequency L and mode K	Real	Watts
FLD(I,L,K,N)	Used in processing the field components; equivalenced to the N th field component	Real	---
DRP(I,L,K)	Derivative of D_r with respect to r at the i th radial point for frequency L and mode K	Real	Coulombs meter $^{-3}$
ETP(I,L,K)	Derivative of E_ϕ with respect to r at the i th radial point for frequency L and mode K	Real	Volts meter $^{-2}$
DTP(I,L,K)	Derivative of D_ϕ with respect to r at the i th radial point for frequency L and mode K	Real	Coulombs meter $^{-3}$
ERDIFF(I,L,K)	Value of the "jump" in E_r at the i th discontinuity in the dielectric	Real	Volts meter $^{-1}$
DTDIFF(I,L,K)	Value of the "jump" in D_ϕ at the i th discontinuity in the dielectric	Real	Coulombs meter $^{-2}$
DZDIFF(I,L,K)	Value of the "jump" in D_z at the i th discontinuity in the dielectric	Real	Coulombs meter $^{-2}$
ERD(I,L,K)	"Smoothed" field component E_r ; $ERD(I,L,K) = ER(I,L,K) - ERDIFF(I,L,K)$	Real	Volts meter $^{-1}$
DTD(I,L,K)	"Smoothed" field component D_ϕ ; $DTD(I,L,K) = DT(I,L,K) - DTDIFF(I,L,K)$	Real	Coulombs meter $^{-2}$
DZD(I,L,K)	"Smoothed" field component D_z ; $DZD(I,L,K) = DZ(I,L,K) - DZDIFF(I,L,K)$	Real	Coulombs meter $^{-2}$

<u>Variable Name</u>	<u>Function</u>	<u>Type</u>	<u>Units</u>
D.2 Subroutine DERIV			
FDRV	First derivative of the dielectric profile at a given point	Real	---
DREL	Dielectric value at a given point	Real	---
FCTR1	Normalized value of r^{-1}	Real	---
FCTR2	Normalized value of k_z^2	Real	---
FCTR3	Normalized value of $\omega_c^2 c^{-2}$	Real	---
FCTR4	$m^2 + 1$	Real	---
FCTR5	$DREL^{-1}$	Real	---

D.3 Subroutine PARDRV

Processing and Control -- The variables FDRV, DREL, FCTR1, FCTR2, FCTR3, FCTR4, and FCTR5 are used here as in subroutine DERIV and will not be repeated. The following variables are defined in Section 3.6

PD(1,1)	PD _{1,1}	Real	---
PD(1,2)	PD _{1,2}	Real	---
PD(1,3)	PD _{1,3}	Real	---
PD(1,4)	PD _{1,4}	Real	---
PD(2,1)	PD _{2,1}	Real	---
PD(2,2)	PD _{2,2}	Real	---
PD(2,3)	PD _{2,3}	Real	---
PD(2,4)	PD _{2,4}	Real	---
PD(3,1)	PD _{3,1}	Real	---
PD(3,2)	PD _{3,2}	Real	---
PD(3,3)	PD _{3,3}	Real	---
PD(3,4)	PD _{3,4}	Real	---

<u>Variable Name</u>	<u>Function</u>	<u>Type</u>	<u>Units</u>
PD(4,1)	PD _{4,1}	Real	---
PD(4,2)	PD _{4,2}	Real	---
PD(4,3)	PD _{4,3}	Real	---
PD(4,4)	PD _{4,4}	Real	---

D.4 Function FNCTL

XEND	Normalized endpoint used by DGEAR	Real	---
FNCTL1	Functional value equal to one of the following equations: TM _{0,n} and TEM modes : equation 93	Real	---
	TE _{0,n} modes : equation 94		

D.5 Function FNCT2

XEND	Normalized endpoint used by DGEAR	Real	---
FC	Functional value equal to Eq. 95	Real	---

D.6 Subroutine NORMAL

Spline Arrays -- The following arrays store the computed spline coefficients generated by the routine ICSCCU and evaluated by ICSEVU and DCSEVU. The arrays below are also used in subroutine ORTHO and function CXINT.

ERS(I,3,2)	Spline coefficients for E _r at ith radial position	Real	---
ETS(I,3,2)	Spline coefficients for E _φ at ith radial position	Real	---
HRS(I,3,2)	Spline coefficients for H _r at ith radial position	Real	---
HTS(I,3,2)	Spline coefficients for H _φ at ith radial position	Real	---

<u>Variable Name</u>	<u>Function</u>	<u>Type</u>	<u>Units</u>
----------------------	-----------------	-------------	--------------

D.7 IMSL and NAG Routines

DGEAR

N	Number of first order differential equations	Integer	---
XP	On input, XP supplies the initial value and is used only on the first call. On output, XP is replaced with the current value of the independent variable at which integration has been completed	Real	---
IWK	Integer work array of length N	Integer	---
WK	Work array of length $4*N+METHT+MITERT$	Real	---

ZREAL1

EPS2	Spread criteria for multiple roots	Real	---
ETA	Used to restart a computation when multiple roots are desired	Real	---

EO4JBE

N	Number of variables	Real	---
INPRINT	Specifies the frequency with which subroutine MONIT is to be called. There are three options: IPRINT > 0: MONIT called once every IPRINT iterations IPRINT = 0: MONIT called at final point only IPRINT < 0: MONIT not called at all	Integer	---

<u>Variable Name</u>	<u>Function</u>	<u>Type</u>	<u>Units</u>
LOCSH	Specifies whether or not the user wishes a "local search" (TRUE or FALSE, respectively) be performed when a point is found which is thought to be a constrained minimum	Logical	---
ETA	Upon judicious choice for the range $0.0 < \text{ETA} < 1.0$, the linear minimization process is made more efficient	Real	---
IBOUND	Specifies whether the problem is unconstrained or bounded. The options are: IBOUND = 0: Variables are bounded and the user supplies L_j and U_j IBOUND = 1: Problem is unconstrained and the function FUNCT is called N times IBOUND = 2: Variables are bounded	Integer	---
LH	Specifies the actual dimension of the NAG subroutine HESL called by E04JBF	Integer	---
IW	Workspace array	Integer	---
LIW	Specifies the actual dimension of IW as declared in the (sub) program from which E04JBF is called	Integer	---
W	Workspace array of at least $9*N$	Real	---
LW	Specifies the actual dimension of W as declared in the (sub) program from which E04JBF is called	Integer	---

<u>Variable</u>	<u>Function</u>	<u>Type</u>	<u>Units</u>
<u>DCADRE</u>			
RERR	Desired relative error in the answer	Real	---

APPENDIX E
VALUES OF THE RADIAL POINTS

The values of the radial points at which the dielectric profile was defined for both cases in Chapter 5 are presented below (in centimeters):

r_1	= 1.0000	r_{24}	= 1.5000
r_2	= 1.0400	r_{25}	= 1.5010
r_3	= 1.0800	r_{26}	= 1.5050
r_4	= 1.1200	r_{27}	= 1.5075
r_5	= 1.1600	r_{28}	= 1.5100
r_6	= 1.2000	r_{29}	= 1.5150
r_7	= 1.2400	r_{30}	= 1.5175
r_8	= 1.2800	r_{31}	= 1.5200
r_9	= 1.3200	r_{32}	= 1.5250
r_{10}	= 1.3600	r_{33}	= 1.5300
r_{11}	= 1.4000	r_{34}	= 1.5400
r_{12}	= 1.4400	r_{35}	= 1.5600
r_{13}	= 1.4600	r_{36}	= 1.6000
r_{14}	= 1.4650	r_{37}	= 1.6400
r_{15}	= 1.4700	r_{38}	= 1.6800
r_{16}	= 1.4750	r_{39}	= 1.7200
r_{17}	= 1.4800	r_{40}	= 1.7600
r_{18}	= 1.4850	r_{41}	= 1.8000
r_{19}	= 1.4900	r_{42}	= 1.8400
r_{20}	= 1.4925	r_{43}	= 1.8800
r_{21}	= 1.4950	r_{44}	= 1.9200
r_{22}	= 1.4990	r_{45}	= 1.9600
r_{23}	= 1.5000	r_{46}	= 2.0000

MISSION
of
Rome Air Development Center

RADC plans and executes research, development, test and selected acquisition programs in support of Command, Control, Communications and Intelligence (C³I) activities. Technical and engineering support within areas of competence is provided to ESD Program Offices (POs) and other ESD elements to perform effective acquisition of C³I systems. The areas of technical competence include communications, command and control, battle management, information processing, surveillance sensors, intelligence data collection and handling, solid state sciences, electromagnetics, and propagation, and electronic, maintainability, and compatibility.

END

8-87

DTIC